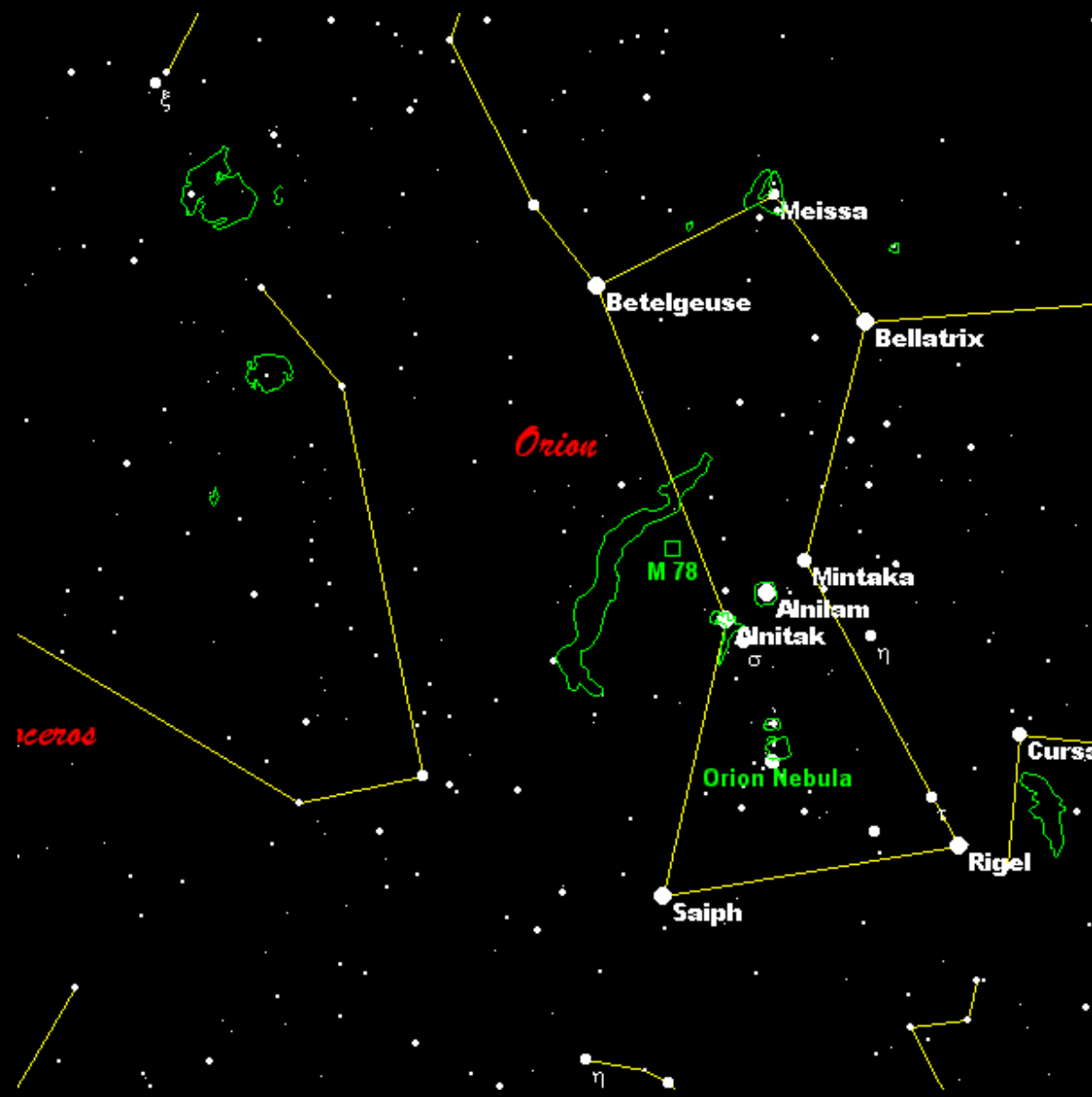


Orione



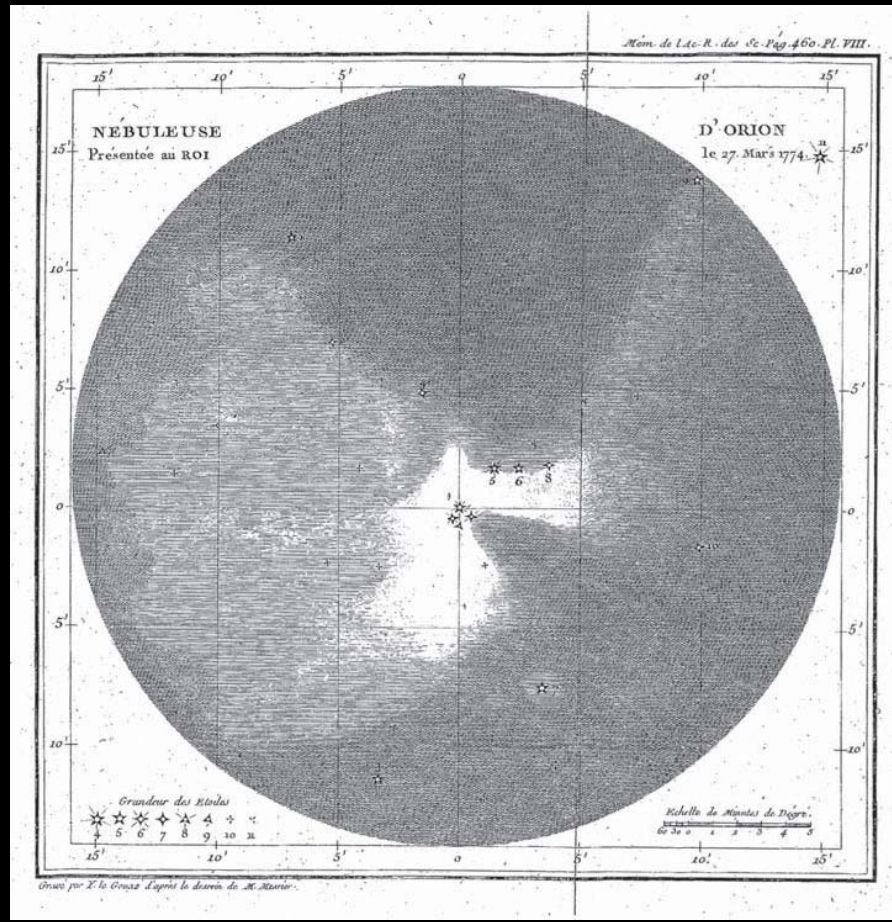
Orione



Nebulosa di Orione

- 1610: de Peiresc riconosce la natura di nebulosa
- 1659: Christiaan Huygens, studio dettagliato

Nebulosa di Orione



Messier

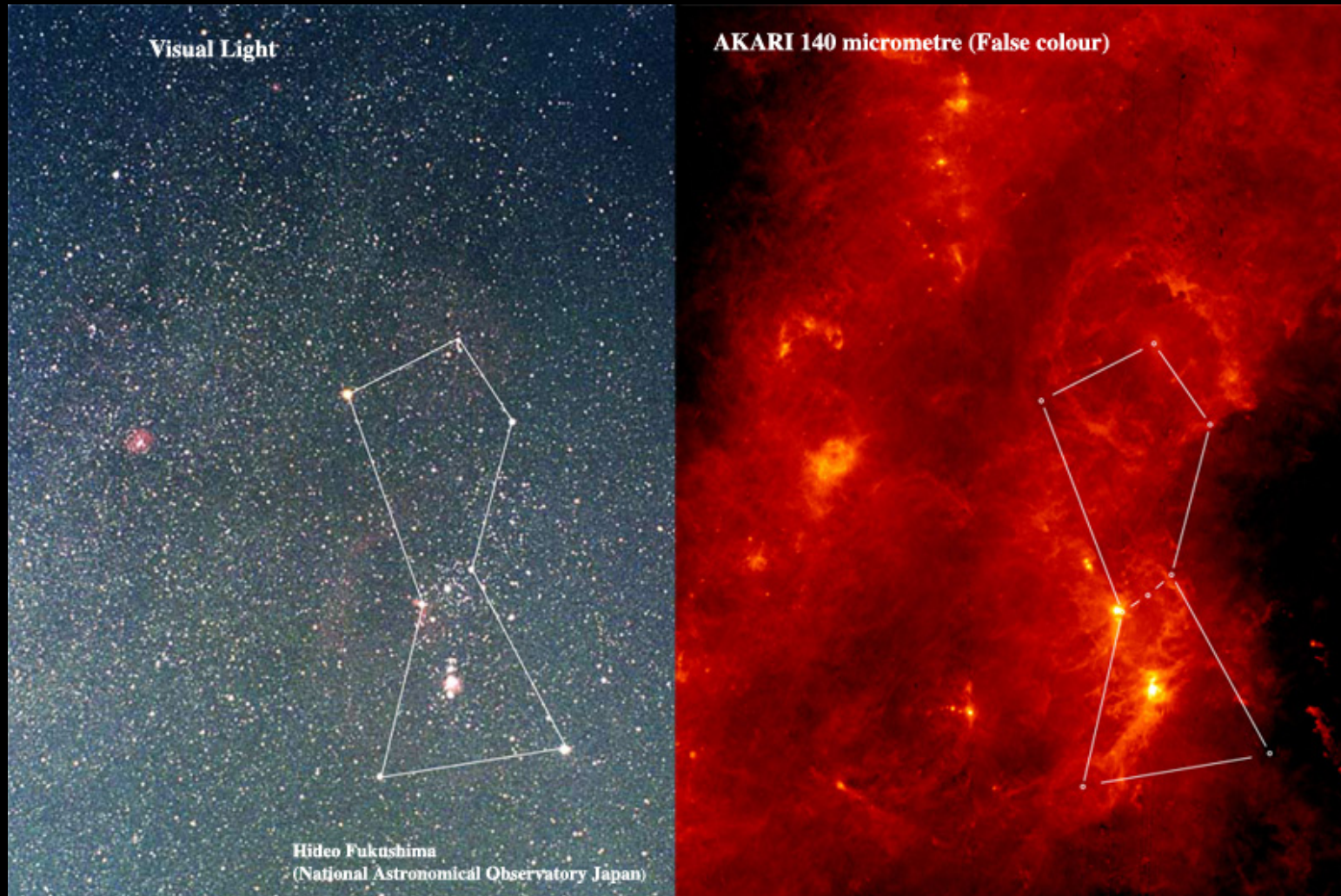
Nebulosa di Orione



Orione



Orione

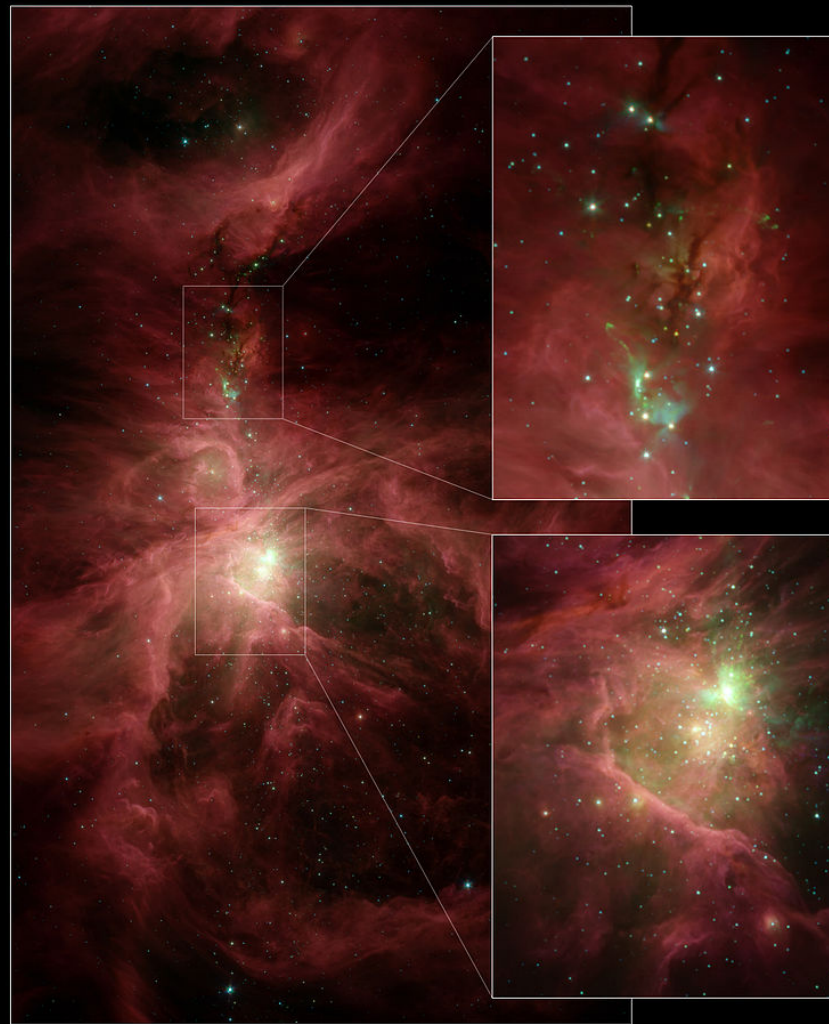


Orione





Nebulosa di Orione



The Great Nebula of Orion (M42)

NASA / JPL-Caltech / S.T. Megeath (University of Toledo, Ohio)

Spitzer Space Telescope • IRAC

ssc2006-16b

Nubi molecolari

- H₂
- decine / centinaia p.c.
- < 1% volume ISM
- Densità medie $10^2\text{-}10^3$ molecole/cm³
- Temperatura 10 / 50 K
(-263/ -223 C)

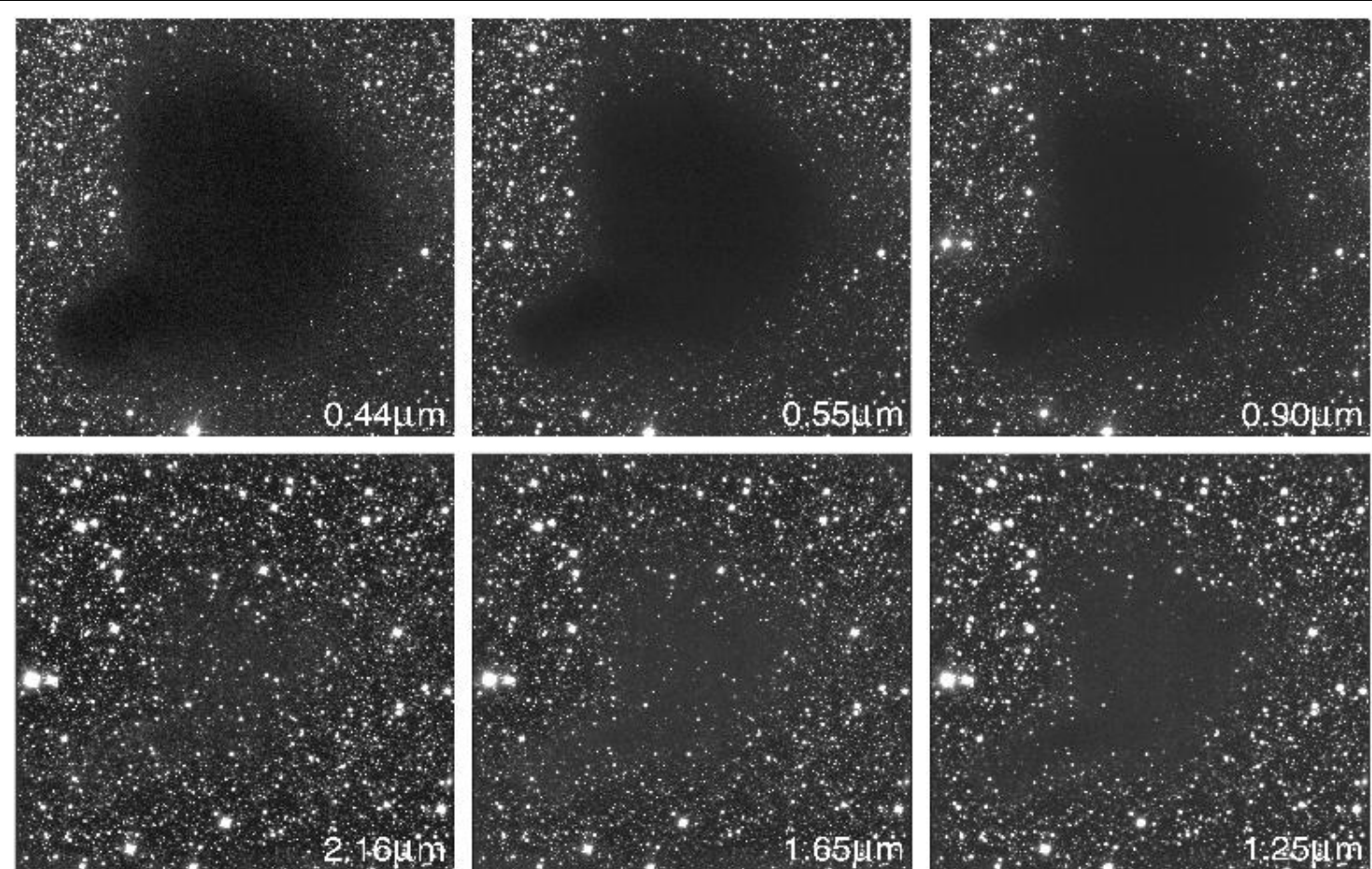


Nubi molecolari

- H_2
- Centinaia di tipi di molecole
- H_2O , NH_3 , $\text{C}_2\text{H}_5\text{OH}$
- Aminoacidi: glicina
 $\text{C}_2\text{H}_5\text{NO}_2$



IC2944

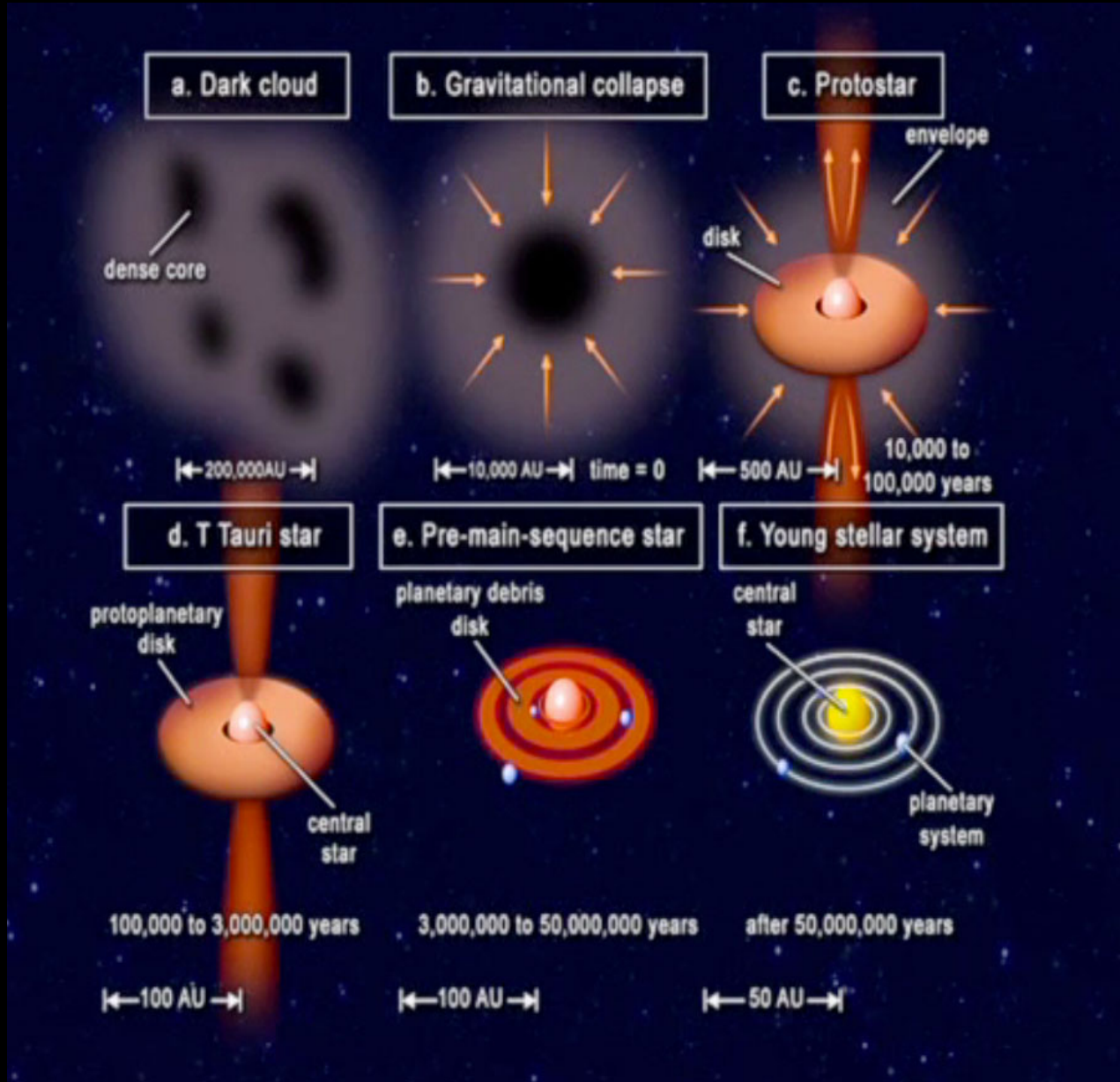


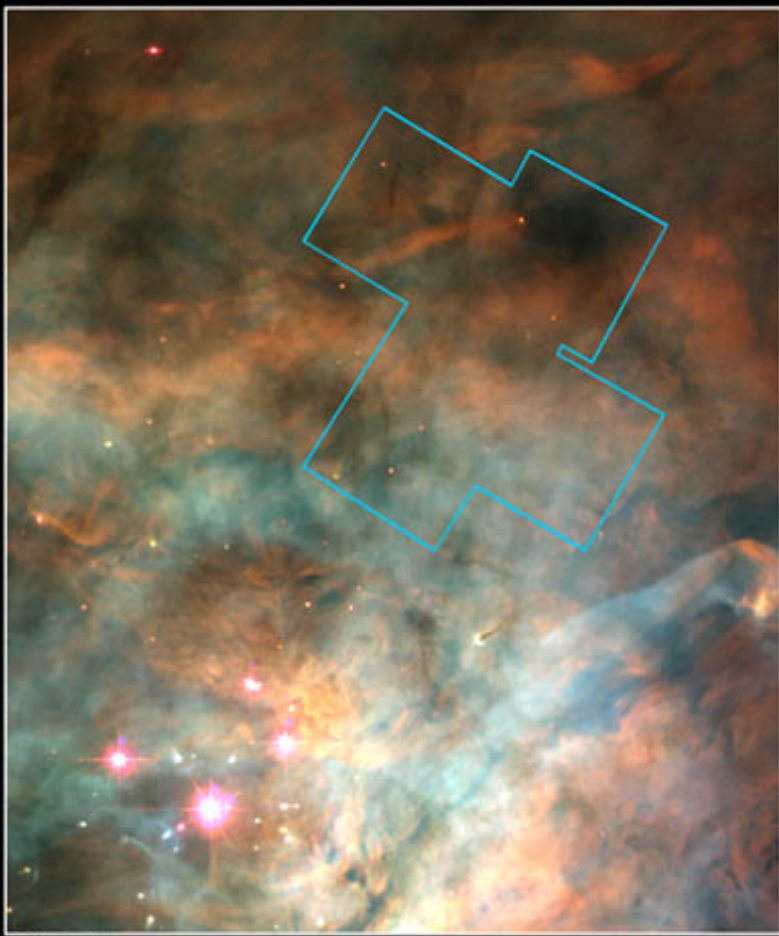
The Dark Cloud B68 at Different Wavelengths (NTT + SOFI)

ESO PR Photo 29b/99 (2 July 1999)

© European Southern Observatory





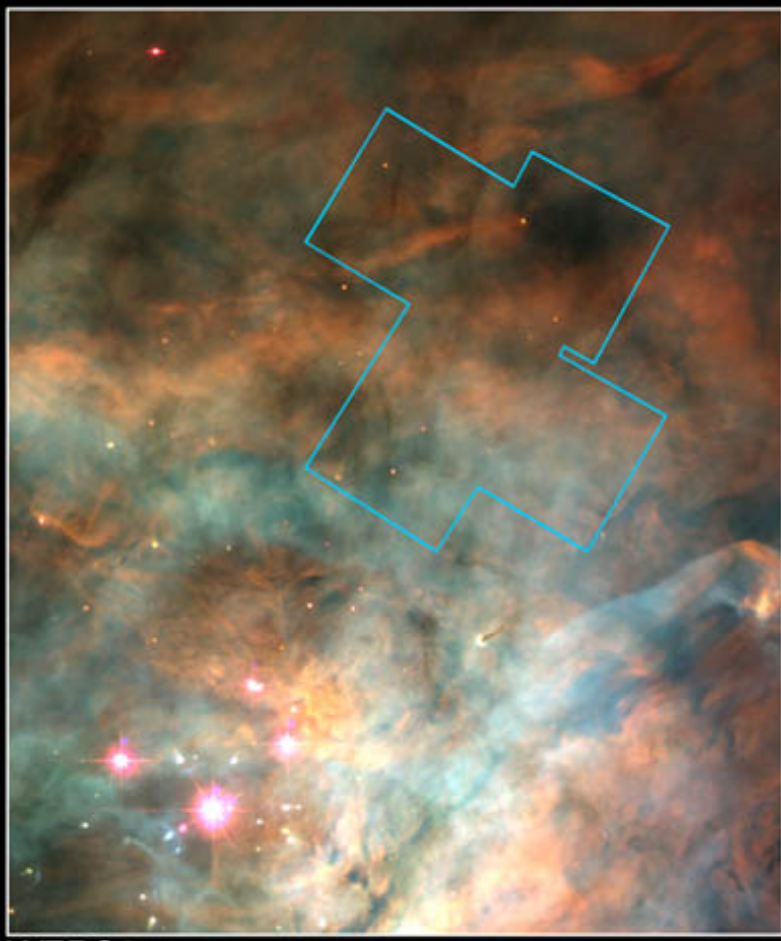


WFPC2

Orion Nebula • OMC-1 Region

PRC97-13 • ST Scl OPO • May 12, 1997

R. Thompson (Univ. Arizona), S. Stolovy (Univ. Arizona), C.R. O'Dell (Rice Univ.) and NASA

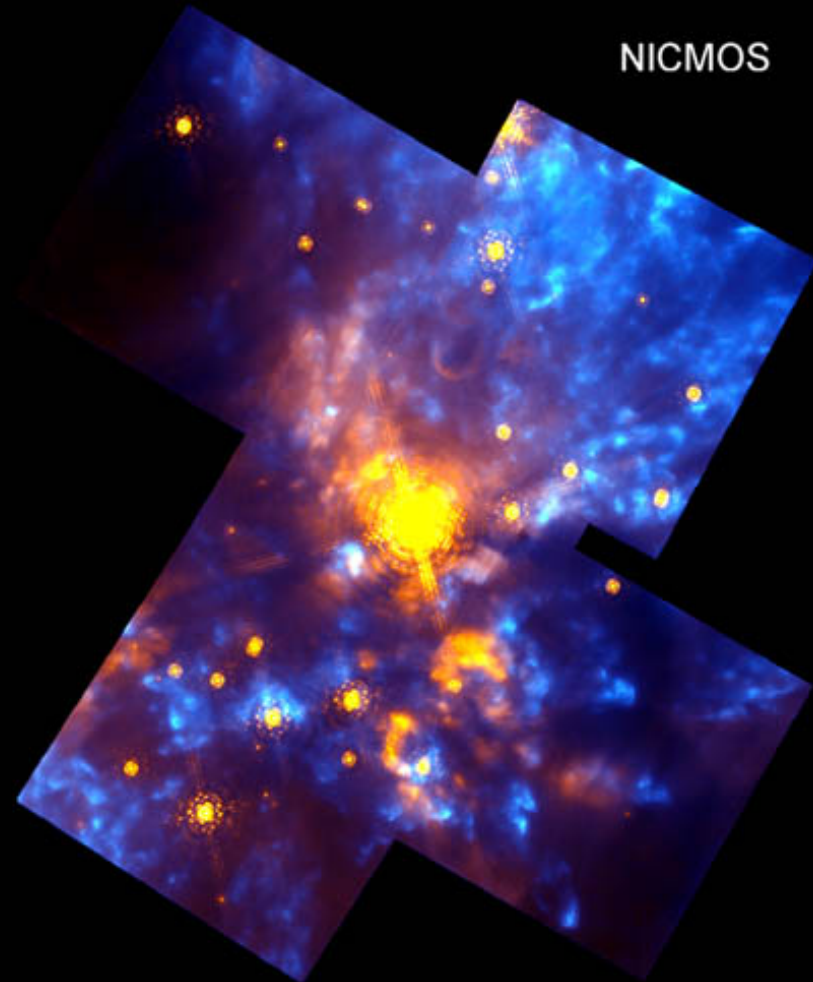


WFPC2

Orion Nebula • OMC-1 Region

PRC97-13 • ST Scl OPO • May 12, 1997

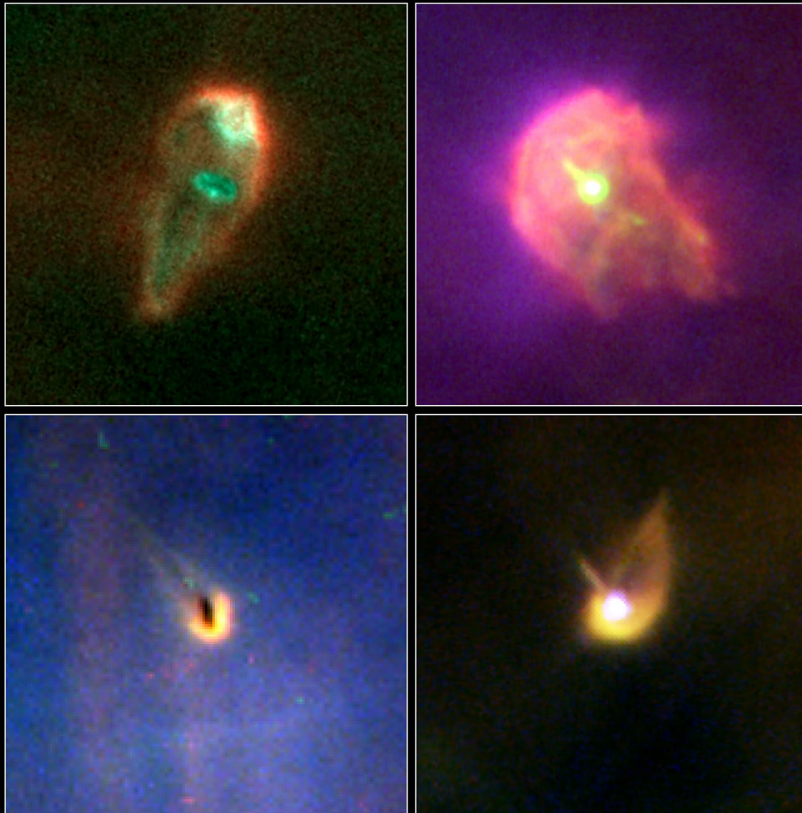
R. Thompson (Univ. Arizona), S. Stolovy (Univ. Arizona), C.R. O'Dell (Rice Univ.) and NASA



Hubble Space Telescope

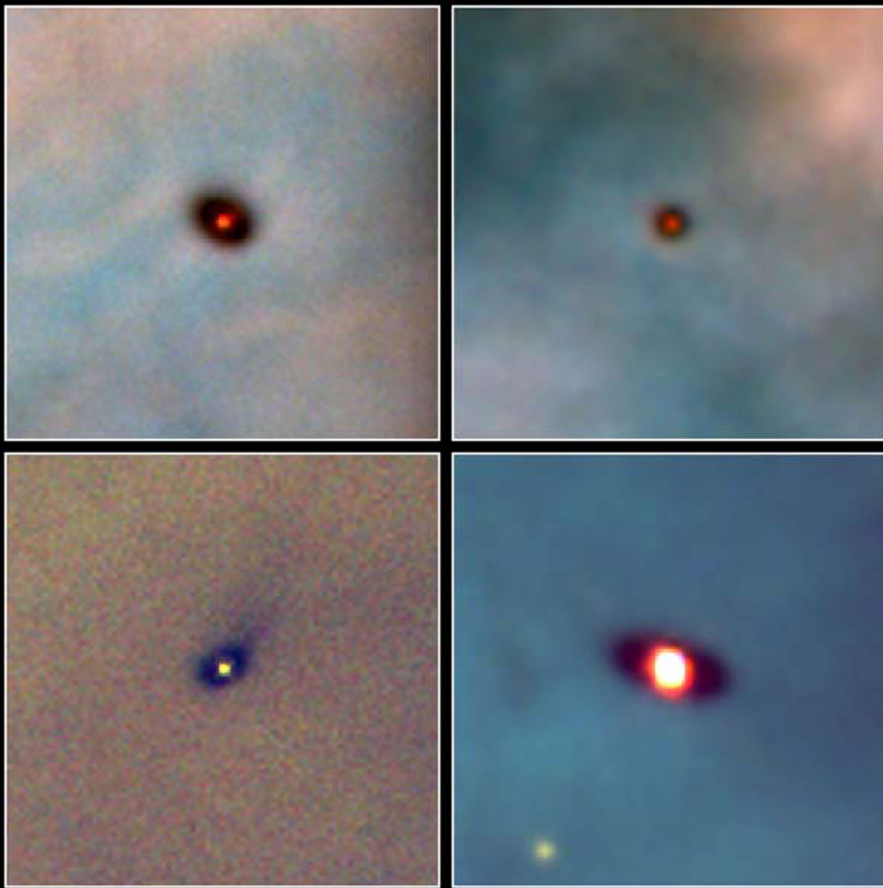


Nebulosa di Orione, HST



Protoplanetary Disks in the Orion Nebula
Hubble Space Telescope • WFPC2

NASA, J. Bally (University of Colorado), H. Throop (SWRI), and C.R. O'Dell (Vanderbilt University)
STScI-PRC01-13



Protoplanetary Disks Orion Nebula

HST • WFPC2

PRC95-45b • ST Scl OPO • November 20, 1995

M. J. McCaughrean (MPIA), C. R. O'Dell (Rice University), NASA

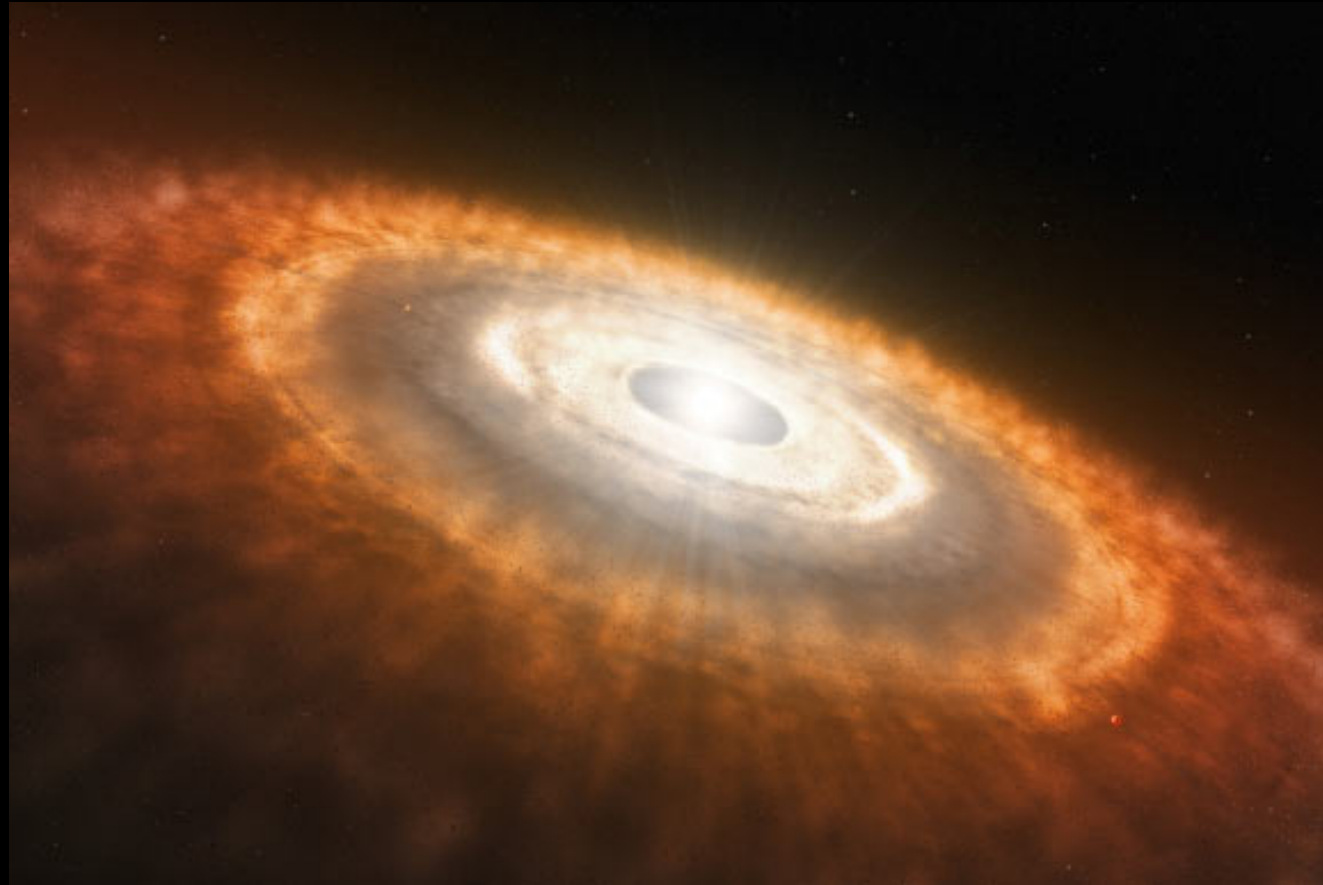


Edge-On Protoplanetary Disk Orion Nebula

PRC95-45c · ST Scl OPO · November 20, 1995

M. J. McCaughrean (MPIA), C. R. O'Dell (Rice University), NASA

HST · WFPC2



Rappresentazione artistica

Disco protoplanetario

- Disco di grani di polvere e di ghiaccio di H₂O, NH₃ e CO

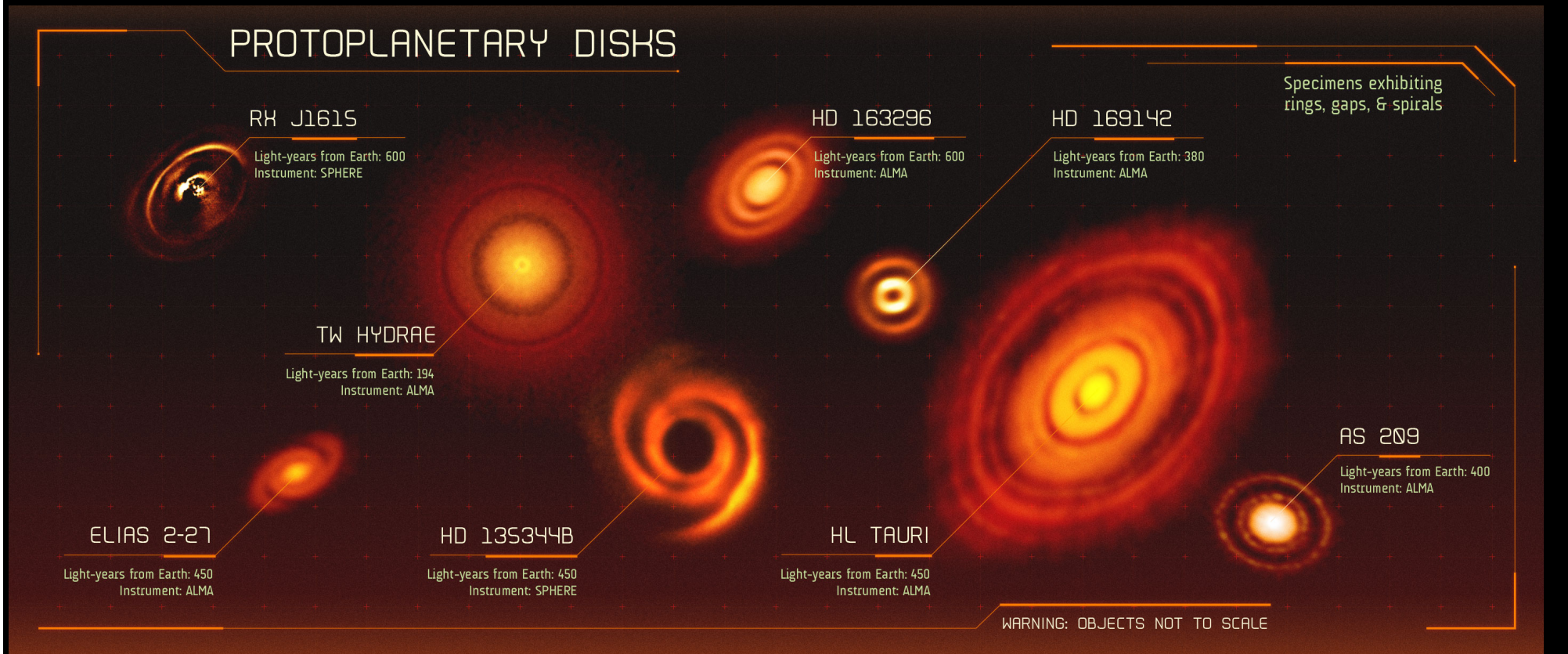


Disco protoplanetario HL Tauri

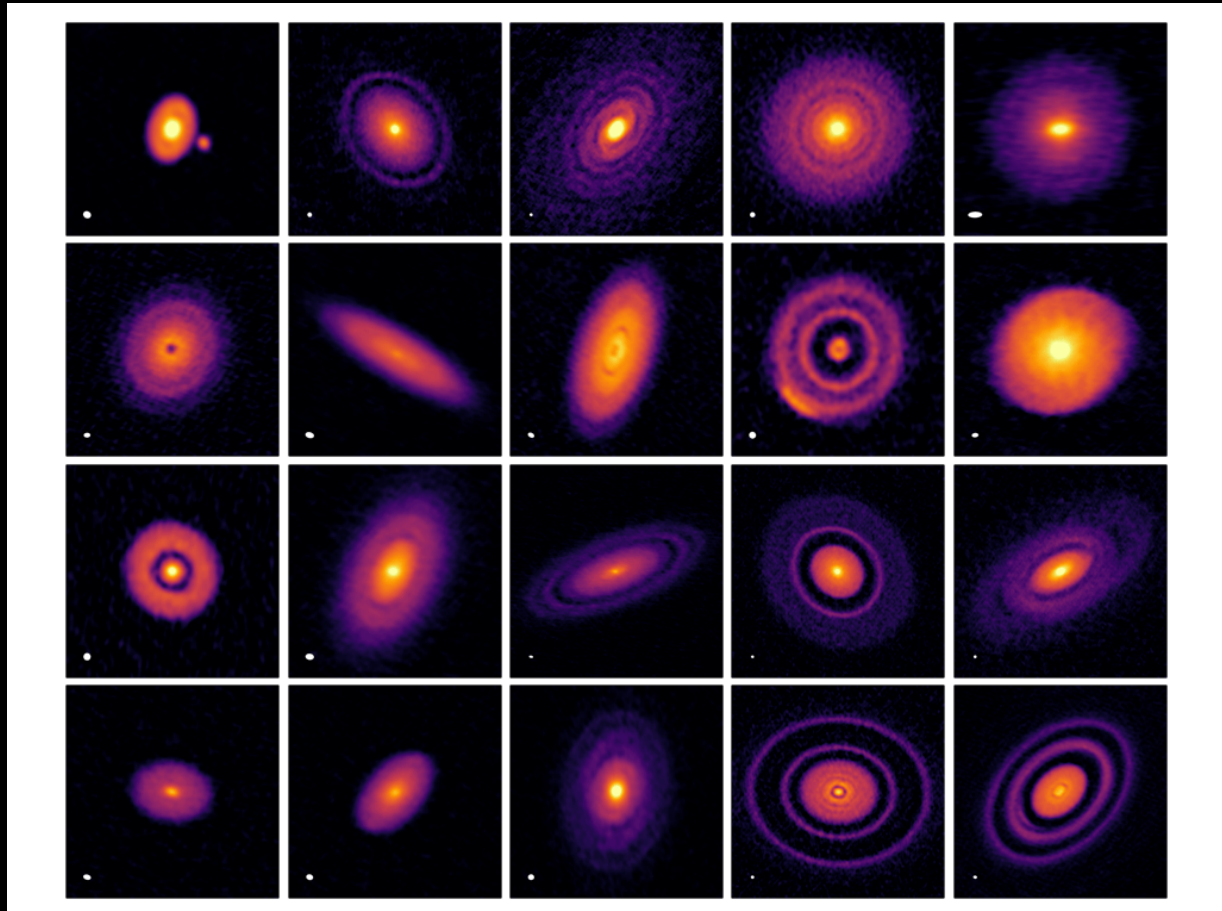


ALMA / Osservazioni Radio

Disco protoplanetario

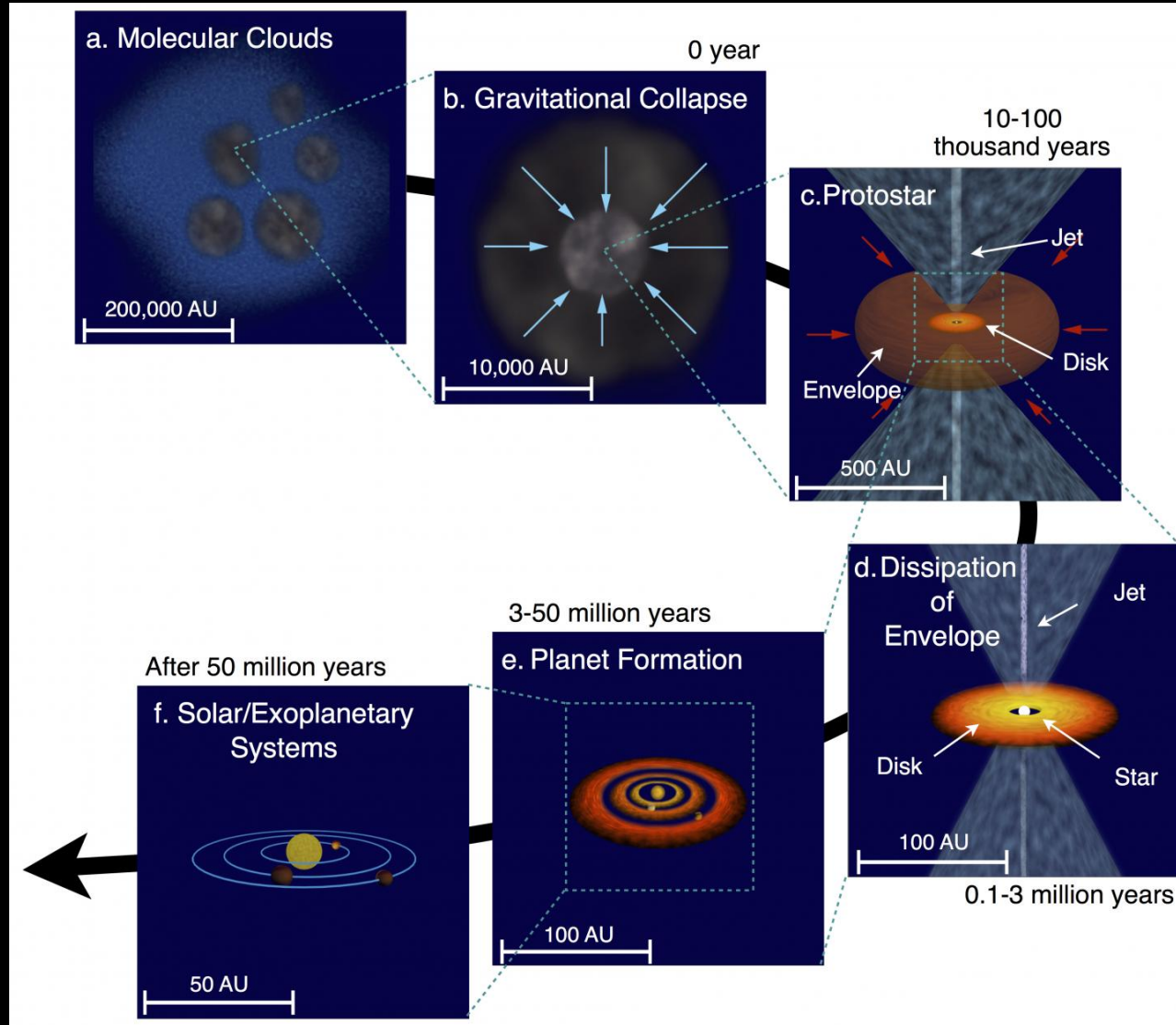


Disco protoplanetario

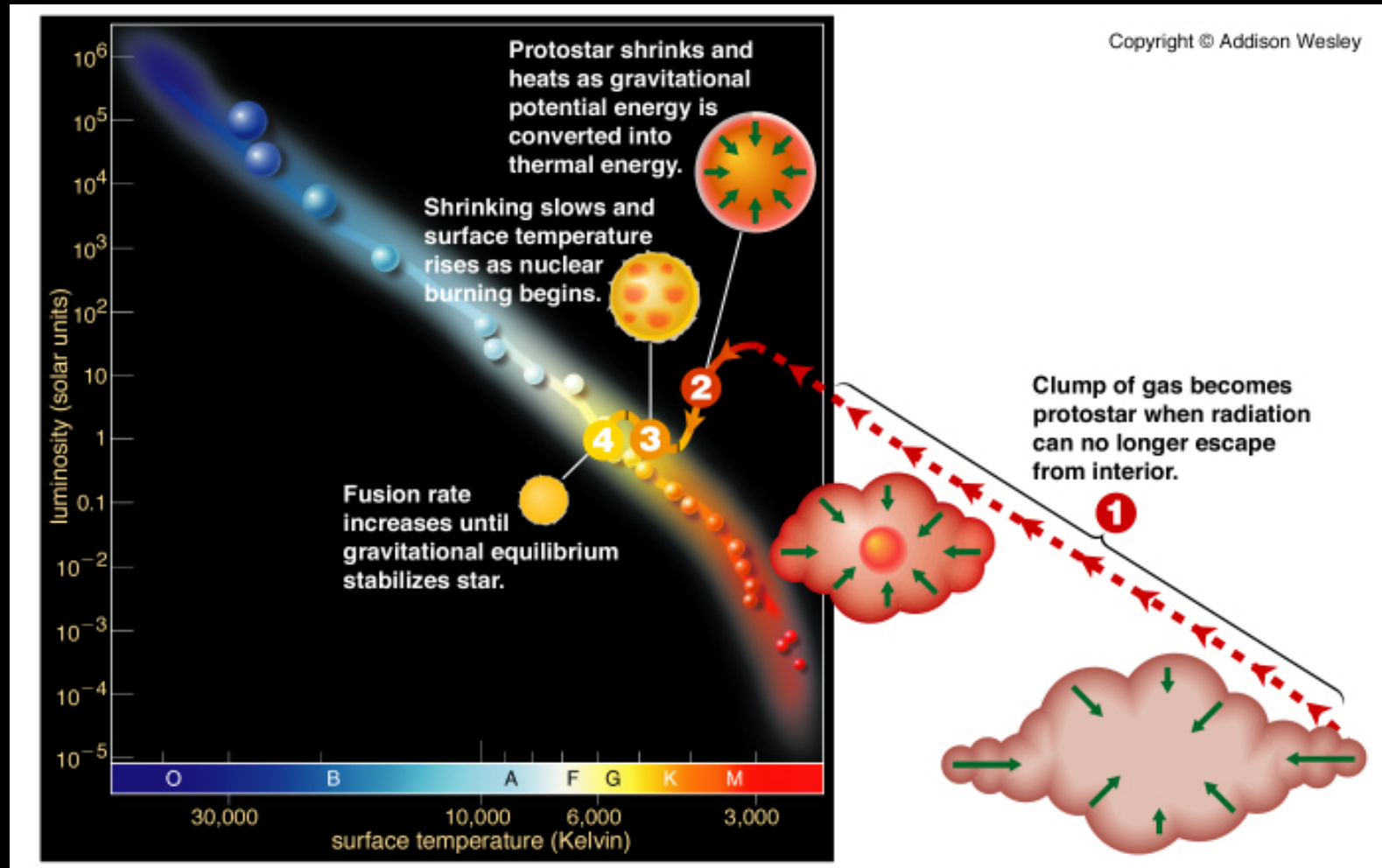


ALMA / DSHARP Osservazioni Radio

Nascita delle stelle e dei pianeti



Stelle di massa piccola e intermedia



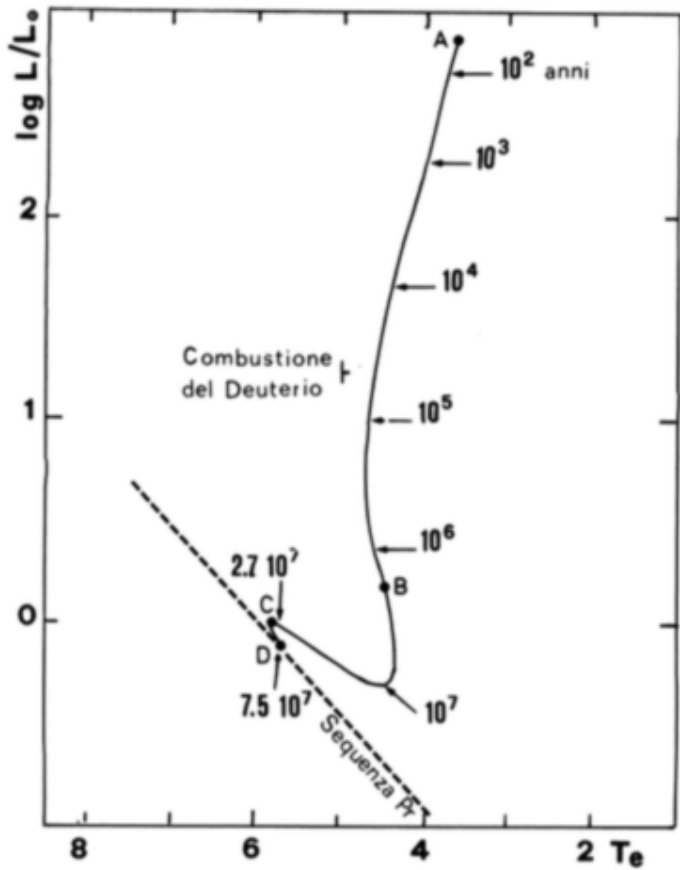
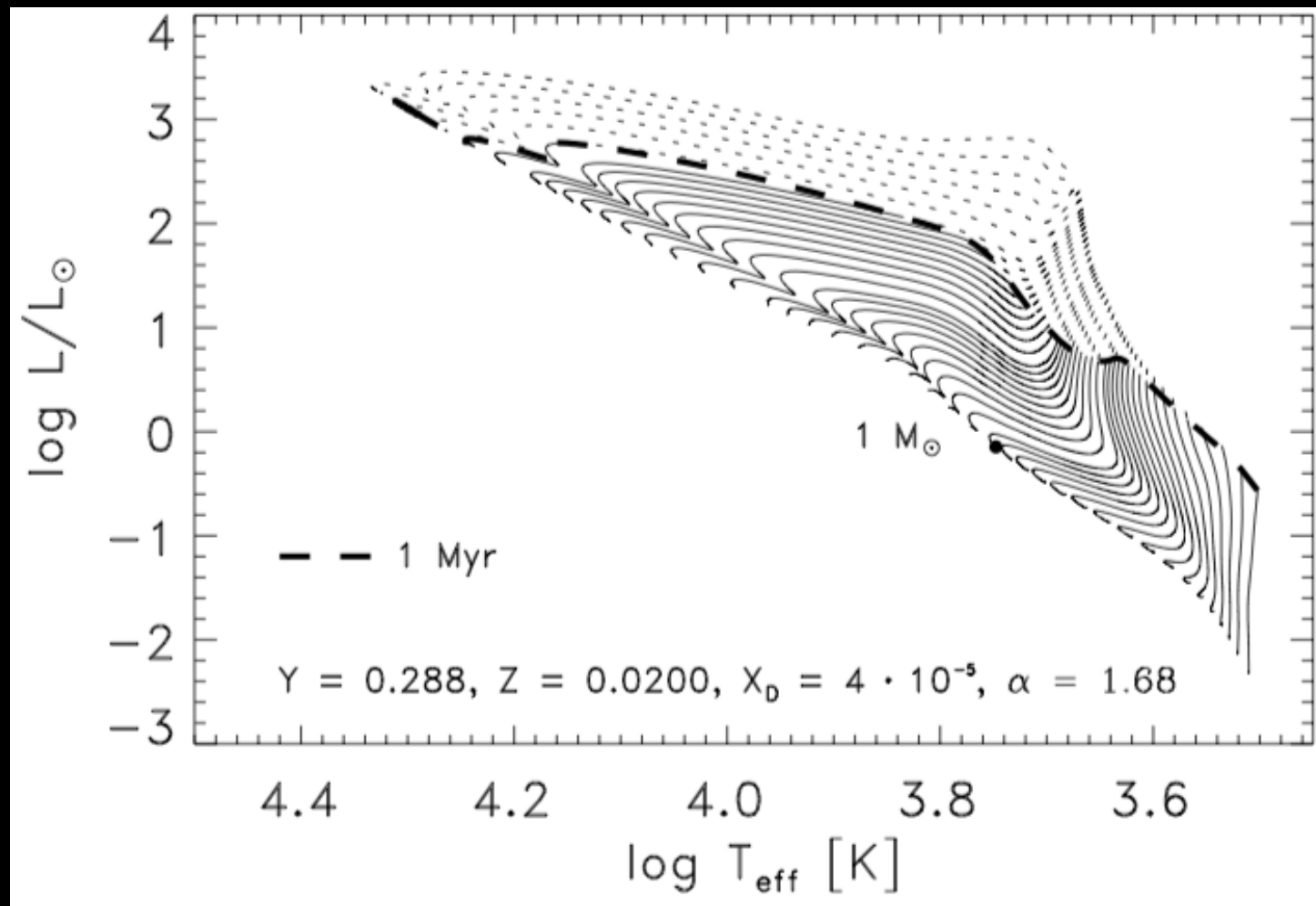


Fig. 5.2. Evoluzione di presequenza per una stella di $1 M_{\odot}$ e composizione chimica solare. A= modello iniziale; B= ultimo modello completamente convettivo; C= primo modello sorretto nuclearmente; D= Sequenza principale di Età Zero (ZAMS). Lungo la traccia sono riportati i tempi di evoluzione ed i modelli in cui si raggiungono le temperature centrali per la combustione del deuterio.

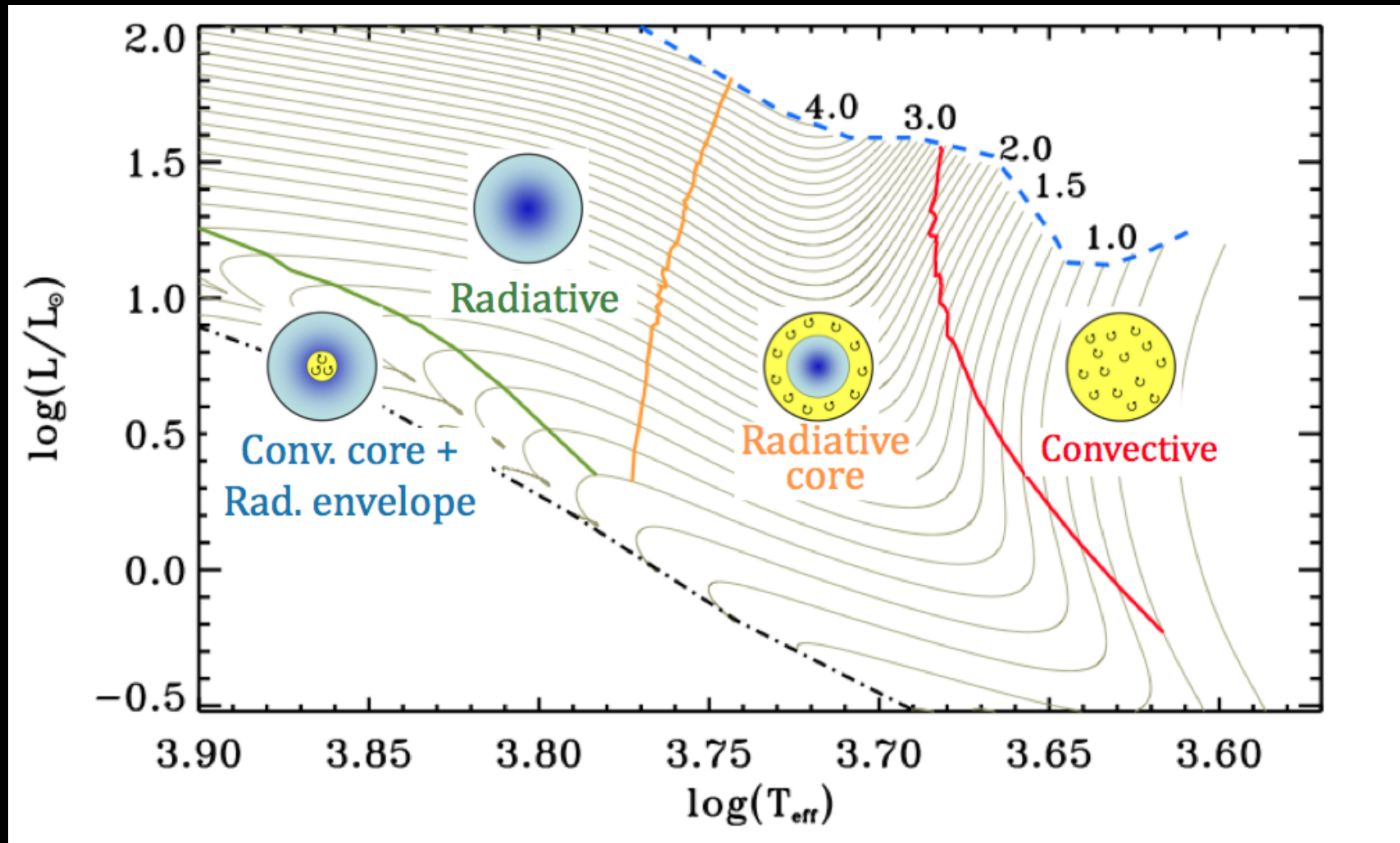
Castellani

Pre-sequenza principale

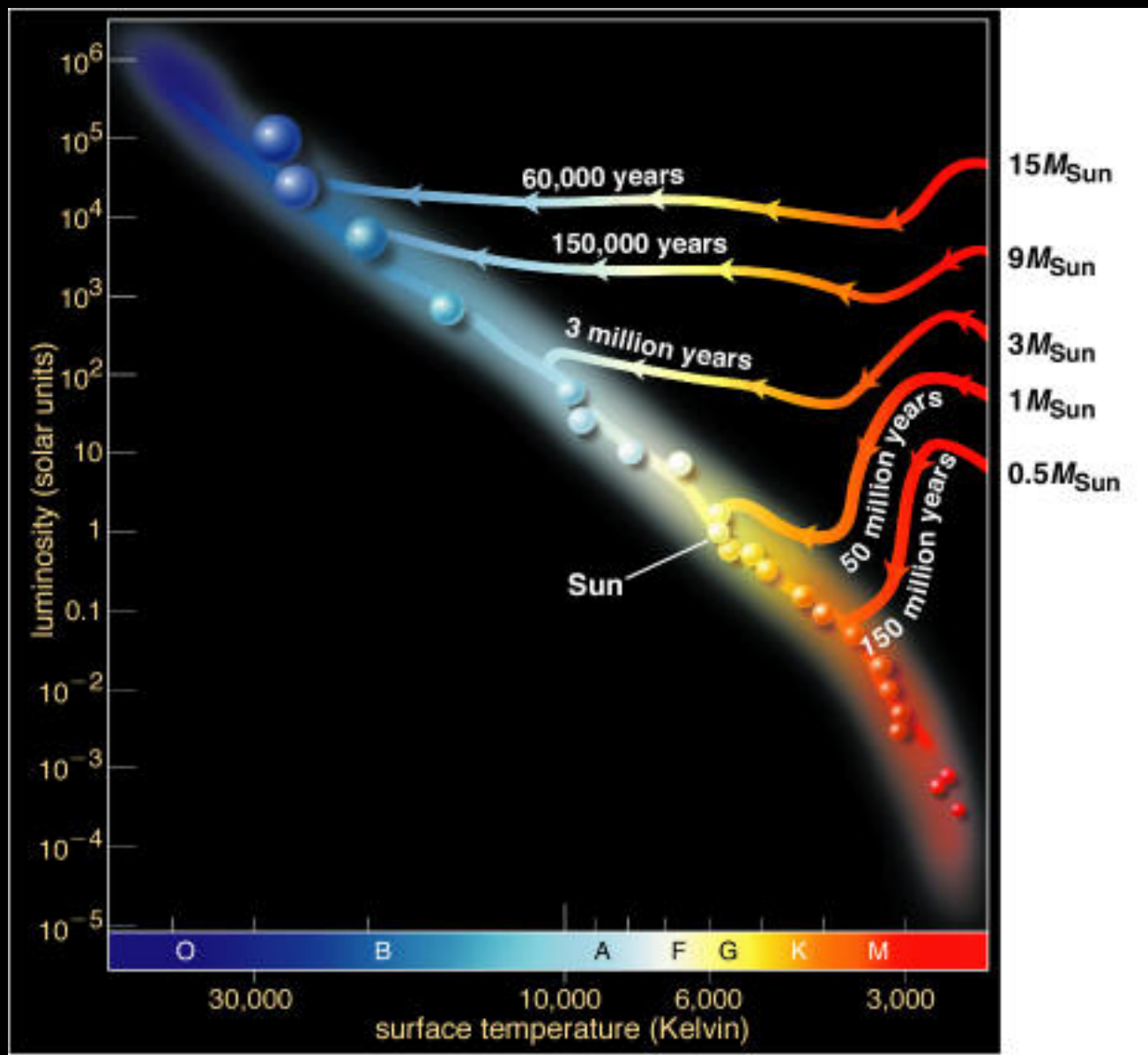


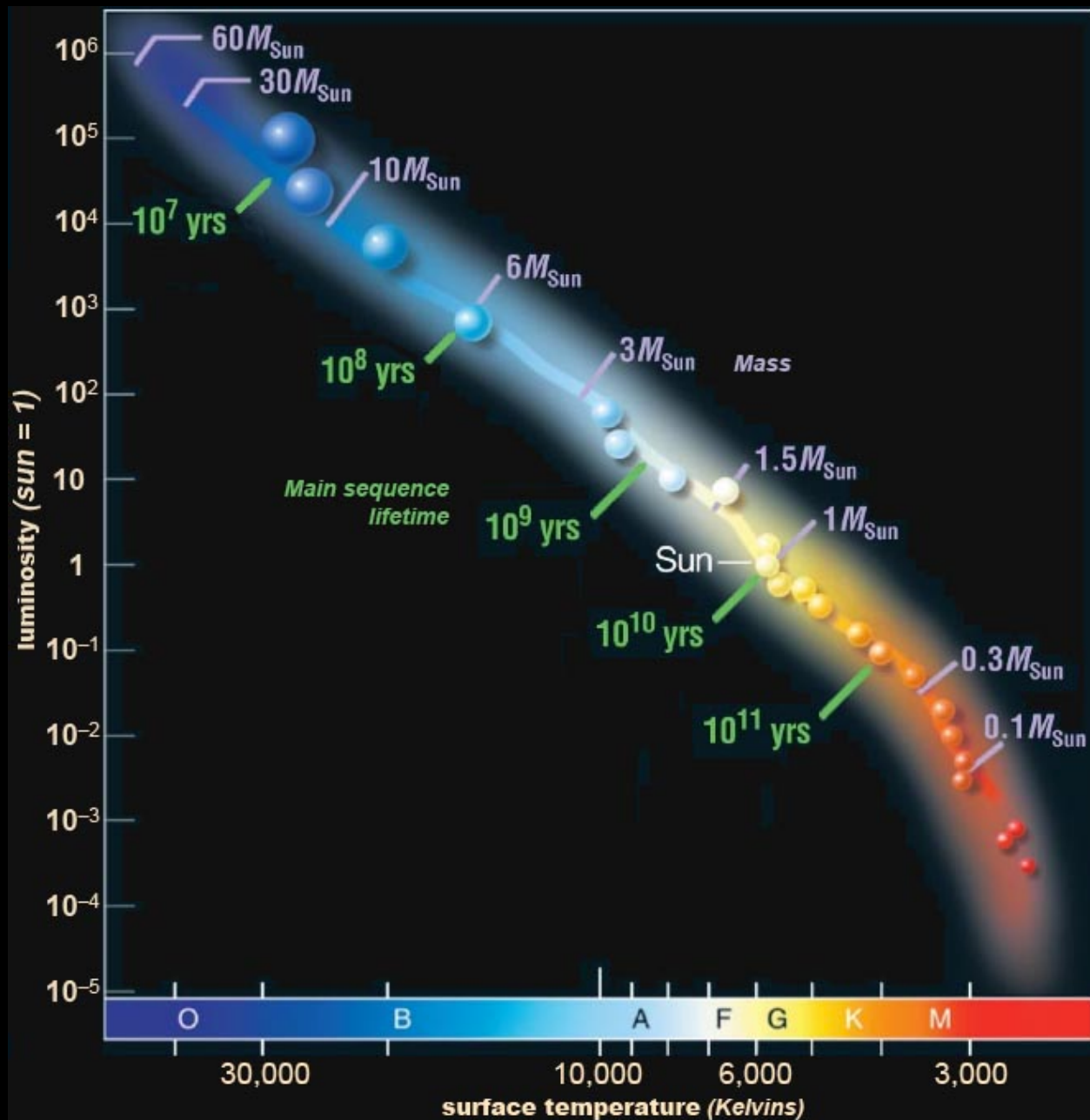
Tognelli, Prada Moroni, Degl’Innocenti 2011

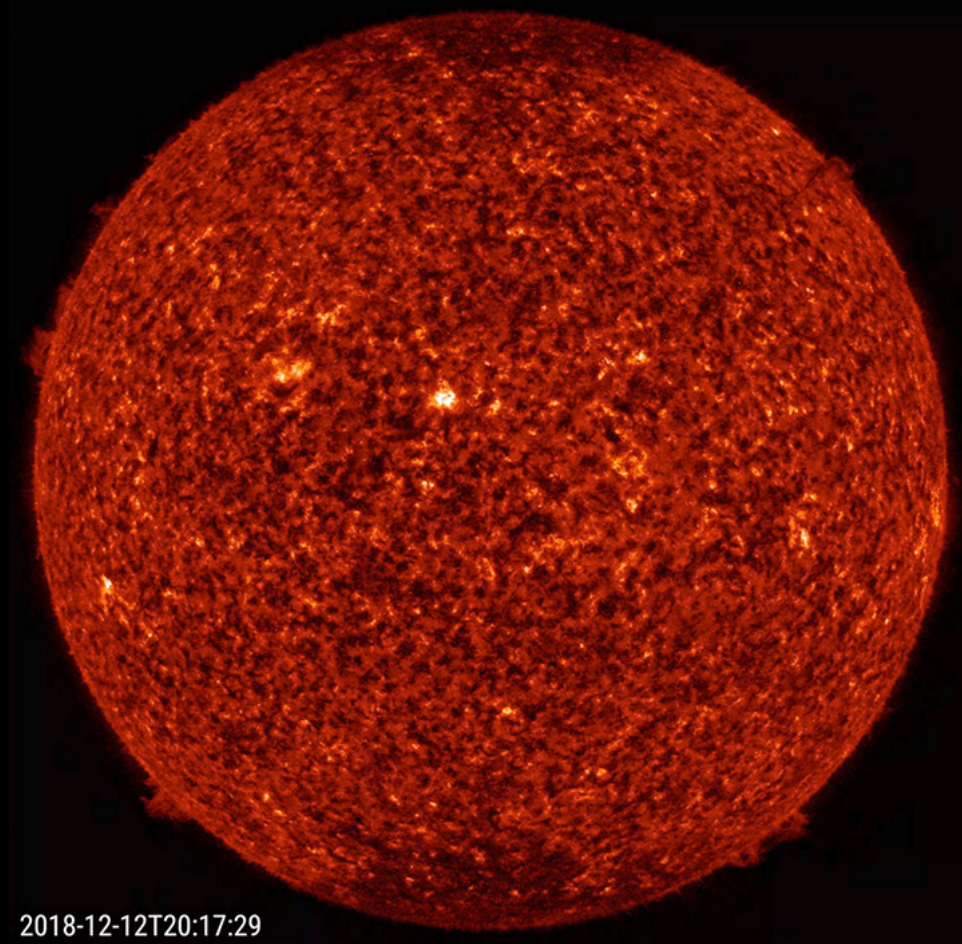
Pre-sequenza principale



Hussain & Alecian 2014



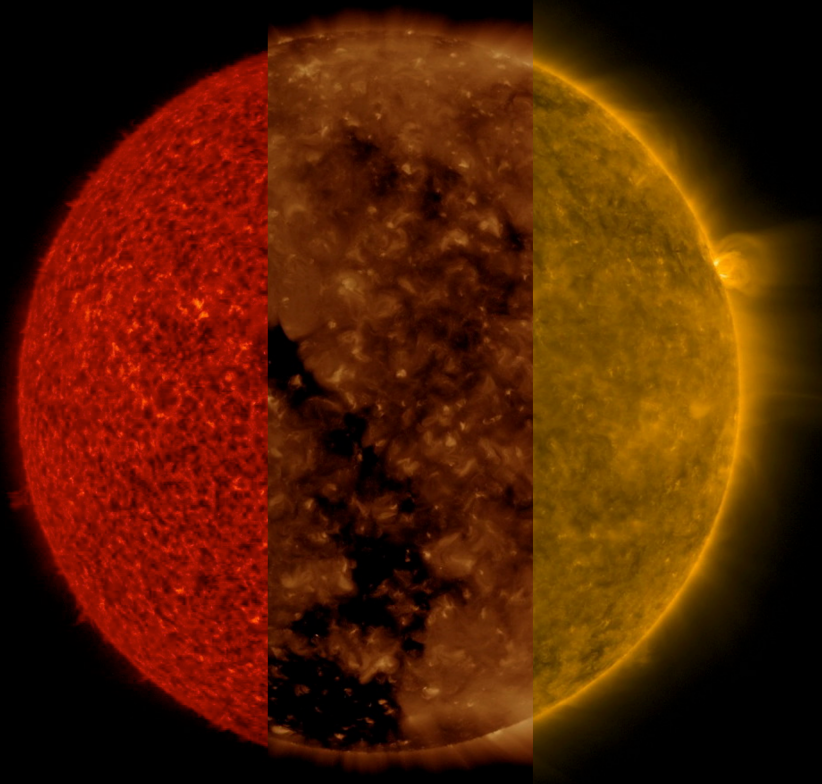




2018-12-12T20:17:29

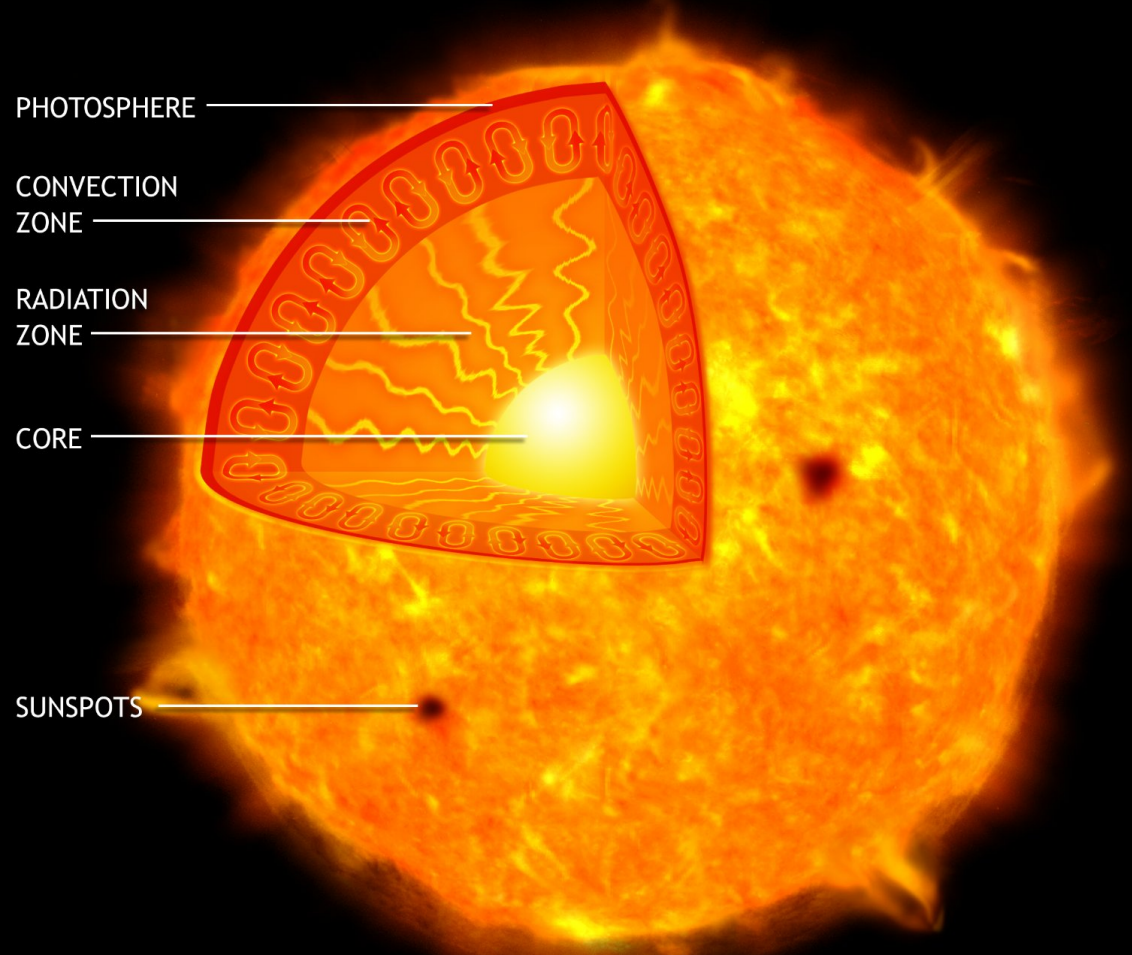
The sun sported four smallish prominences along its edge at about the same time (Dec. 12-14, 2018). They were at the positions of 2 o'clock, 5 o'clock, 7 o'clock, and 10 o'clock. The largest and most active of the prominences was at the 7 o'clock point. Prominences are clouds of charged particles suspended above the sun by magnetic forces. These were observed in a wavelength of extreme ultraviolet light. The video clip covers almost two days' of activity: it consists of 335 frames being shown at 20 frames per second. Credit: Solar Dynamics Observatory, NASA.

Search Tag(s): *aia, 304, prominence*



We ran together three sequences of the sun taken in three different extreme ultraviolet wavelengths to better illustrate how different features that appear in one sequence are difficult if not impossible to see in the others (Mar. 20-21, 2018). In the red sequence (304 Angstroms), we can see very small spicules and some small prominences at the sun's edge, which are not easy to see in the other two sequences. In the second clip (193 Angstroms), we can readily observe the large and dark coronal hole, though it is difficult to make out in the others. In the third clip (171 wavelengths), we can see strands of plasma waving above the surface, especially above the one small, but bright, active region near the right edge. And these are just three of the 10 extreme ultraviolet wavelengths in which SDO images the sun every 12 seconds every day. That's a lot of data and a lot of science. Credit: Solar Dynamics Observatory, NASA.

Search Tag(s): *aia, 193, 171, 304, prominence*



1. Large κ and low T
(outer layers of cool stars)
2. Large $L_r/4\pi r^2$
(cores of massive stars)

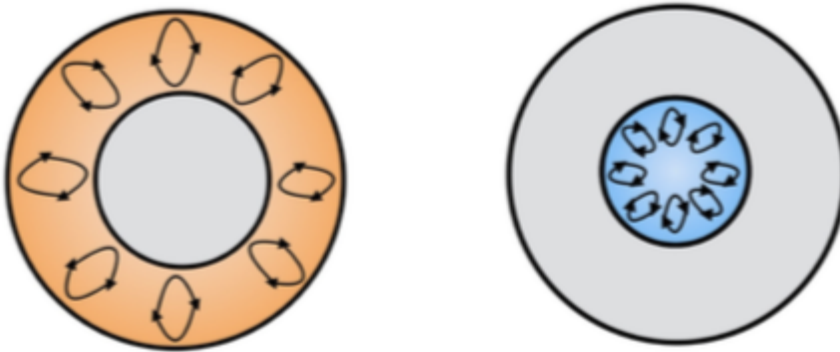


Figure 7.5. Schematic drawing of envelope convection in cool stars and core convection in massive stars. The gray regions are in radiative equilibrium.

Lamers

Sequenza Principale

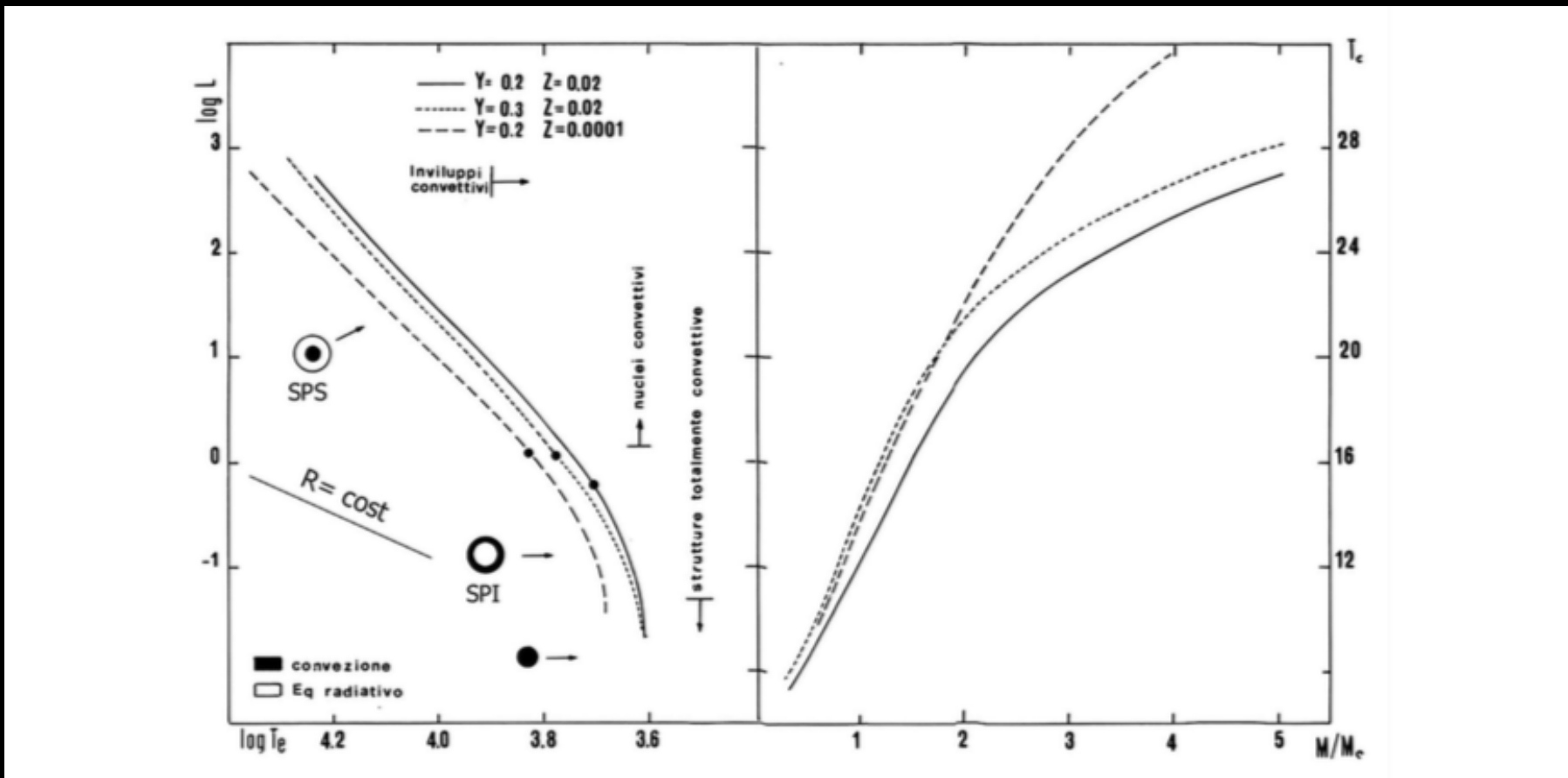


Fig. 5.8. A sinistra: distribuzione nel diagramma HR di strutture di sequenza principale per le indicate composizioni chimiche. Il punto lungo le sequenze segnala la collocazione dei modelli di $1 M_\odot$. E' indicata una retta $R = \text{cost}$ ($\log L \propto 4 \log T_e$). A destra: andamento delle temperature centrali (in milioni di gradi) al variare della massa negli stessi modelli.

Castellani

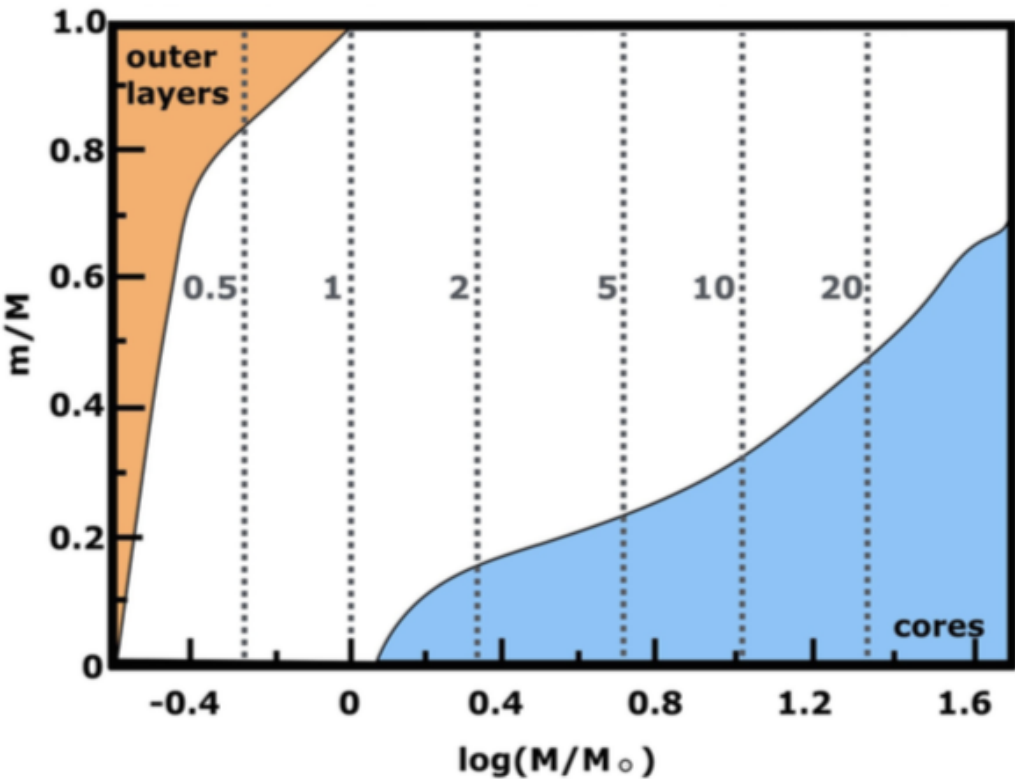
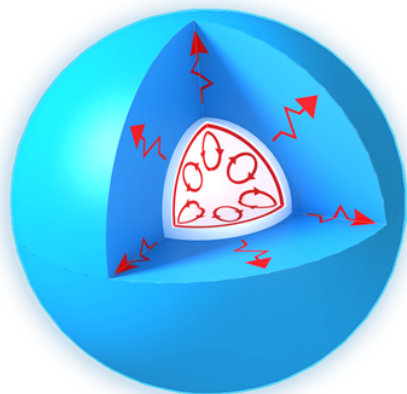


Figure 7.6. Occurrence of convection in stars at the beginning of the core H-fusion phase (ZAMS). The mass of convective envelopes (orange) and convective cores (blue) is expressed as a fraction of the stellar mass, from $m/M = 0$ in the core to $m/M = 1$ at the surface. The vertical lines indicate the stellar mass. (Reproduced from Kippenhahn & Weigert 1990. © Springer-Verlag Berlin Heidelberg 2012.)

Lamers

Heat Transfer of Stars

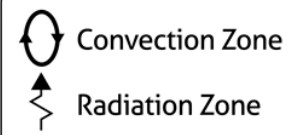
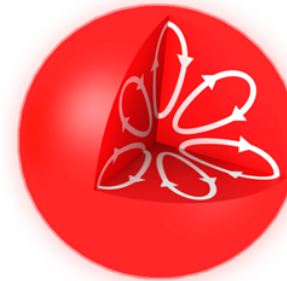
> 1.5 solar masses



0.5 - 1.5 solar masses



< 0.5 solar masses



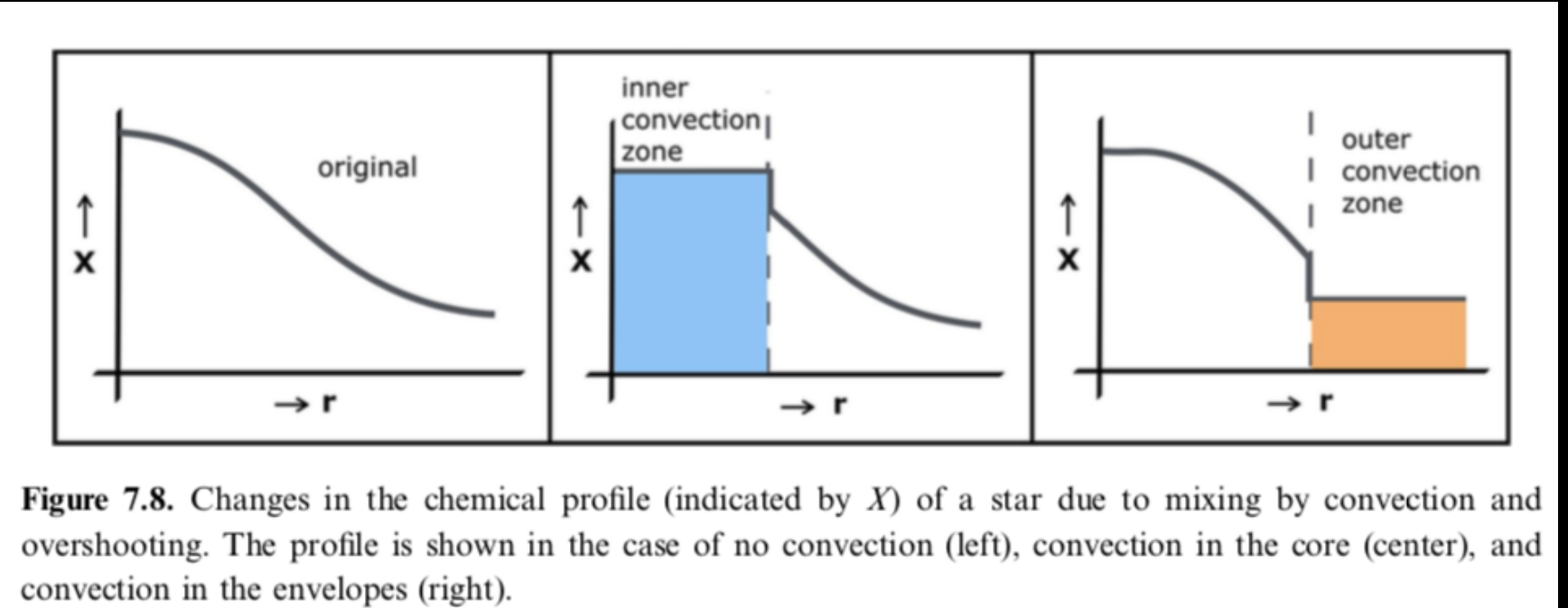


Figure 7.8. Changes in the chemical profile (indicated by X) of a star due to mixing by convection and overshooting. The profile is shown in the case of no convection (left), convection in the core (center), and convection in the envelopes (right).

Lamers

Main Sequence of very low-mass stars

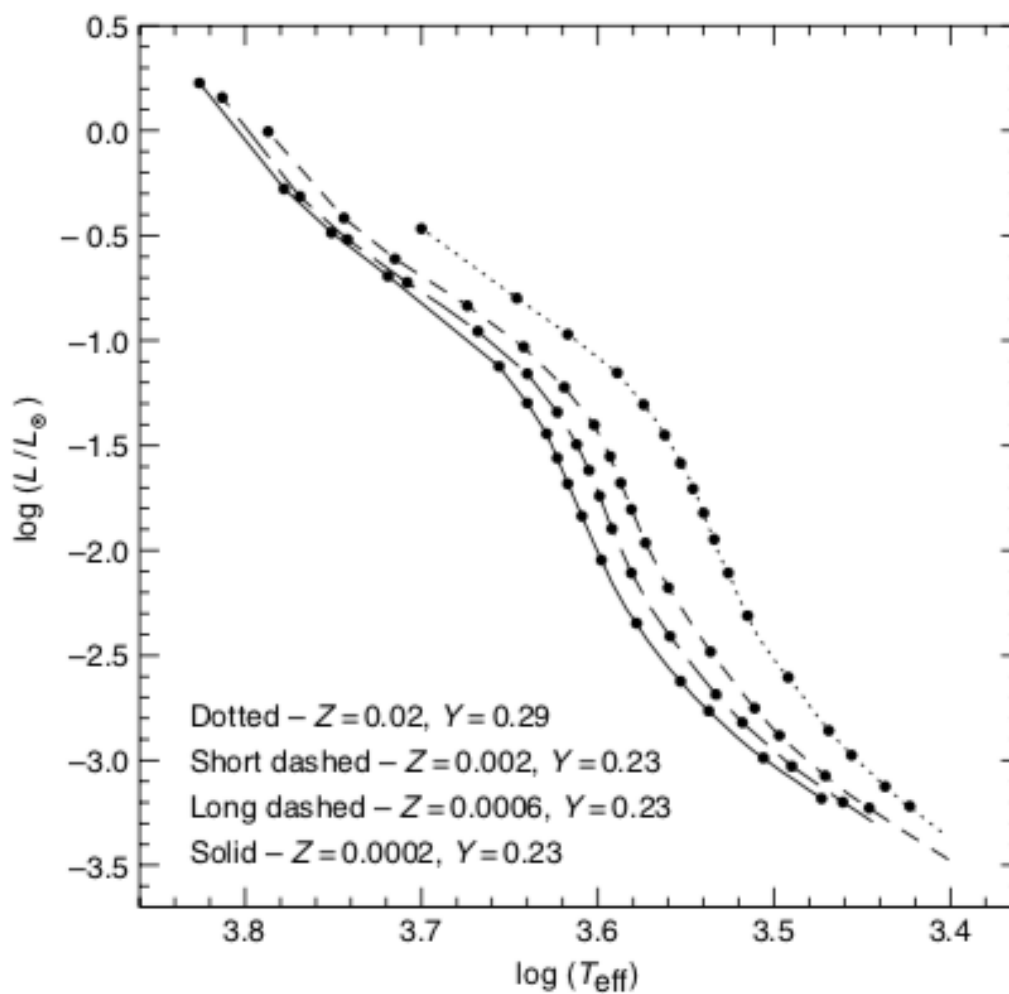


Figure 5.10 The MS location of very low-mass stars with different initial chemical compositions at an age of 10 Gyrs. The solid dots along each sequence mark the location of the following masses (from top to bottom): $M/M_{\odot} = 0.80, 0.70, 0.65, 0.60, 0.50, 0.45, 0.40, 0.35, 0.30, 0.25, 0.20, 0.15, 0.12, 0.11, 0.10, 0.095$

$$L \propto M^3$$

Due to the several approximations made in this sketchy derivation, one has to expect that the relation $L \propto M^3$ is only roughly followed by ‘real’ stars. Empirical data for stars of approximately solar chemical composition provide $L \propto M^{3.6}$ for masses between ~ 2 and $20M_{\odot}$, $L \propto M^{4.5}$ in the range between ~ 2 and $0.5M_{\odot}$, and $L \propto M^{2.6}$ in the range between ~ 0.5 and $0.2M_{\odot}$. Figure 5.11 shows a theoretical mass-luminosity relation for ZAMS stars in the mass range $0.1M_{\odot}–10M_{\odot}$ provided by detailed evolutionary computations, that displays trends with mass roughly consistent with the observations.

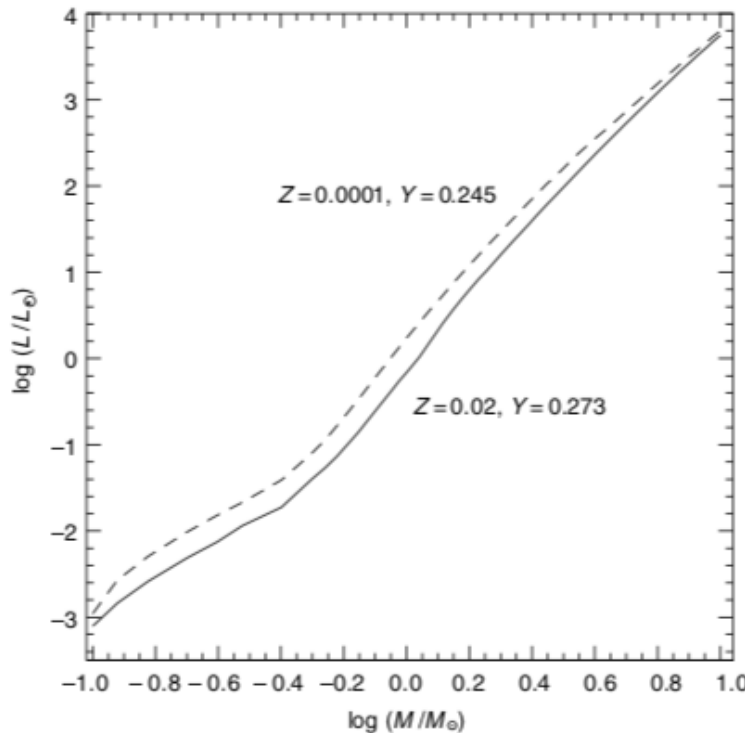


Figure 5.11 The mass-luminosity relation for ZAMS stars in the mass interval $0.1M_{\odot}–10M_{\odot}$, for two initial chemical compositions

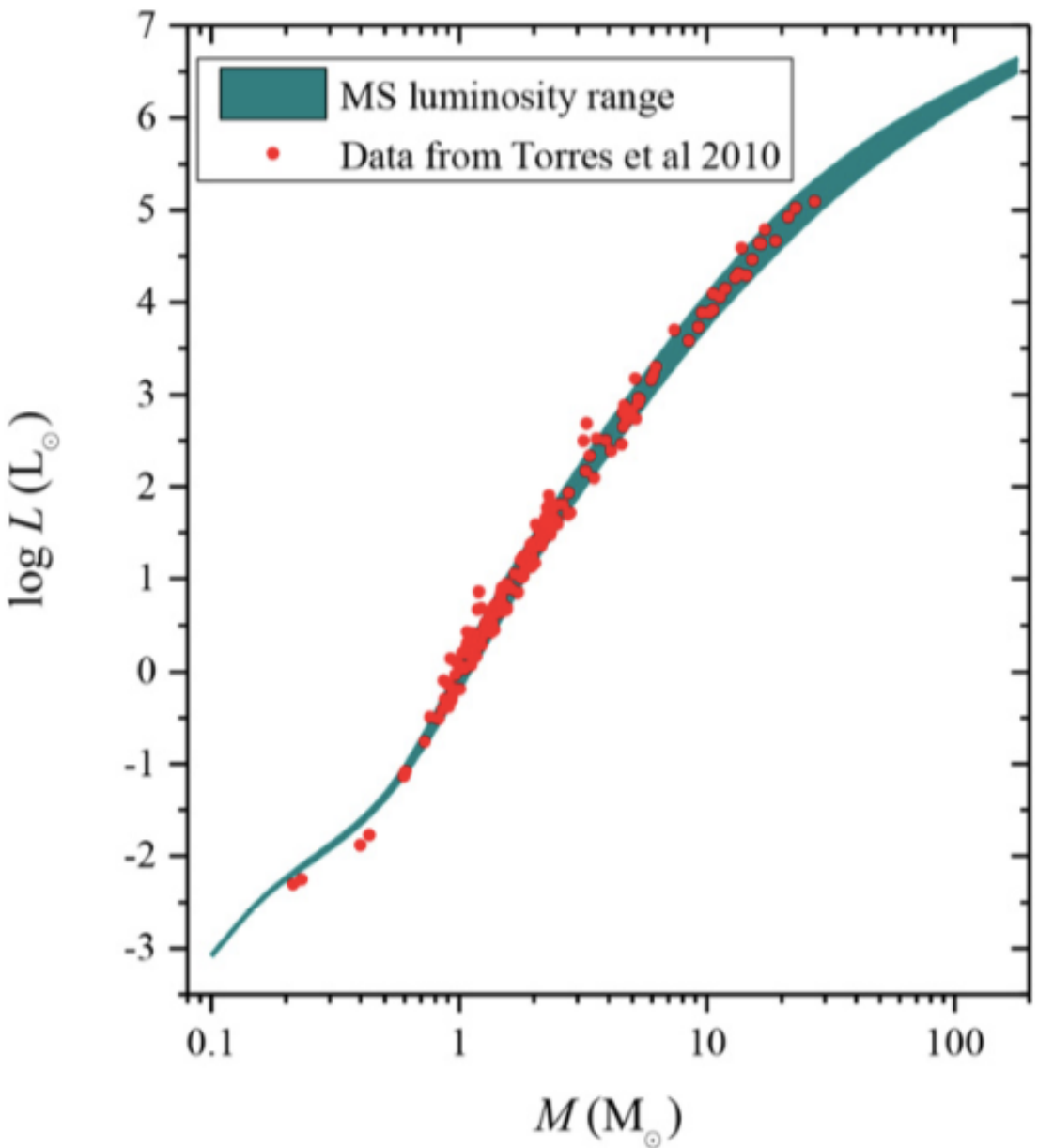


Figure 14.4. MS luminosity range for models of solar composition.

McDonald

Turn off

126

THE HYDROGEN BURNING PHASE

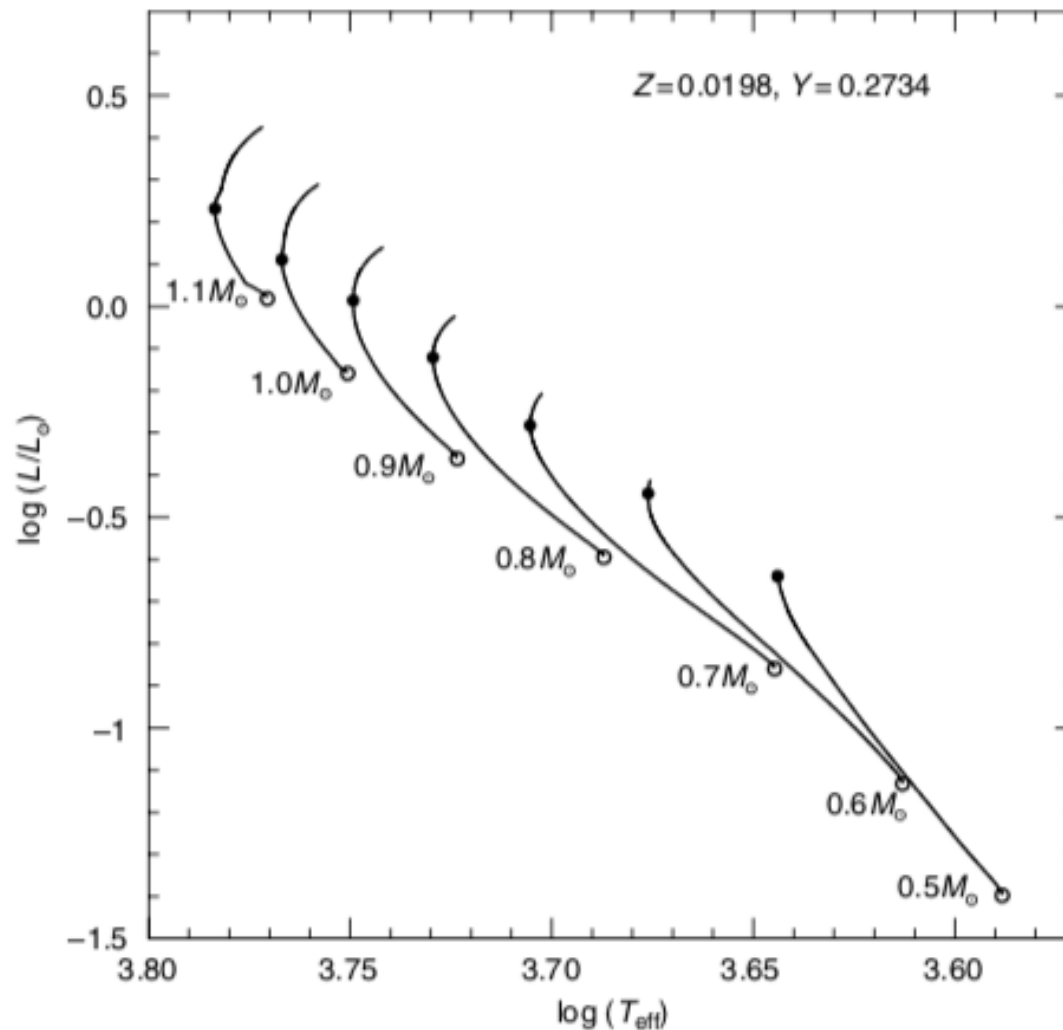


Figure 5.3 The HRD for low-mass stars of different mass during the core H-burning phase. The solid dot marks the location of the turn off along each track

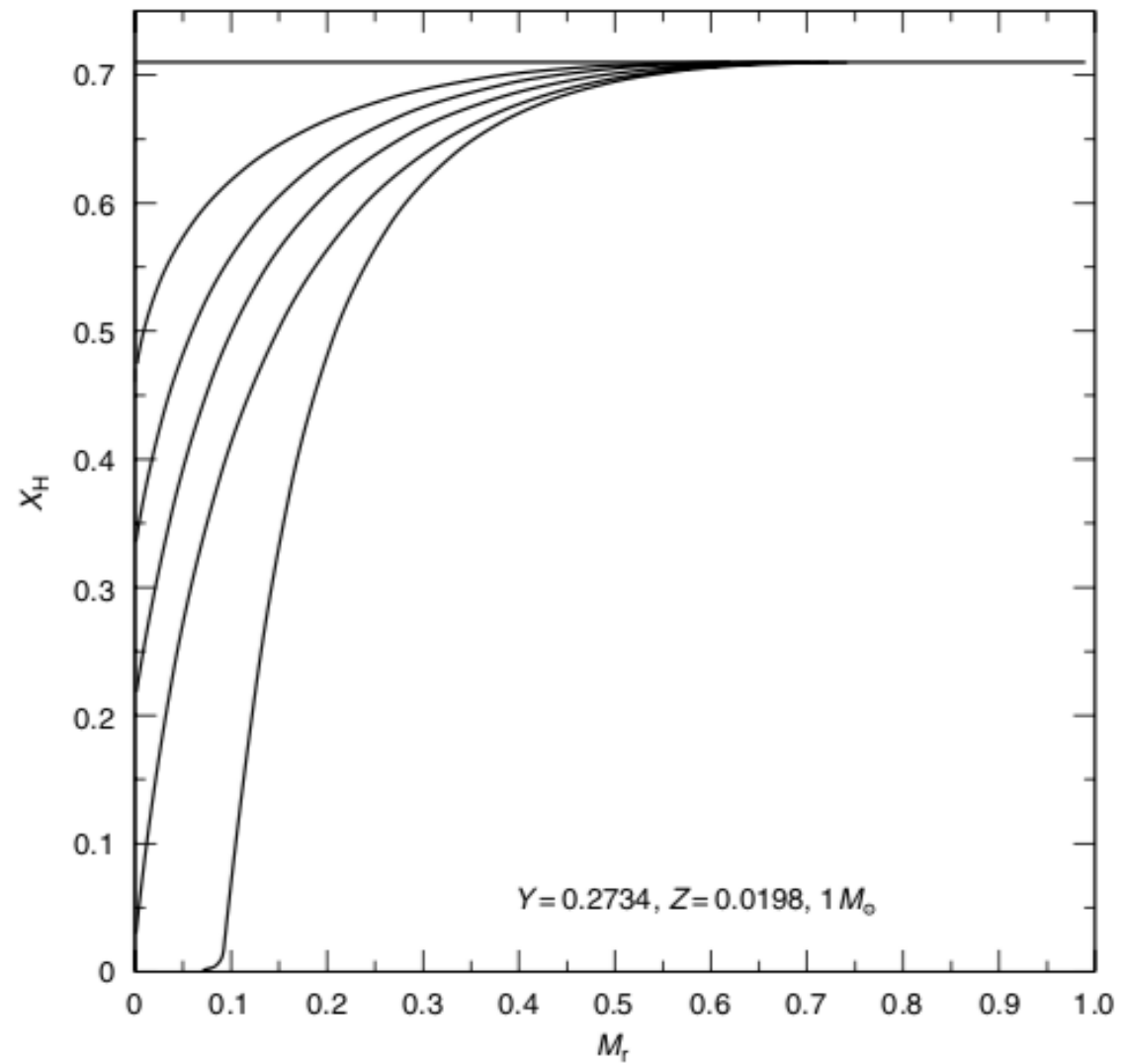


Figure 5.2 The chemical profile of hydrogen in a $1M_{\odot}$ star at different stages during the core H-burning phase

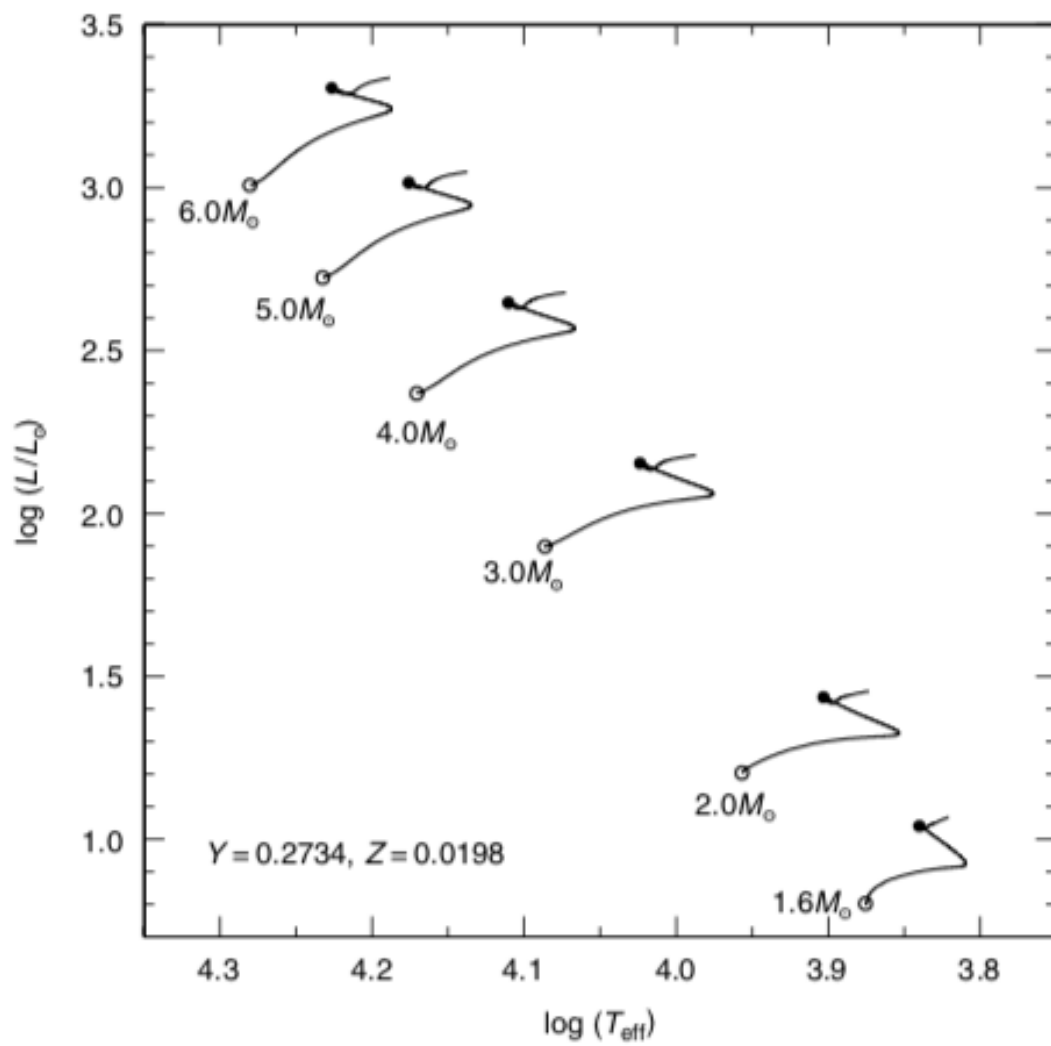


Figure 5.5 Evolutionary tracks of different intermediate-mass stars during the core H-burning phase. The solid dot marks the evolutionary stage equivalent to the turn off point in less massive stars

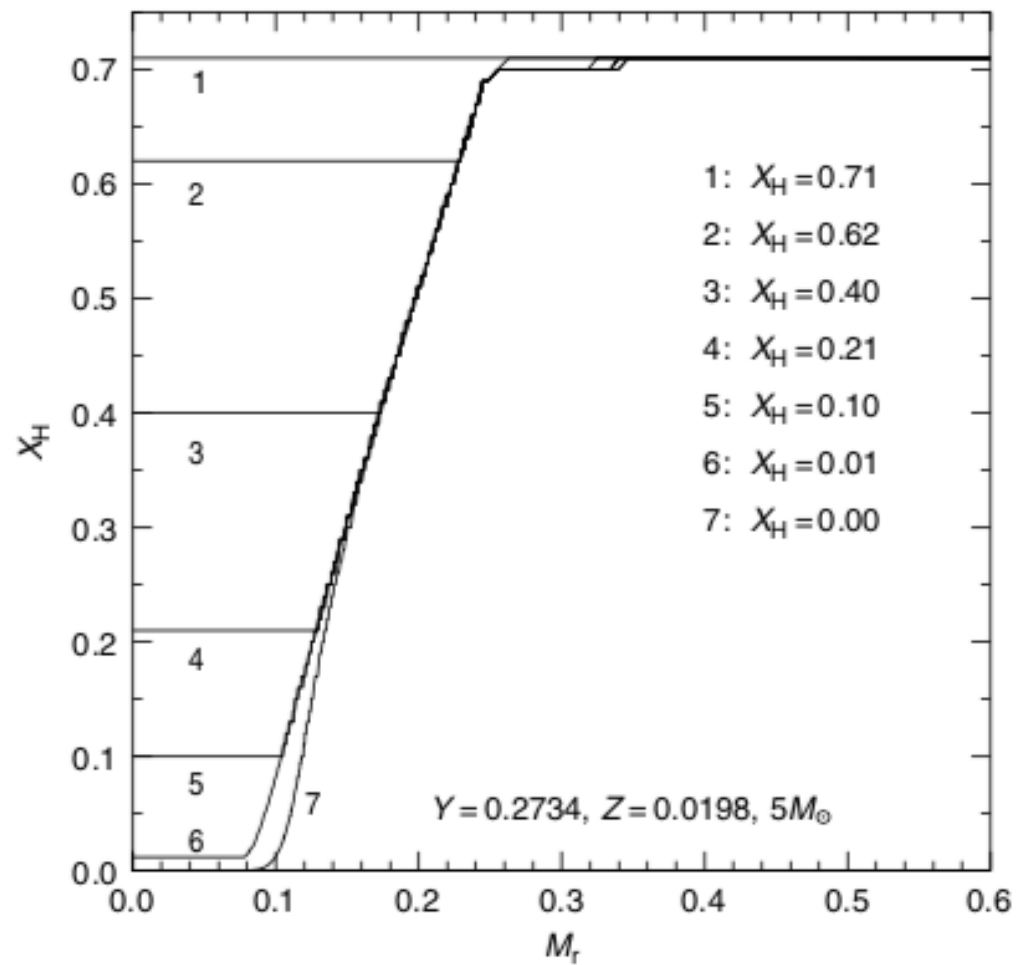


Figure 5.6 The chemical profile of hydrogen in a $5M_{\odot}$ star at different stages during the core H-burning phase

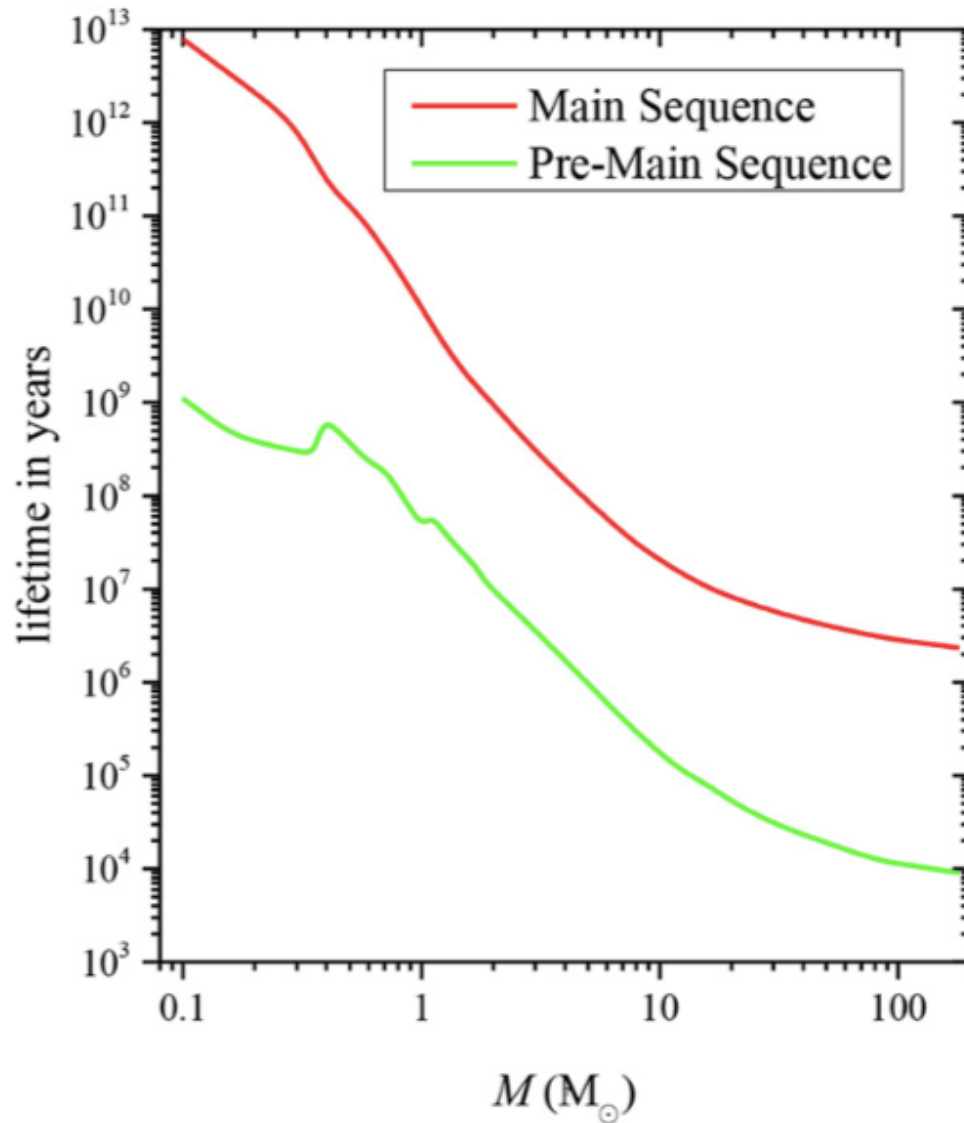


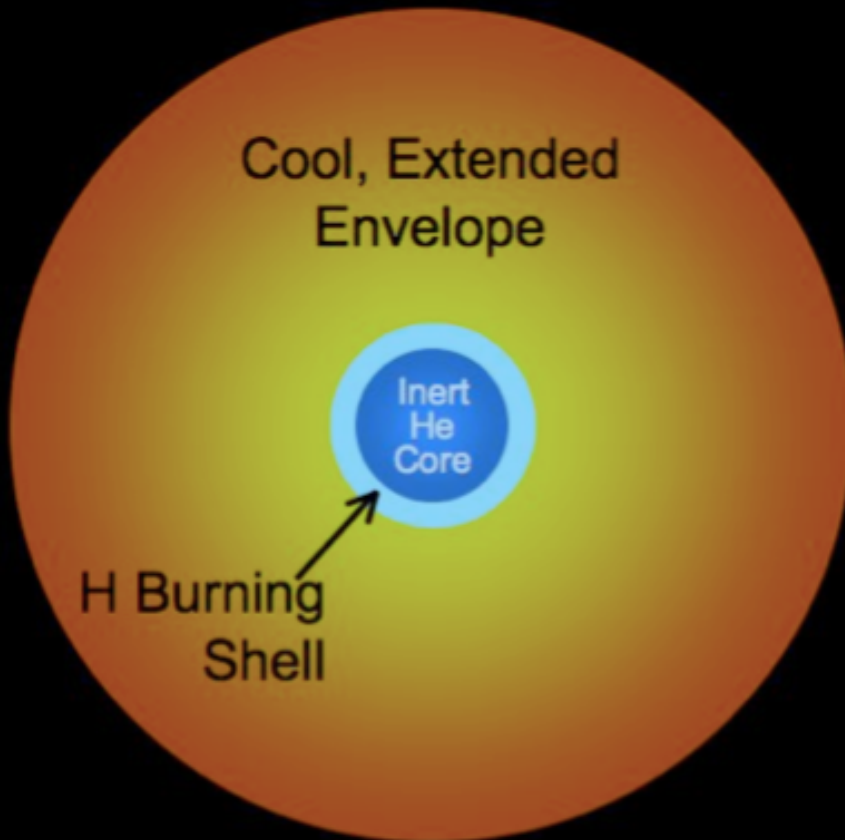
Figure 14.1. PMS and MS lifetimes for solar composition stellar models.

McDonald

Table 5.1 Selected properties of core H-burning stars with different masses and solar chemical composition: surface luminosity, effective temperature, central temperature, central density and mass-size of the convective core at the ZAMS, and the core H-burning lifetime. The units are K for temperatures and g cm⁻³ for the density

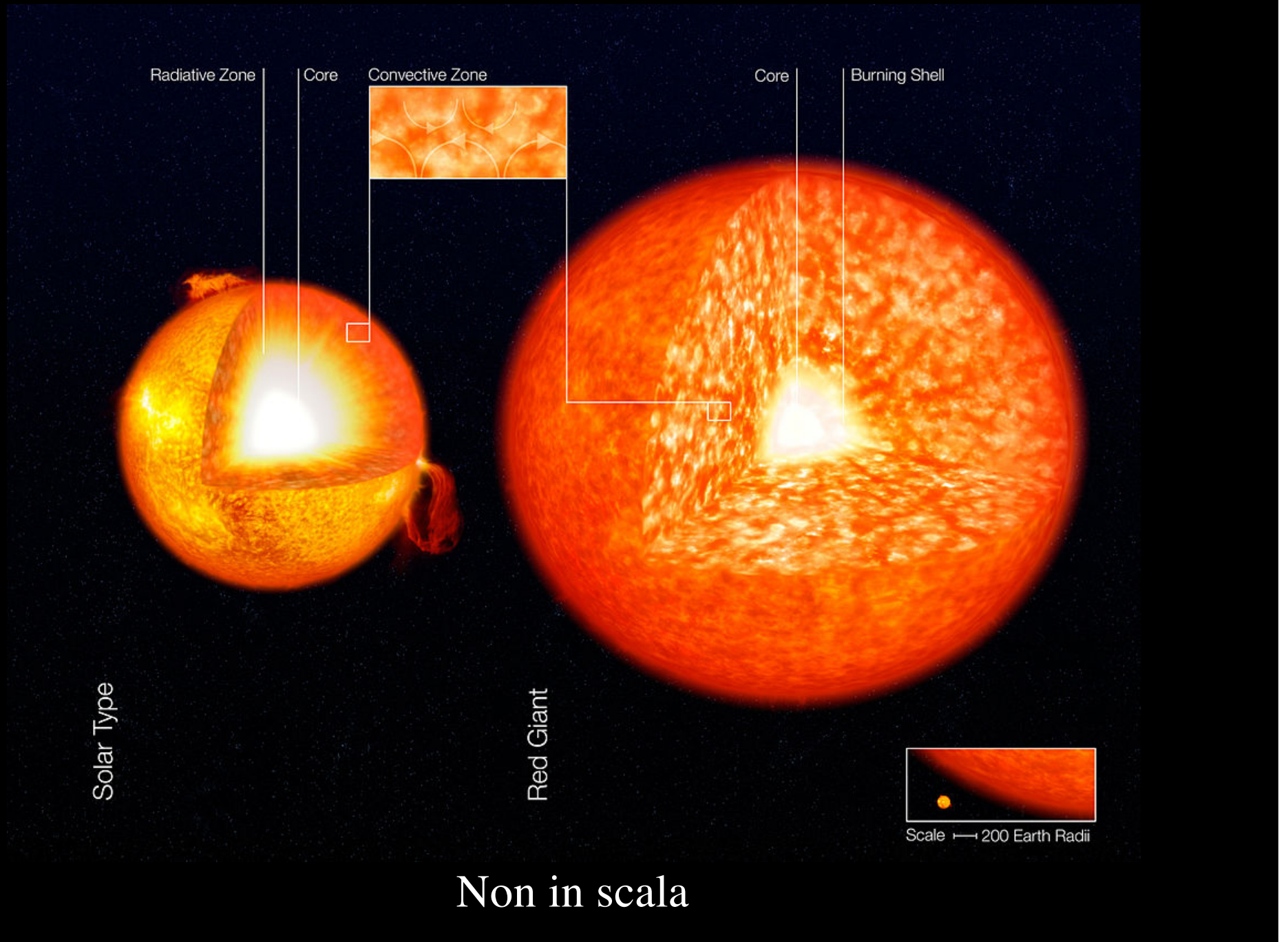
$M(M_{\odot})$	$\log(L/L_{\odot})$	$\log(T_{\text{eff}})$	$\log(T_c)$	$\log(\rho_c)$	$M_{\text{cc}}(M_{\odot})$	t_{He} (Myr)
0.5	-1.397	3.588	6.948	1.857	-	128543.7
0.6	-1.133	3.613	6.984	1.872	-	77015.7
0.7	-0.860	3.645	7.021	1.887	-	44031.9
0.8	-0.595	3.687	7.062	1.898	-	26952.3
0.9	-0.363	3.723	7.101	1.900	-	17360.2
1.0	-0.161	3.751	7.133	1.890	-	11513.3
1.1	0.018	3.771	7.158	1.874	0.000	7913.1
1.2	0.213	3.790	7.184	1.887	0.000	5640.7
1.3	0.400	3.813	7.217	1.928	0.085	4138.5
1.4	0.556	3.831	7.248	1.932	0.111	3043.3
1.5	0.691	3.851	7.268	1.918	0.136	2312.5
1.6	0.812	3.874	7.284	1.900	0.168	1844.3
1.7	0.923	3.897	7.297	1.879	0.199	1520.8
1.8	1.019	3.919	7.306	1.851	0.232	1333.3
1.9	1.113	3.939	7.315	1.829	0.266	1142.9
2.0	1.207	3.956	7.325	1.807	0.299	946.5
2.1	1.290	3.973	7.332	1.786	0.335	836.0
2.2	1.371	3.988	7.339	1.762	0.358	727.1
2.3	1.448	4.003	7.346	1.742	0.394	637.8
2.5	1.591	4.030	7.357	1.700	0.447	502.3
2.6	1.657	4.042	7.362	1.679	0.492	447.9
2.8	1.783	4.065	7.372	1.640	0.542	360.9
3.0	1.898	4.086	7.380	1.603	0.603	296.6
4.0	2.368	4.171	7.414	1.446	0.922	138.1
5.0	2.724	4.232	7.437	1.325	1.242	78.5
6.0	3.007	4.280	7.455	1.227	1.549	51.0
7.0	3.238	4.320	7.470	1.147	1.887	36.3
8.0	3.433	4.352	7.482	1.079	2.309	27.7
9.0	3.601	4.380	7.493	1.022	2.672	22.1
10.0	3.749	4.404	7.502	0.972	3.159	18.3

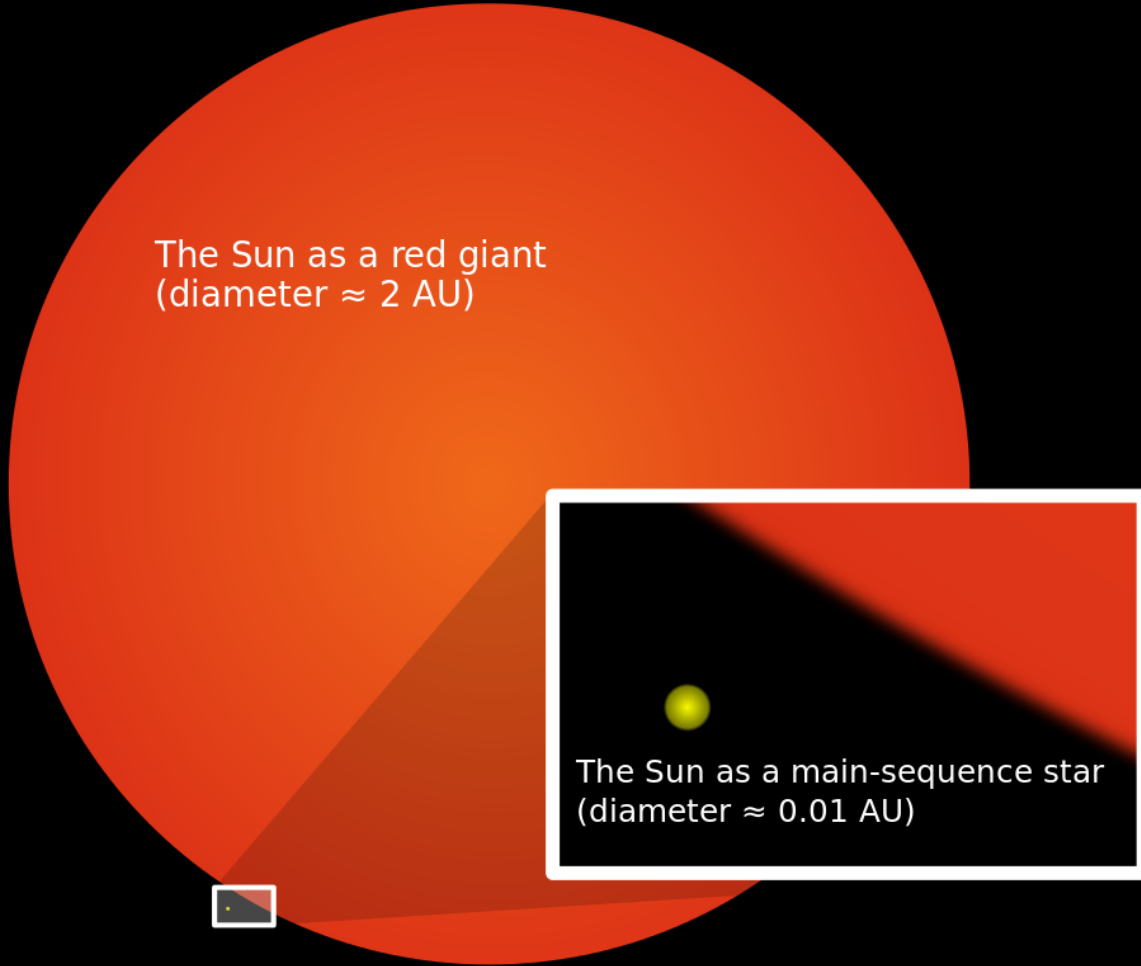
Red Giant Star



Non in scala

Red Giant Star





He Flash

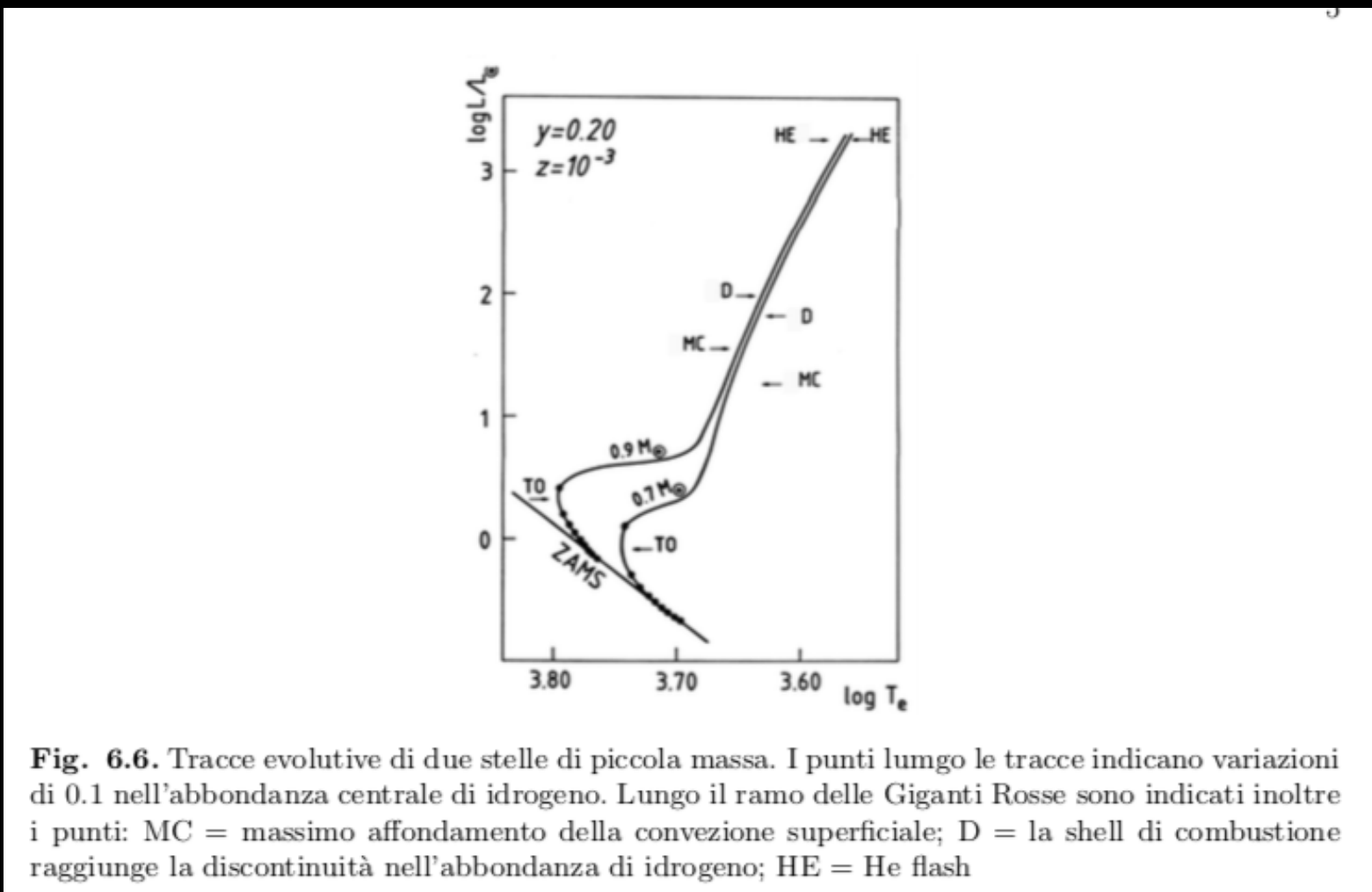


Fig. 6.6. Tracce evolutive di due stelle di piccola massa. I punti lungo le tracce indicano variazioni di 0.1 nell'abbondanza centrale di idrogeno. Lungo il ramo delle Giganti Rosse sono indicati inoltre i punti: MC = massimo affondamento della convezione superficiale; D = la shell di combustione raggiunge la discontinuità nell'abbondanza di idrogeno; HE = He flash

Castellani

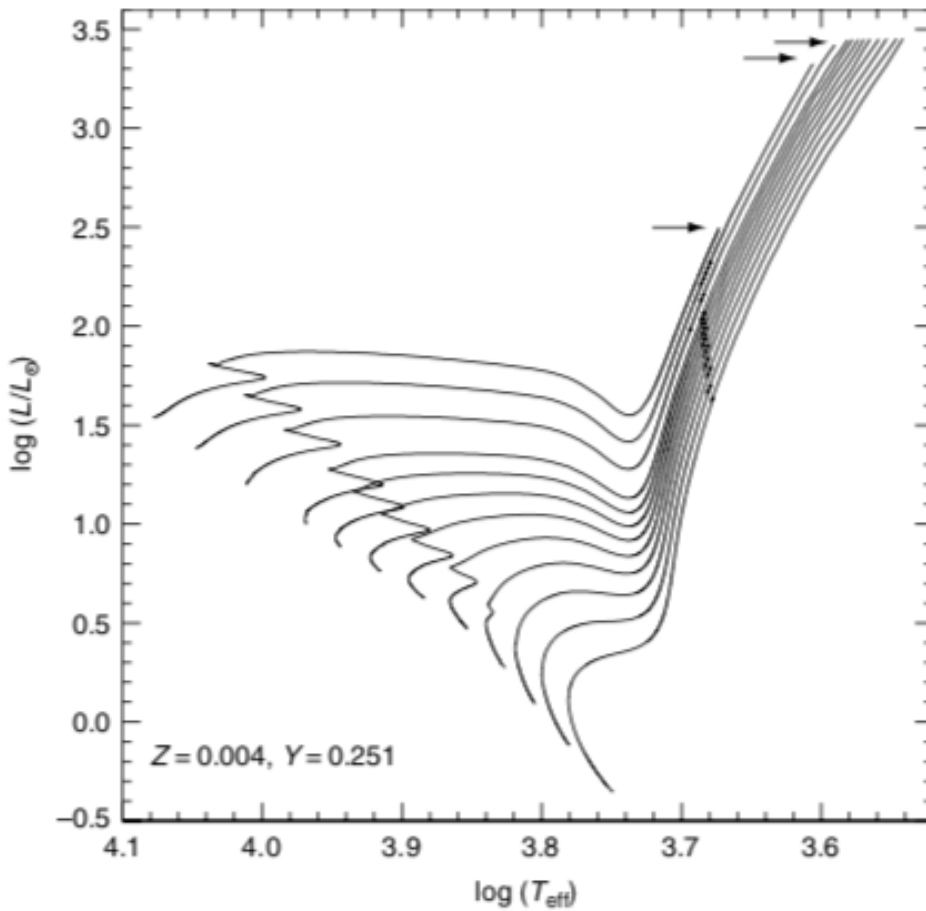
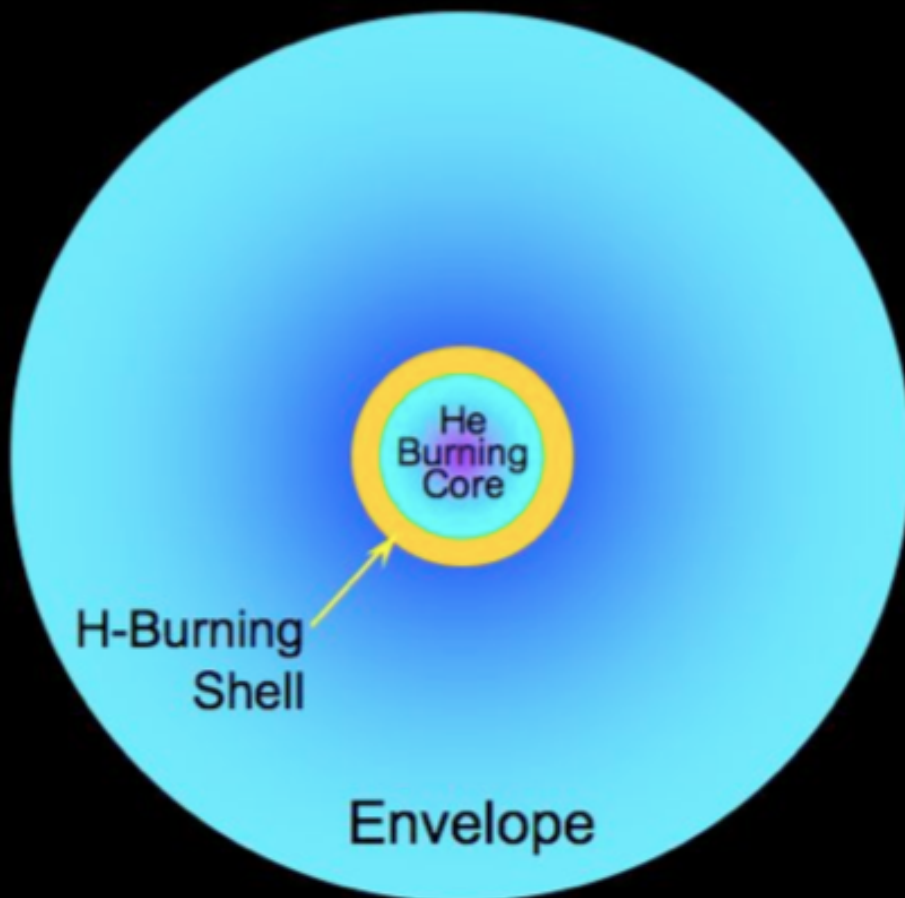


Figure 5.13 The HRD for both the core and shell H-burning phases of low-mass stars for the labelled chemical composition. The RG phase begins when the stars start to evolve at almost constant T_{eff} and increasing luminosity. The various evolutionary tracks correspond to the following stellar masses: $M/M_\odot = 0.8, 0.9, 1.0, 1.1, 1.2, 1.3, 1.4, 1.5, 1.6, 1.8, 2.0, 2.2$. The arrows mark the location of the tip of the RGB for the $2.2M_\odot$ and $2M_\odot$ models, and for those less massive (that has an approximately constant luminosity)

Horizontal Branch Star



Non in scala

Horizontal Branch Stars

8

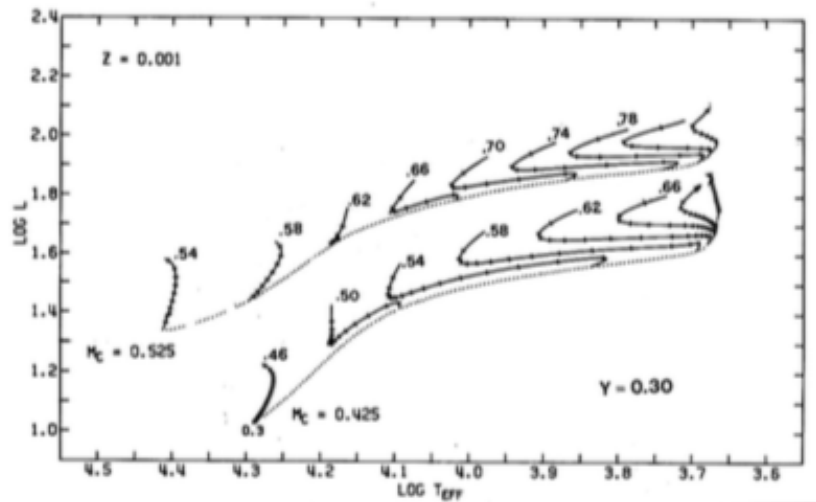


Fig. 7.9. Tracce evolutive nel diagramma HR di strutture in fase di combustione di elio per due diverse assunzioni sulla massa del nucleo di He M_c e al variare della massa totale. Le linee a punti mostrano, per ogni M_c , la collocazione dei modelli iniziali

Castellani

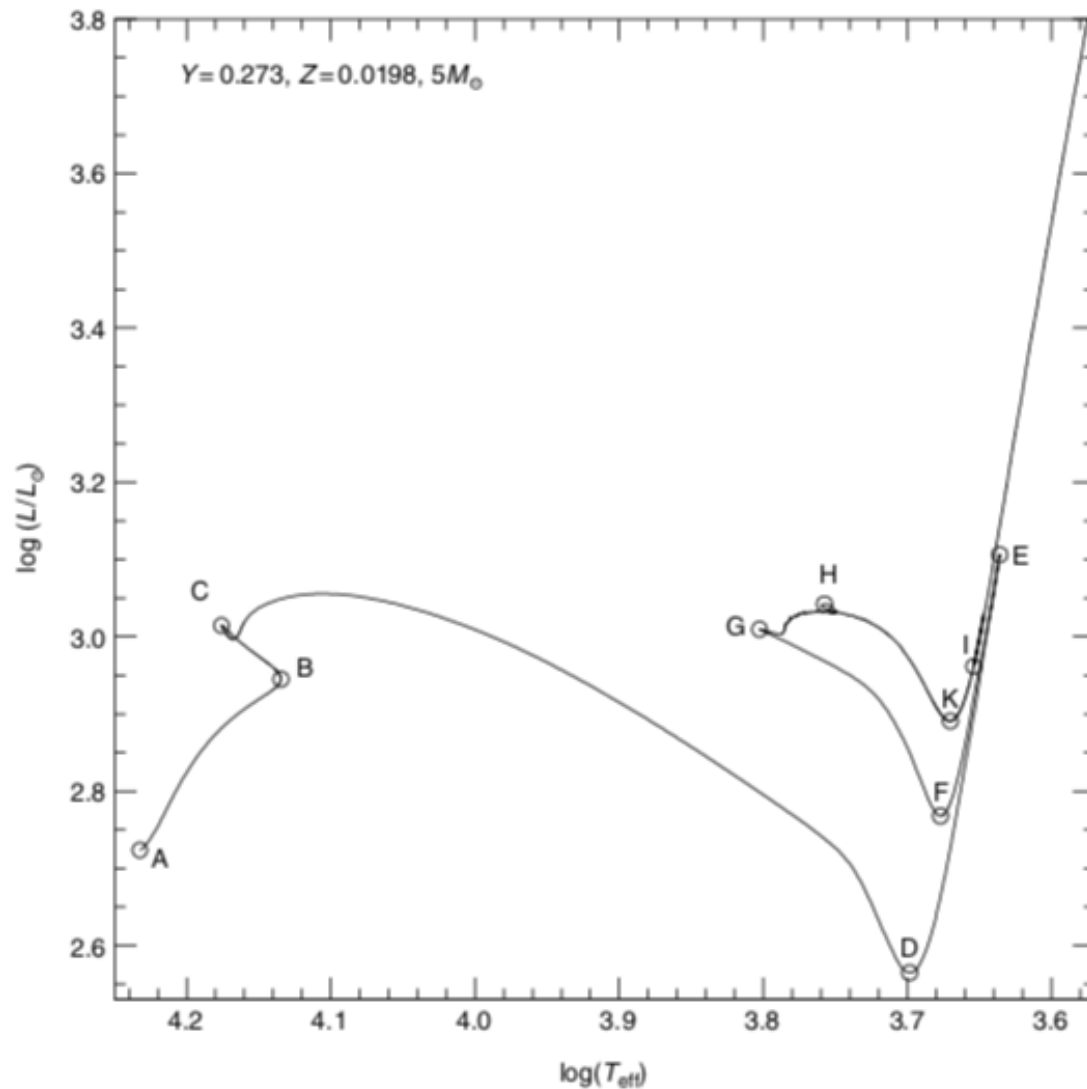


Figure 6.8 The evolutionary track of a $5M_{\odot}$ model during the H- and He-burning phases. The different evolutionary stages discussed in the text are marked A-K

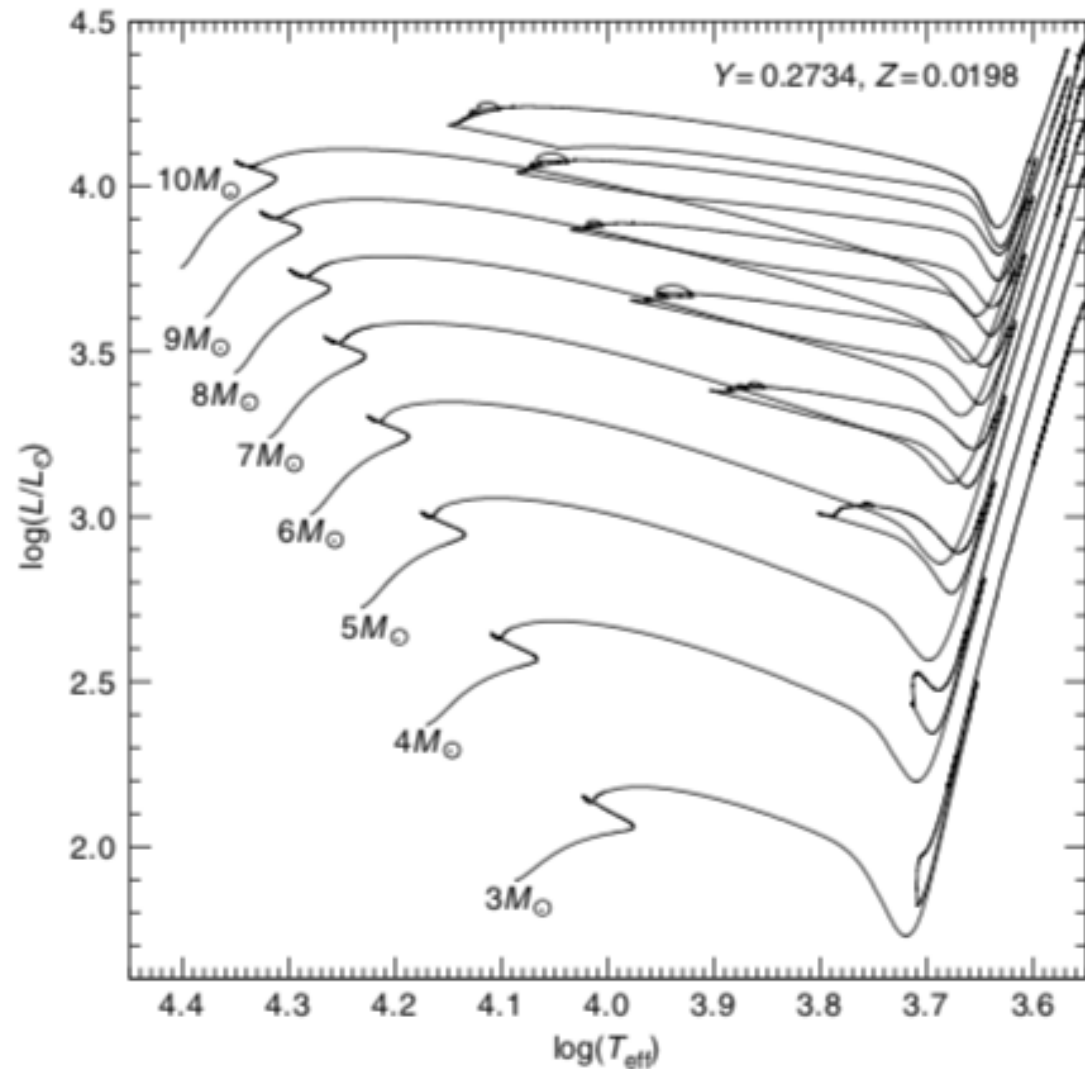


Figure 6.10 The HRD of evolutionary tracks for different intermediate-mass stars with solar chemical composition

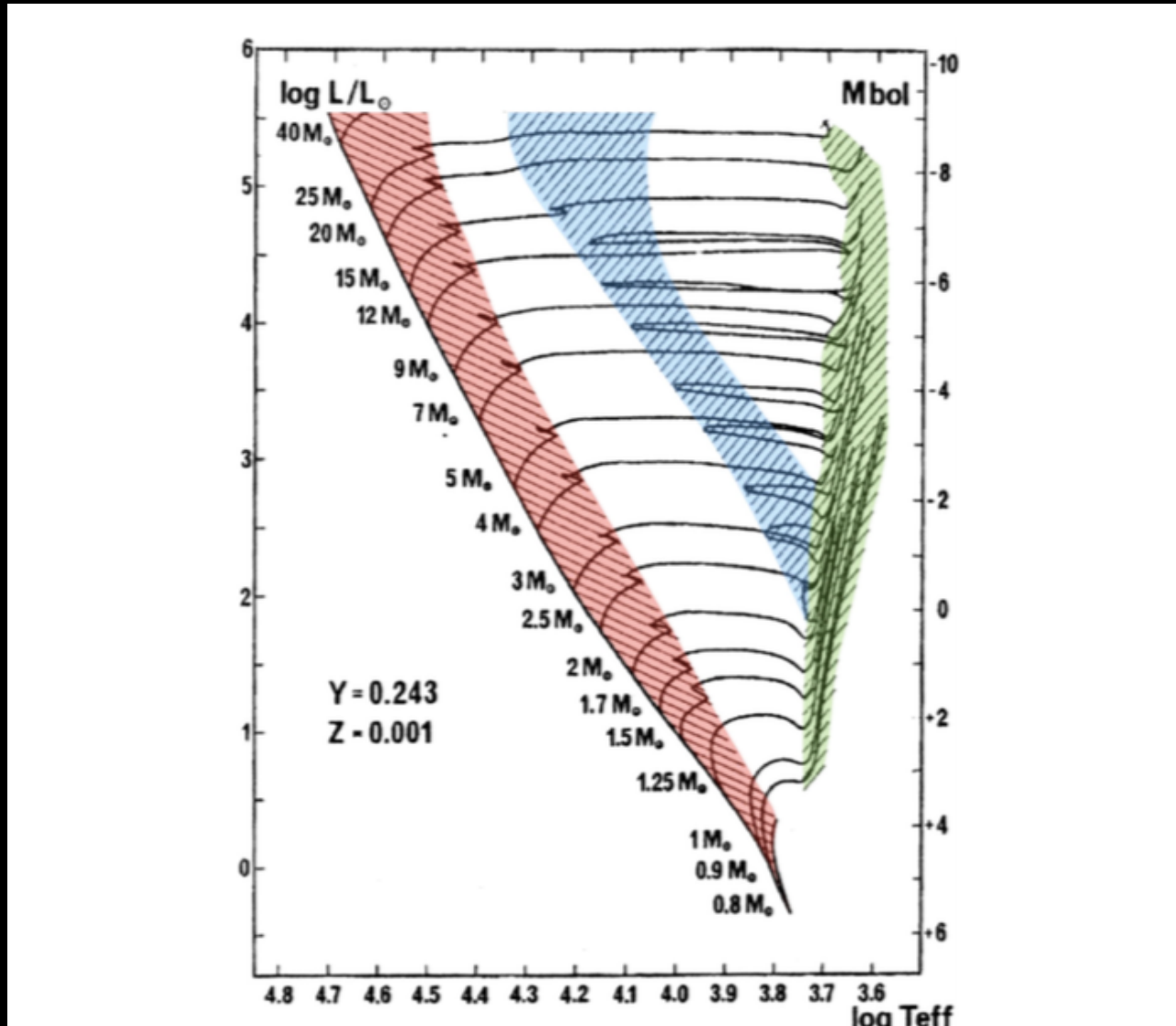
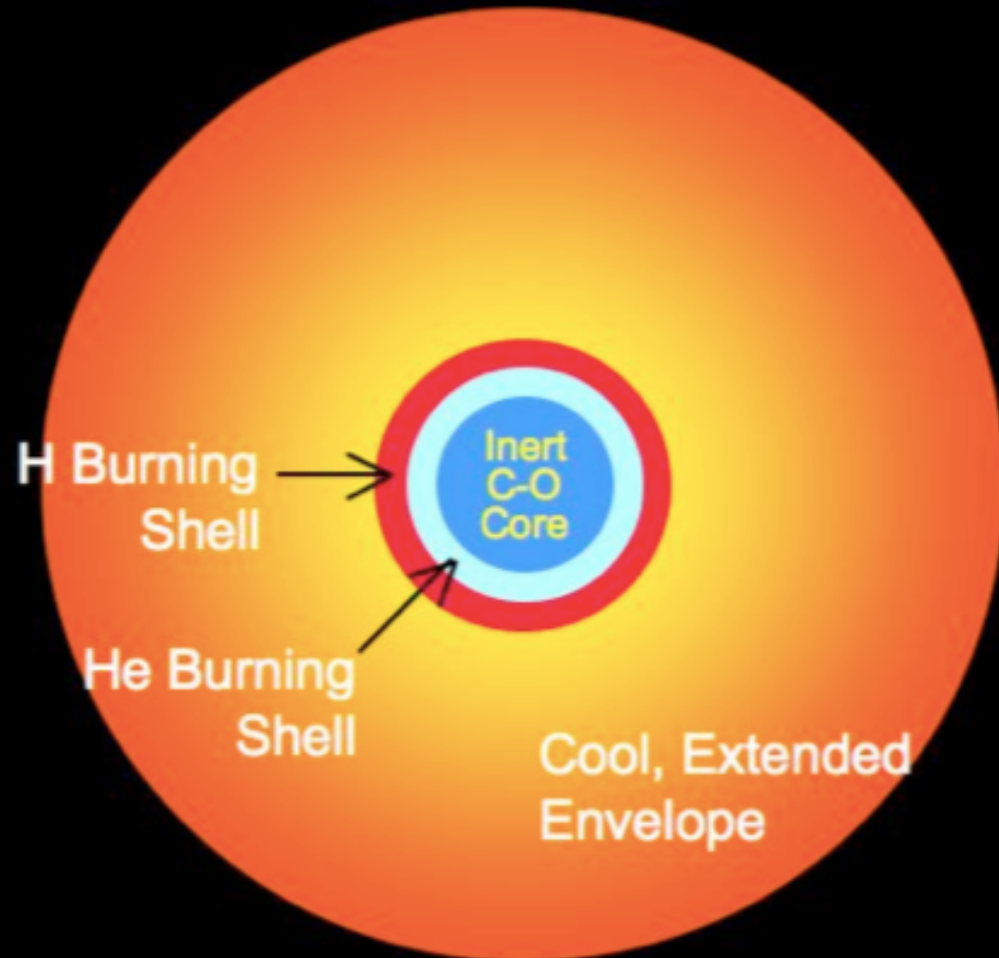


Figure 14.2. Predicted evolutionary tracks of low-metallicity stars. The core H- and core He-fusion phases are shown in red and blue, respectively. The green region indicates the Hayashi line of stars at $T_{\text{eff}} \approx 4000$ to 5000 K with extended convective envelopes. (Reproduced from Schaller et al. 1992, with permission. © ESO.)

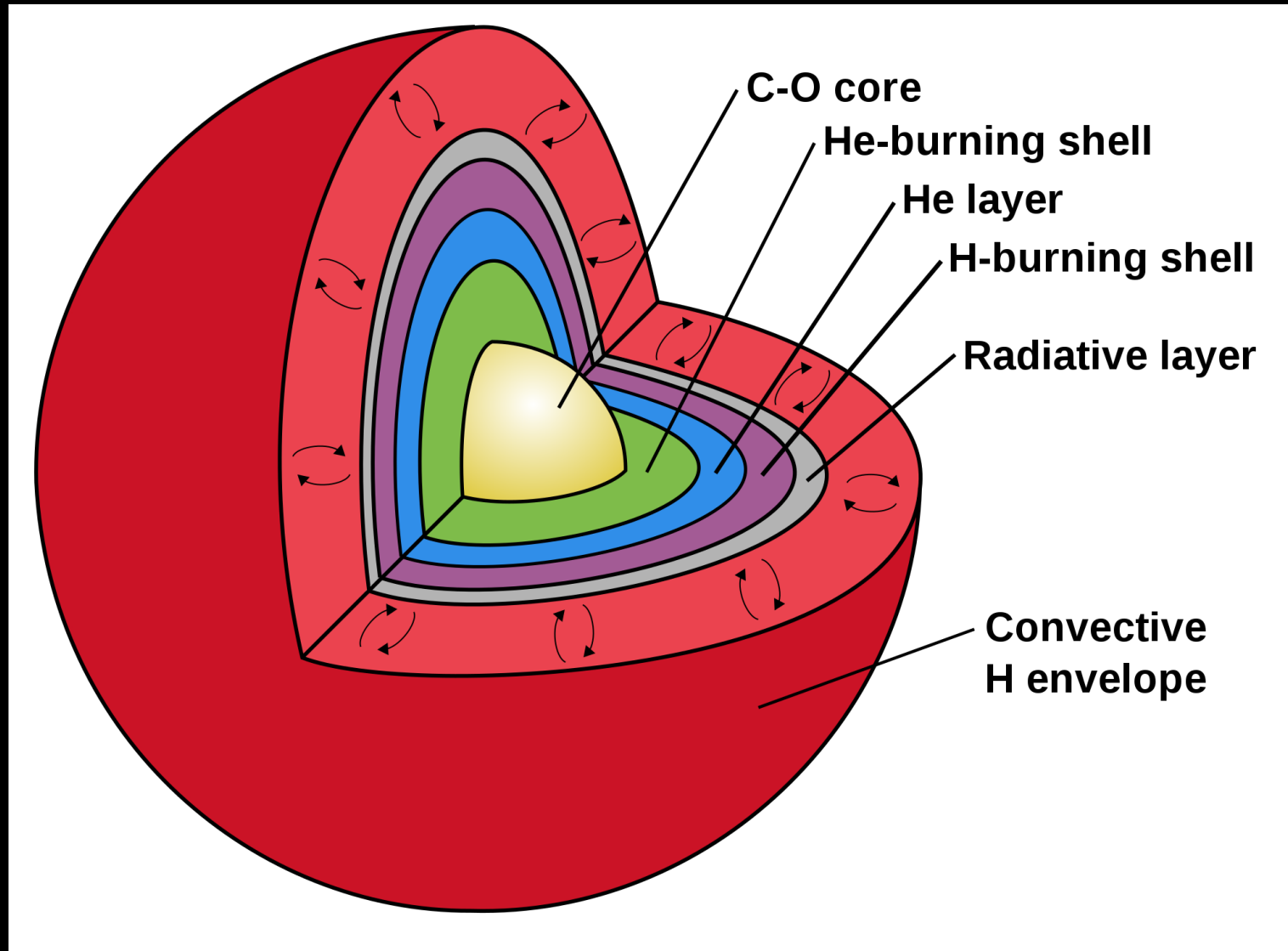
Lamers

Asymptotic Giant Branch Star



Non in scala

Asymptotic Giant Branch Star



Non in scala

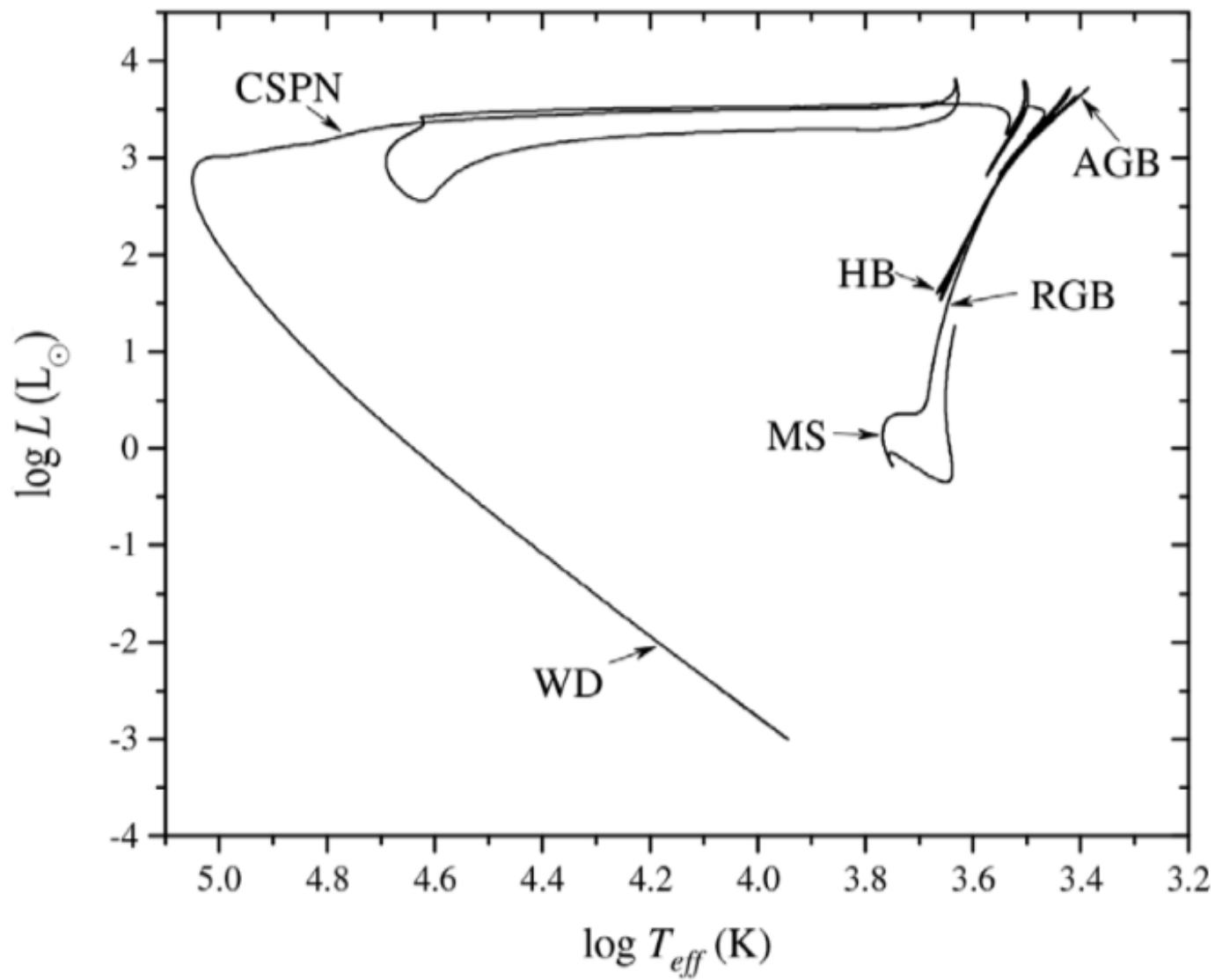


Figure 20.1. Complete evolutionary path in the HRD of a $1 M_\odot$ model from the PMS to a cool WD.

McDonald

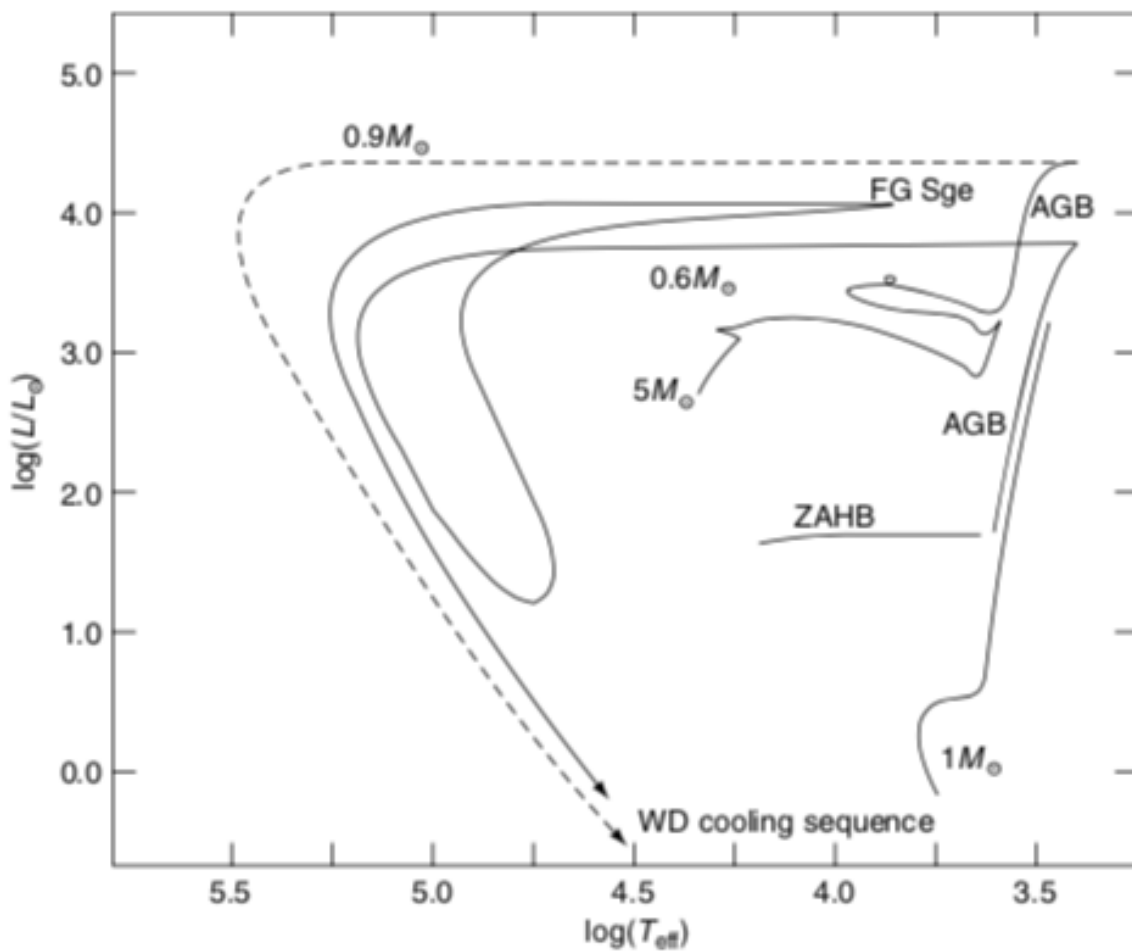


Figure 7.4 Evolutionary tracks from the MS to the WD cooling sequence. The dashed line is the evolutionary track of the $0.9 M_{\odot}$ object left at the end of the AGB, whose initial MS mass was equal to $5 M_{\odot}$; the solid line labelled $0.6 M_{\odot}$ is the evolutionary track of an object whose initial mass was equal to $1 M_{\odot}$. This star experiences a final He flash in the shell before reaching the WD cooling sequence. The location of the observational counterpart represented by the star FG Sagittae is also shown

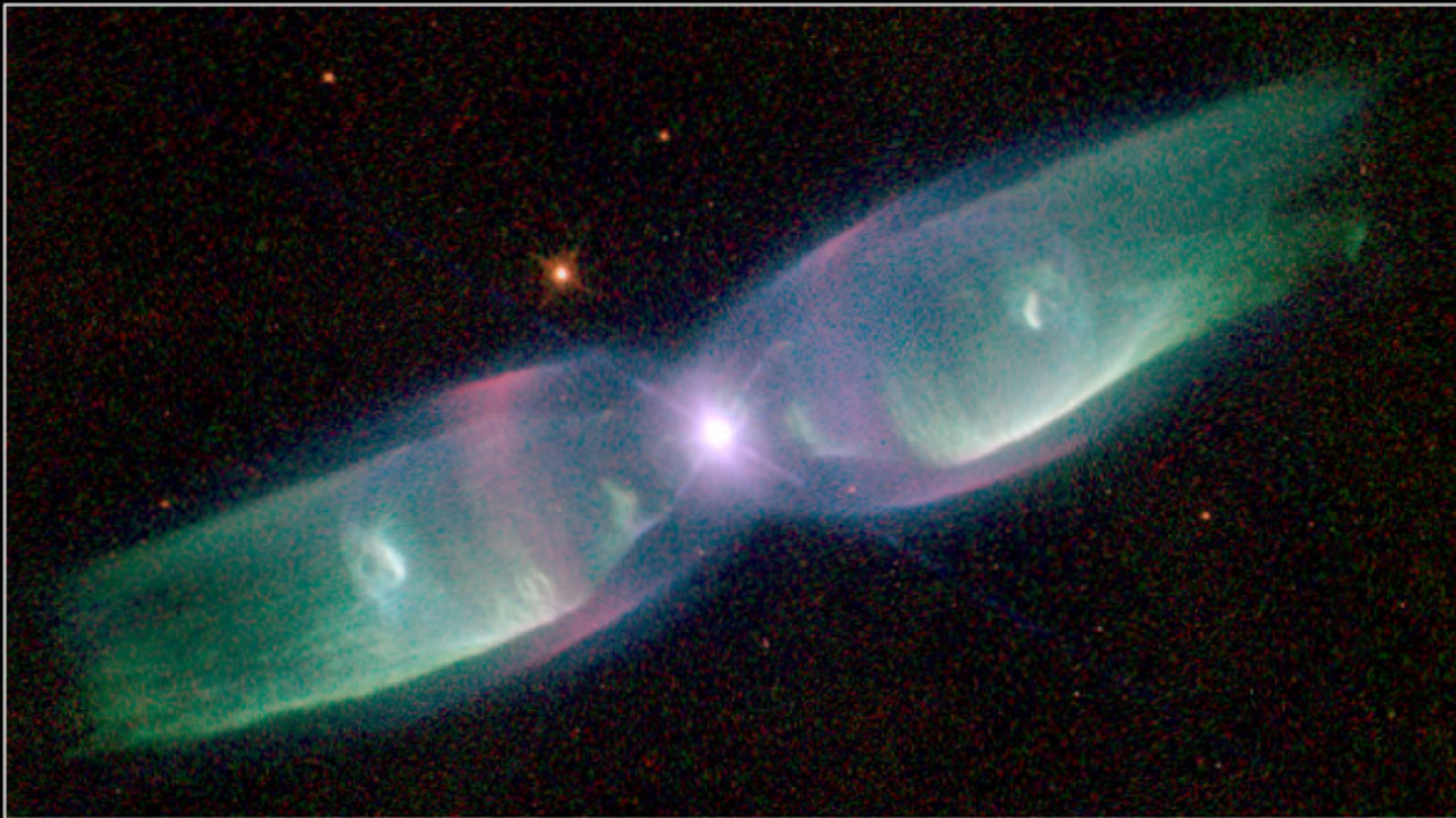


NGC 6543

PR95-01a · ST Scl OPO · January 1995 · P. Harrington (U.MD), NASA

HST · WFPC2

12/13/94 zgl



Planetary Nebula M2-9

PRC97-38a • ST Scl OPO • December 17, 1997
B. Balick (University of Washington) and NASA

HST • WFPC2

Planetary Nebula NGC 6751



Hubble
Heritage

PRC00-12 • Space Telescope Science Institute • NASA and The Hubble Heritage Team (STScI/AURA)

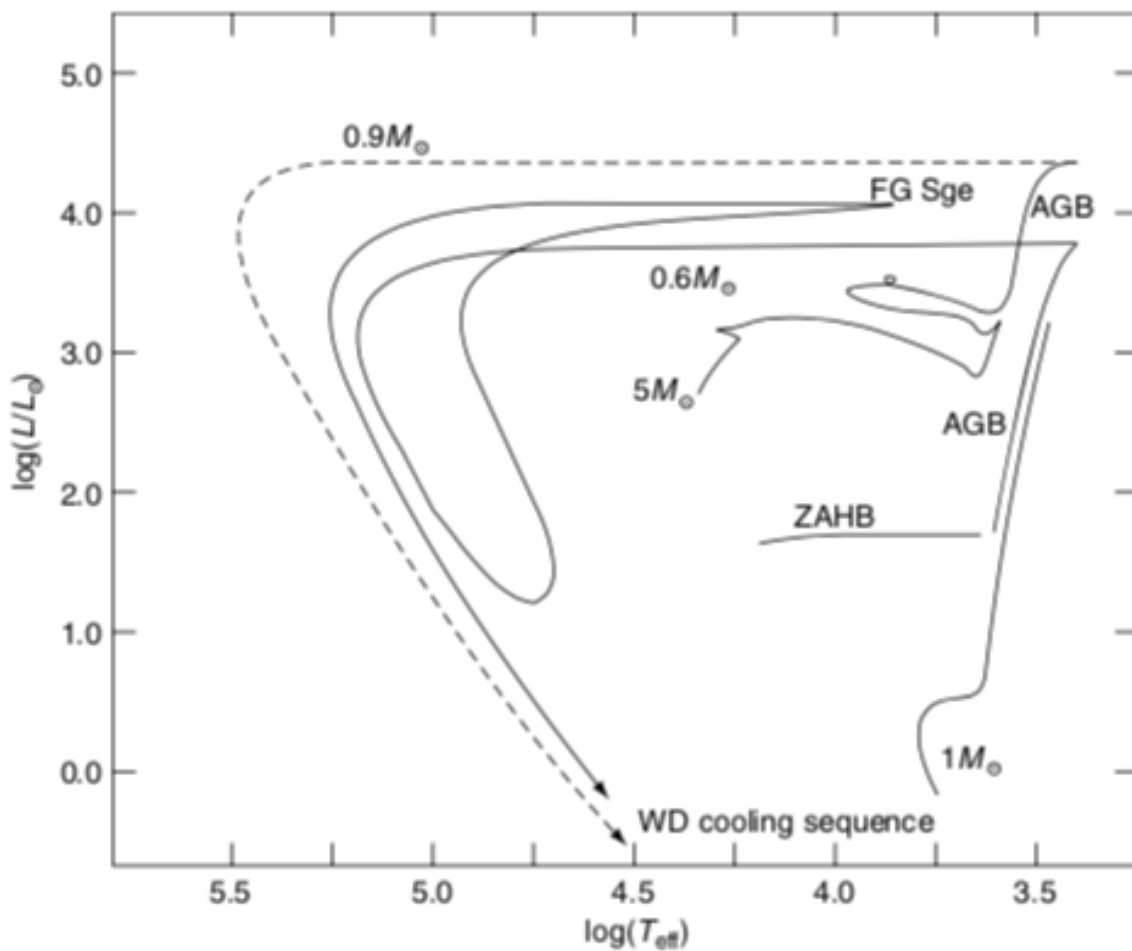
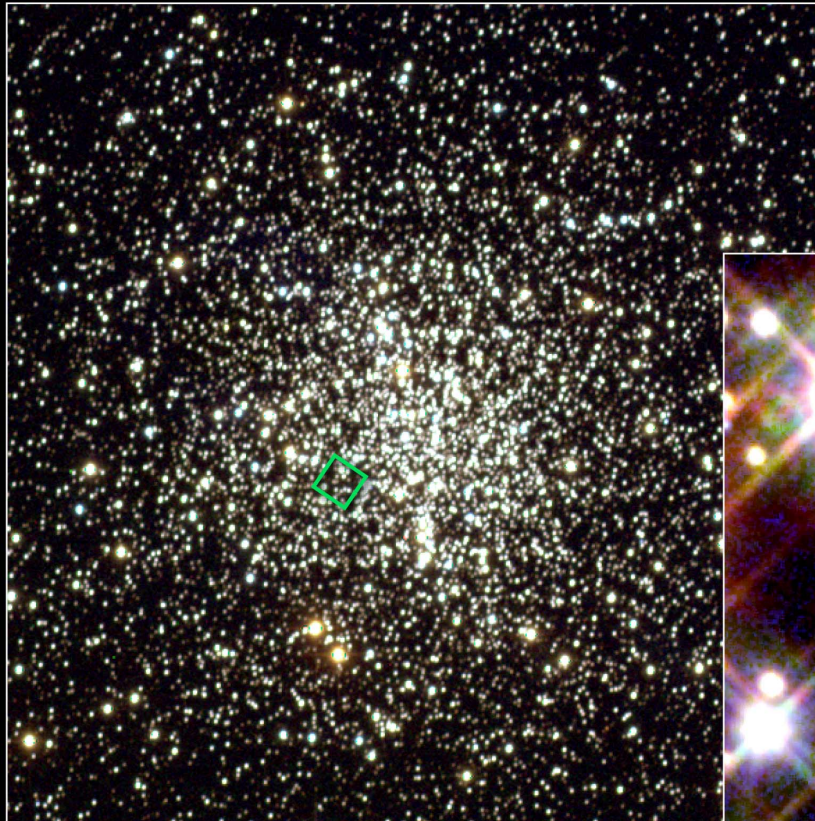
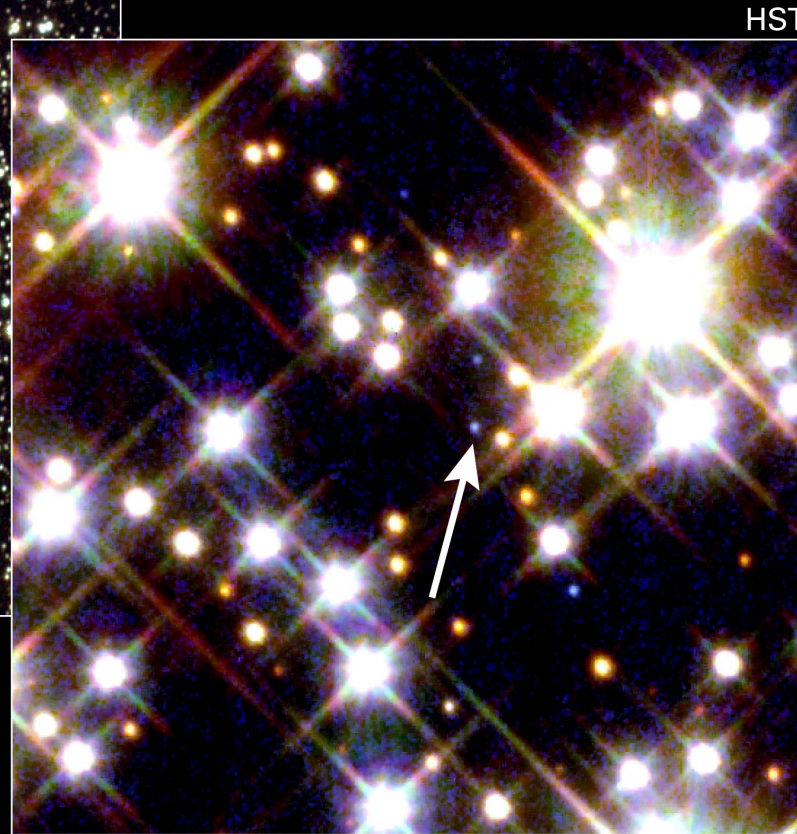


Figure 7.4 Evolutionary tracks from the MS to the WD cooling sequence. The dashed line is the evolutionary track of the $0.9 M_{\odot}$ object left at the end of the AGB, whose initial MS mass was equal to $5 M_{\odot}$; the solid line labelled $0.6 M_{\odot}$ is the evolutionary track of an object whose initial mass was equal to $1 M_{\odot}$. This star experiences a final He flash in the shell before reaching the WD cooling sequence. The location of the observational counterpart represented by the star FG Sagittae is also shown

Nane bianche



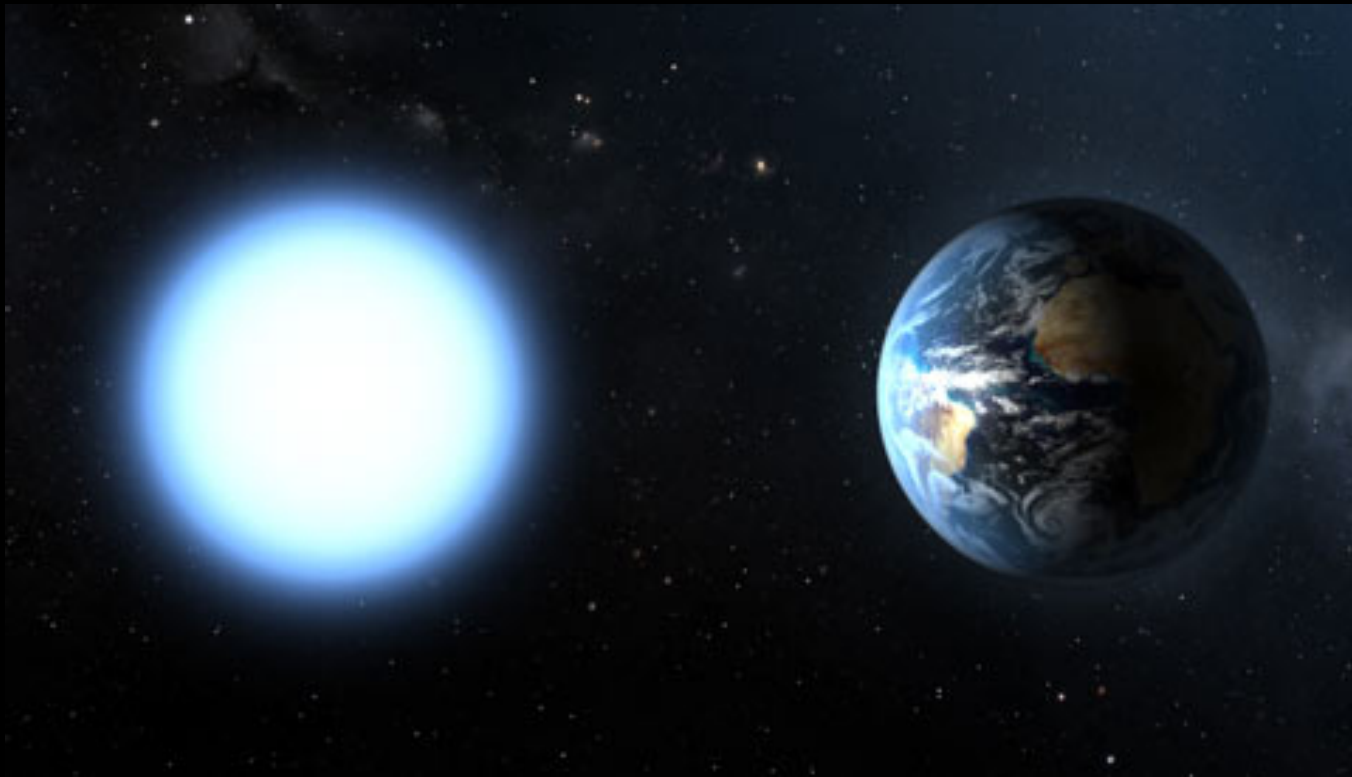
Globular Cluster M4
Location of white dwarf
companion to pulsar B1620-26

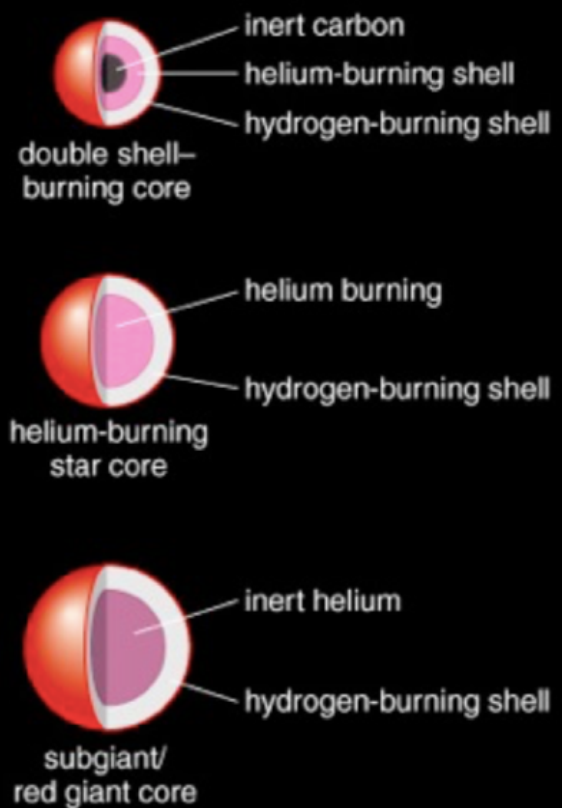
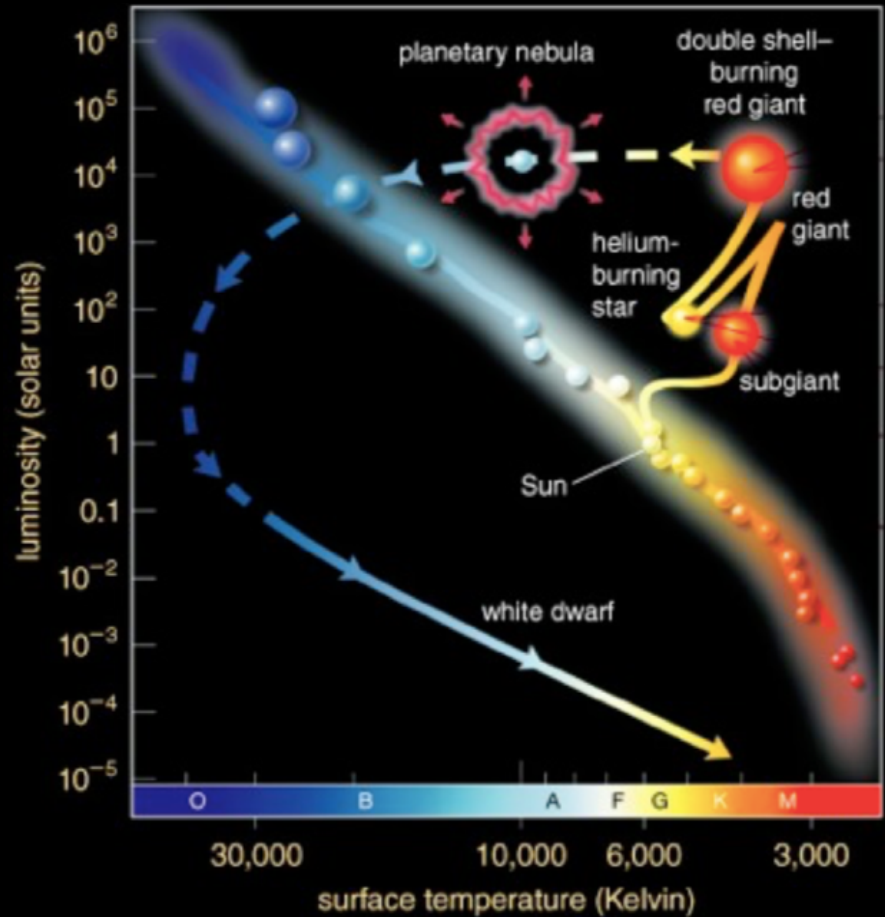


Hubble Space Telescope • WFPC2

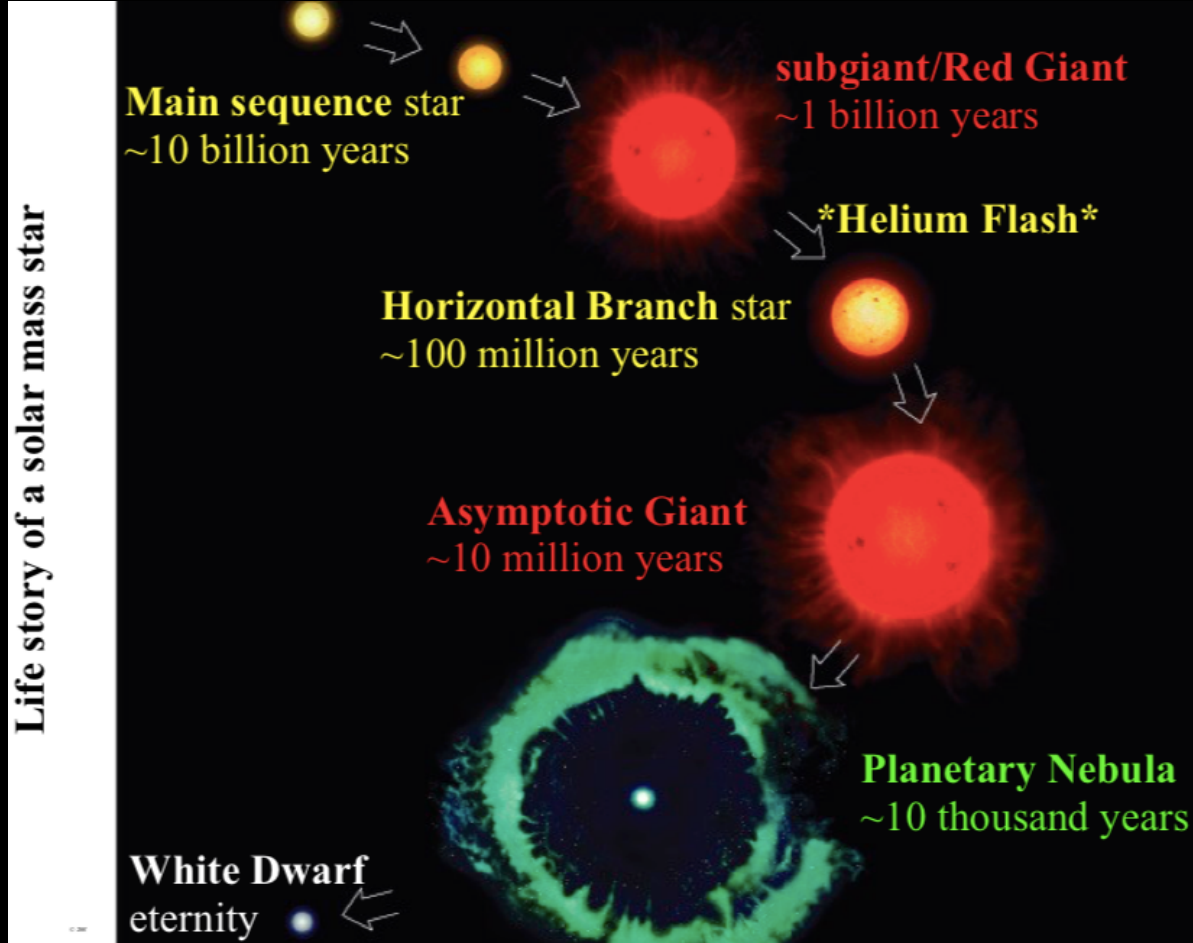
NASA and H. Richer (University of British Columbia)
STScI-PRC03-19b

Nane bianche

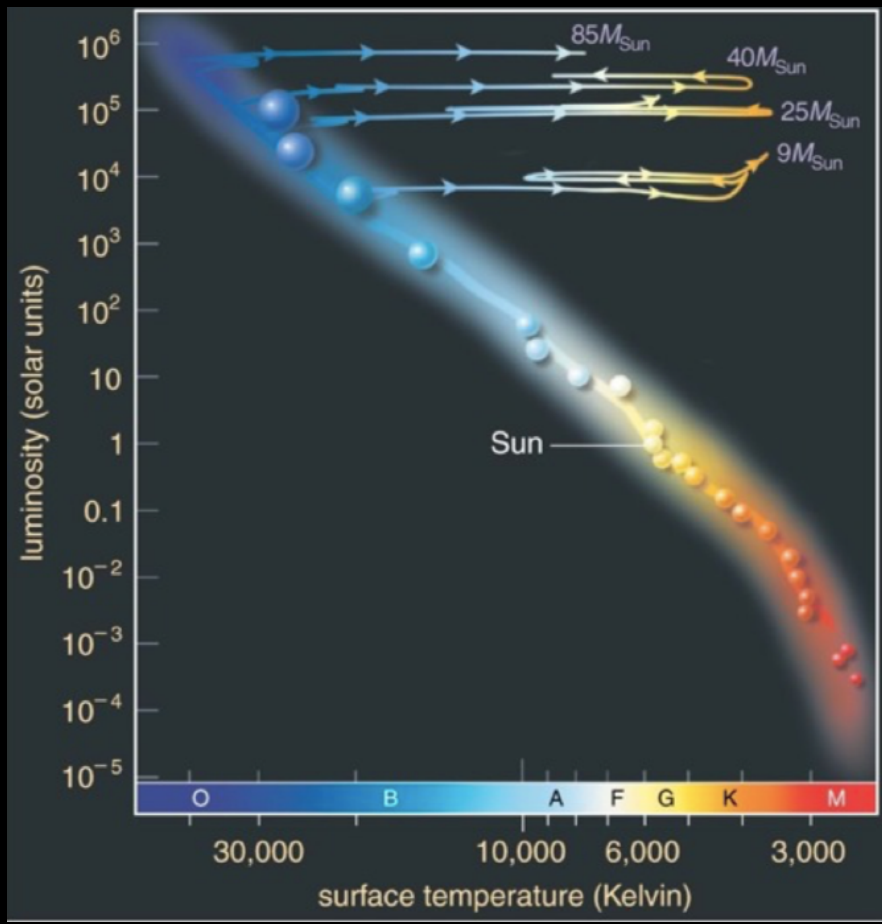




Life story of a solar mass star



Stelle di grande massa



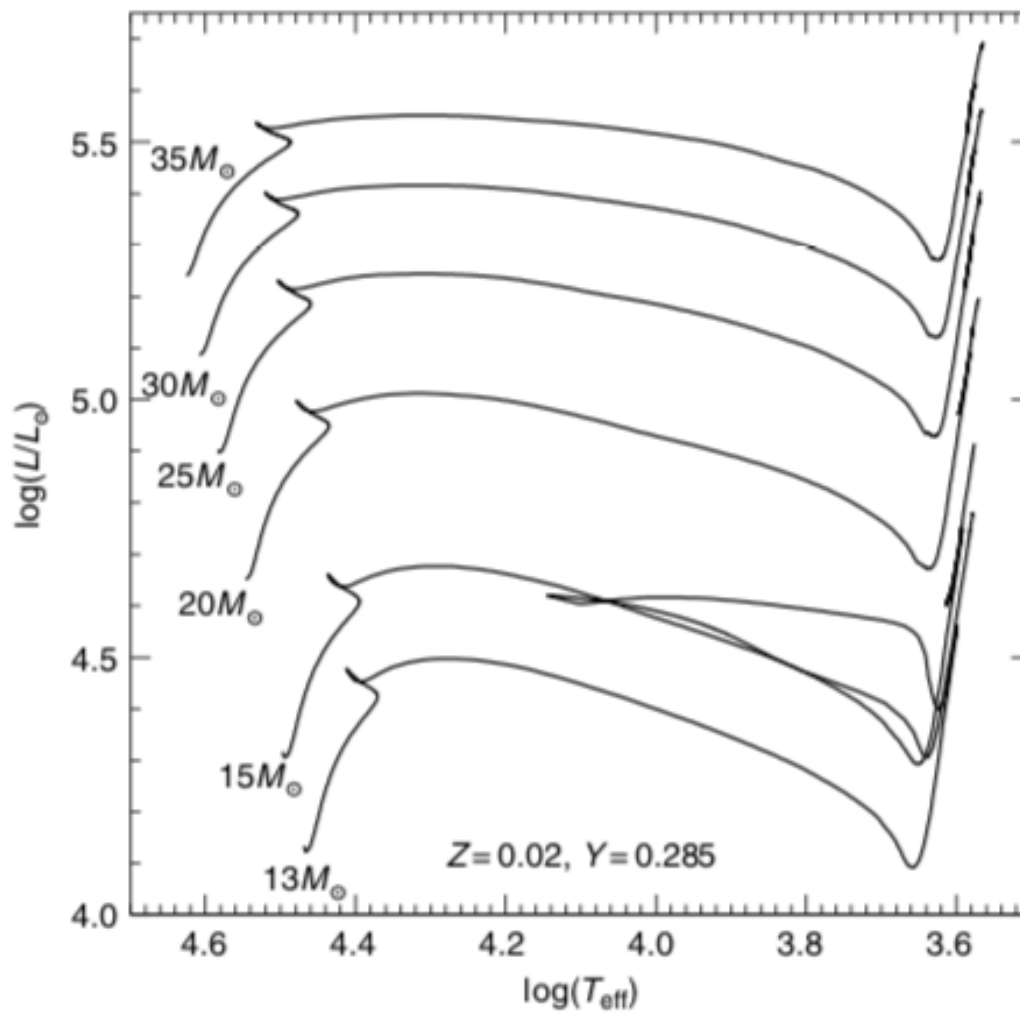
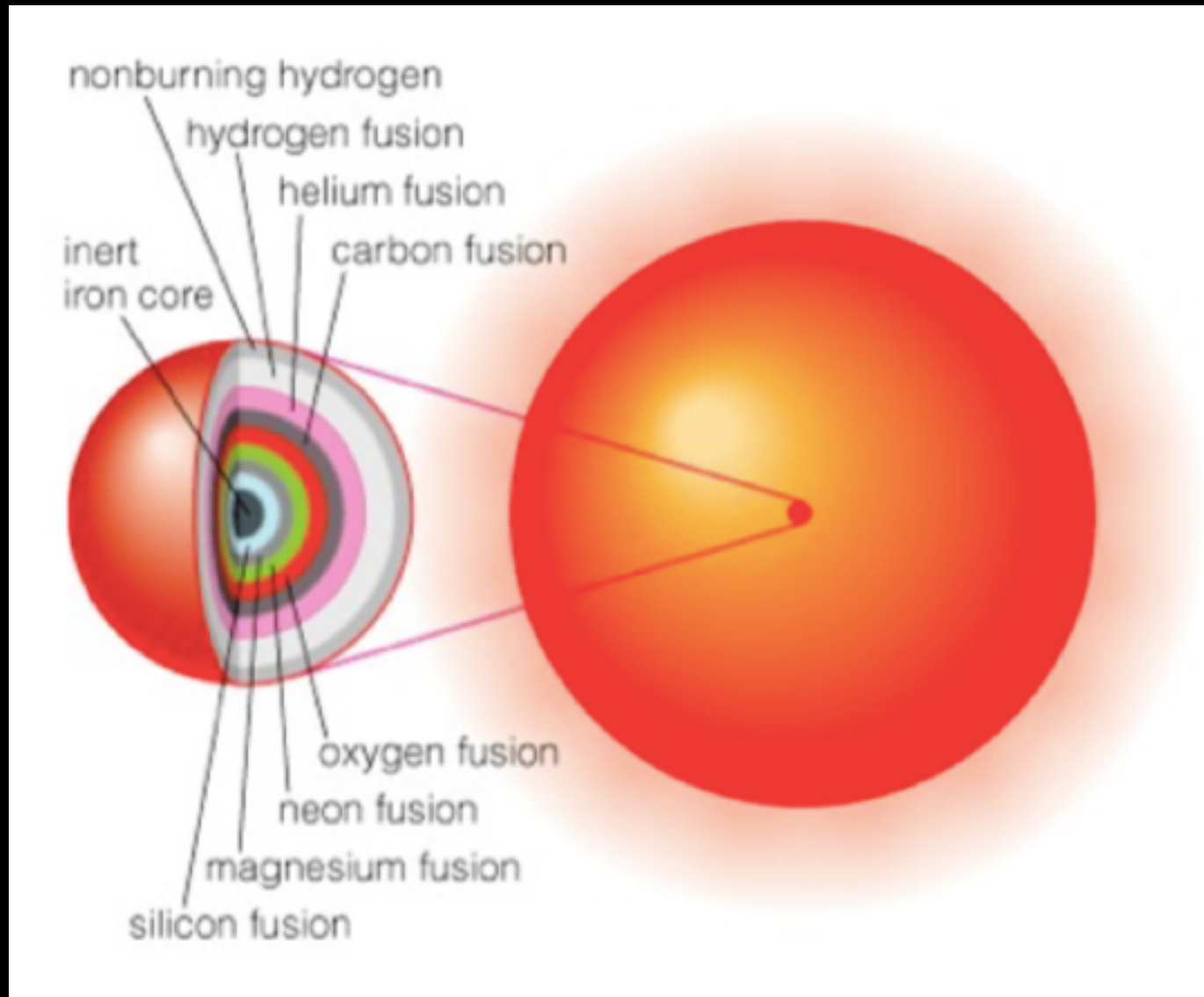
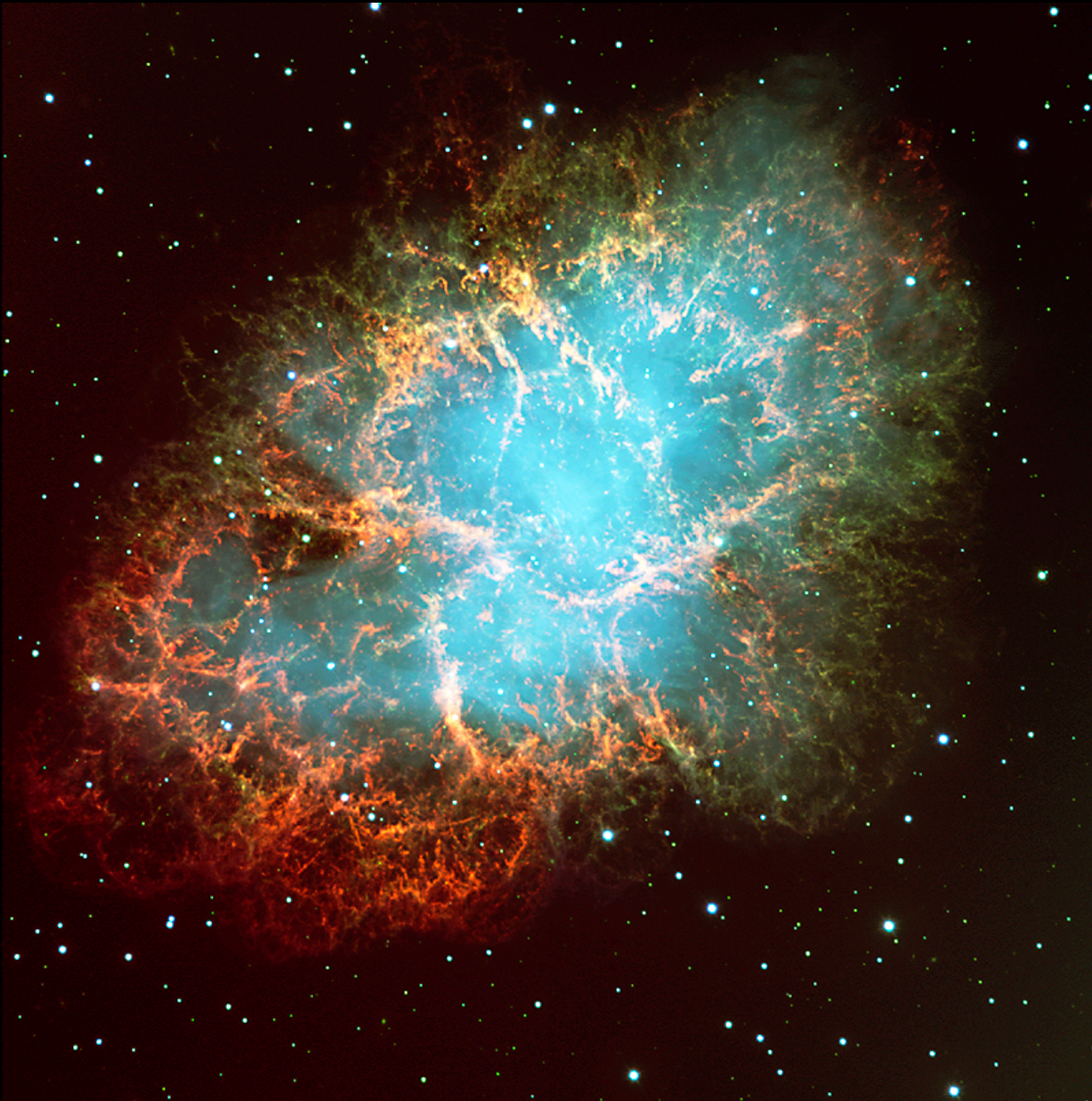


Figure 7.12 Evolutionary tracks of massive stars with different masses (courtesy of M. Limongi)





The Crab Nebula in Taurus (VLT KUEYEN + FORS2)

ESO PR Photo 40f/99 (17 November 1999)

© European Southern Observatory



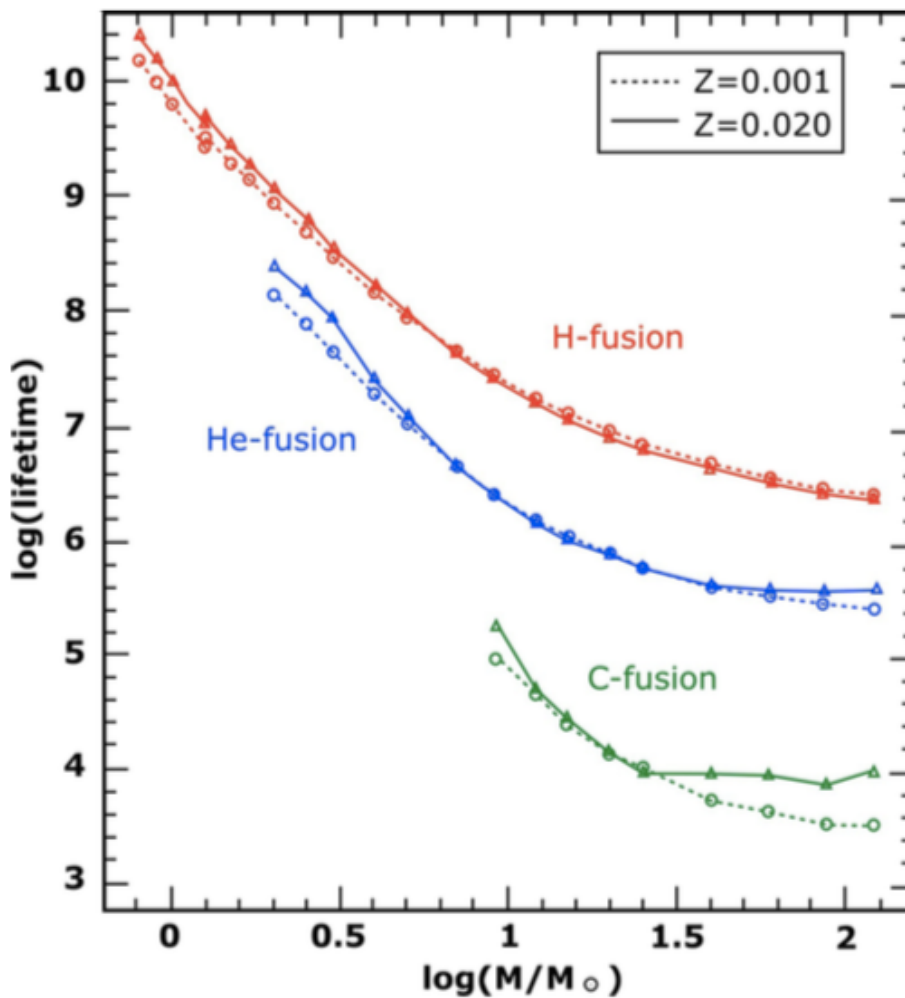


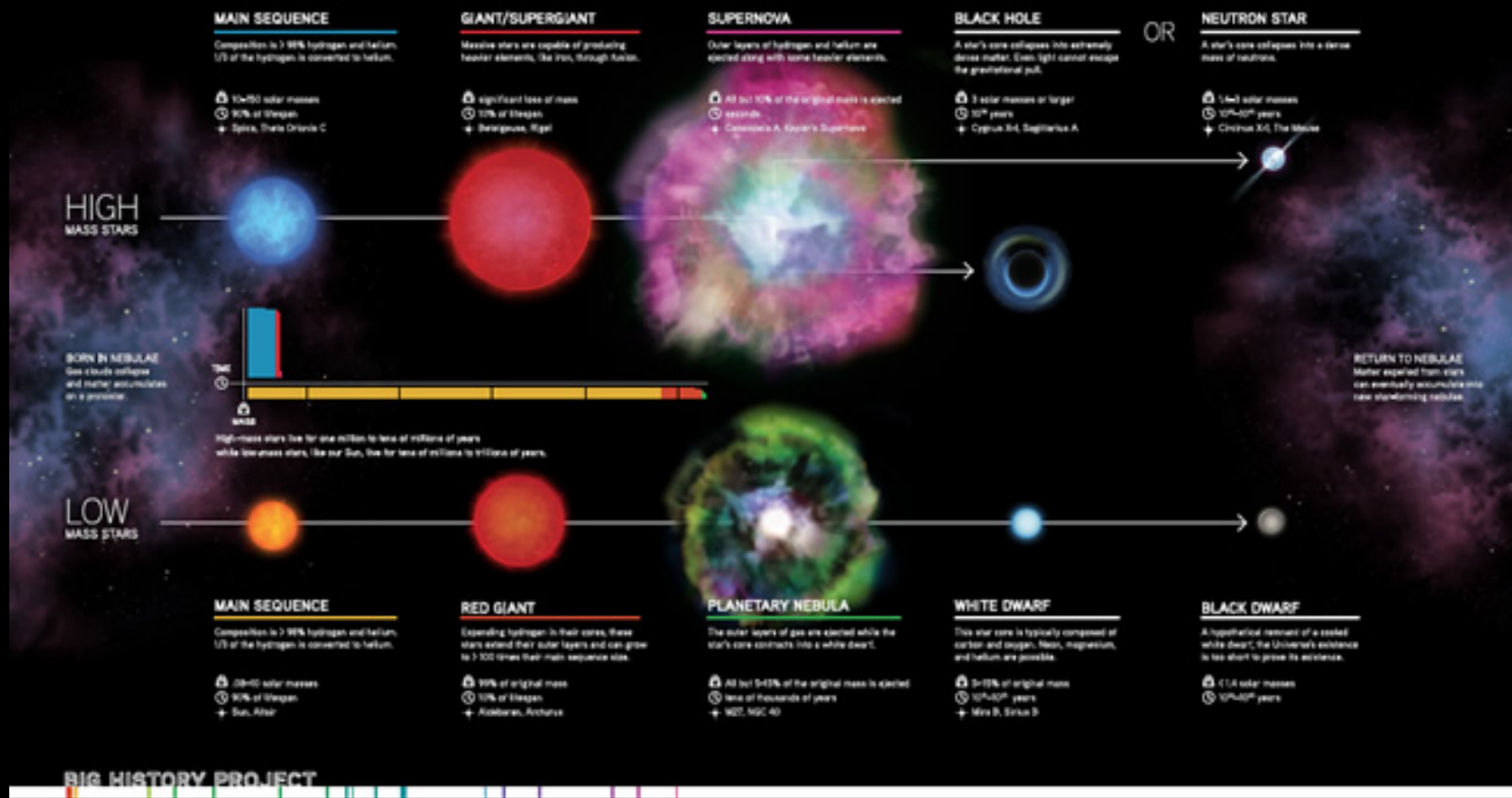
Figure 24.3. Lifetimes of H-fusion, He-fusion, and C-fusion in stars of $M_i = 1$ to $120M_\odot$ for two metallicities: $Z = 0.02$ and 0.001 (Reproduced from Schaller et al. 1992, with permission. © ESO.)

Lamers

Table 7.1 Selected quantities for $15M_{\odot}$, $20M_{\odot}$ and $25M_{\odot}$ stars with solar chemical composition ([130]). The evolutionary lifetimes refer to the core burning phases and M_{∞} corresponds to the maximum mass of the convective core, M_{HeC} and M_{CO} are the mass of the He core and CO core at the central exhaustion of H and He, respectively. M_{Fe} is the mass of the iron core of the last model computed by [130]

Quantity	$15M_{\odot}$	$20M_{\odot}$	$25M_{\odot}$
H-burning			
t_{H} (Myr)	10.70	7.48	5.93
$M_{\infty}(M_{\odot})$	6.11	9.30	13.77
$M_{\text{HeC}}(M_{\odot})$	4.10	5.94	8.01
He-burning			
t_{He} (Myr)	1.40	0.93	0.68
$M_{\infty}(M_{\odot})$	2.33	3.63	5.23
$M_{\text{CO}}(M_{\odot})$	2.39	3.44	4.90
C-burning			
t_{C} (10^3 yr)	2.60	1.45	0.97
$M_{\infty}(M_{\odot})$	0.41		
Ne-burning			
t_{Ne} (yr)	2.00	1.46	0.77
$M_{\infty}(M_{\odot})$	0.66	0.50	0.50
O-burning			
t_{O} (yr)	2.47	0.72	0.33
$M_{\infty}(M_{\odot})$	0.94	1.12	1.15
Si-burning: radiative core			
$t_{\text{Si-rad}}$ (10^{-2} yr)	29.00	2.80	1.94
$\log T_c$	9.420	9.443	9.434
$\log \rho_c$	8.092	7.818	7.798
Si-burning: convective core			
$t_{\text{Si-conv}}$ (10^{-3} yr)	20.00	3.50	3.41
$M_{\infty}(M_{\odot})$	1.14	1.11	1.12
$M_{\text{Fe}}(M_{\odot})$	1.43	1.55	1.53

THE LIFE CYCLES OF STARS

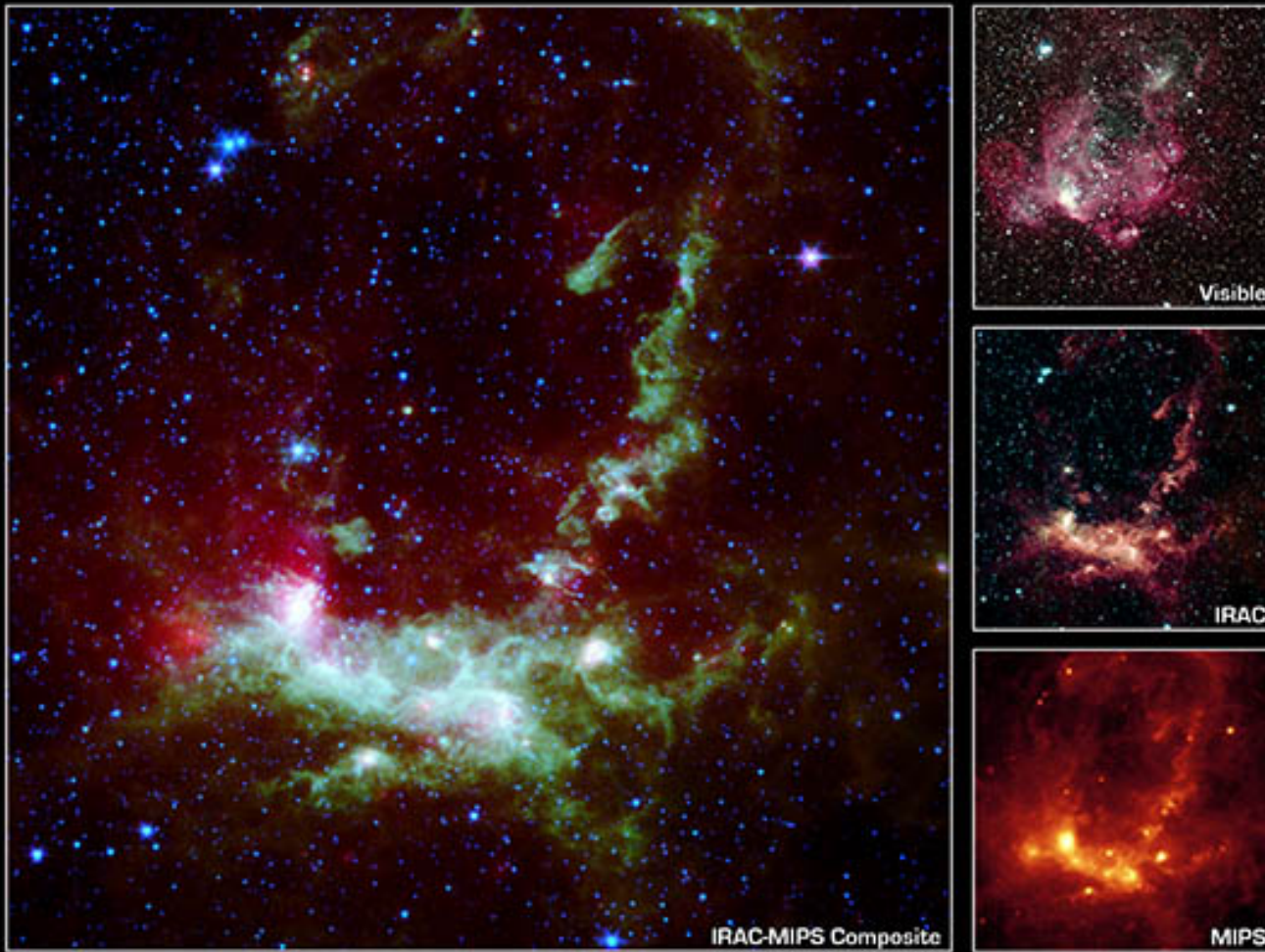


Henize 206



- Nebulosa
- Grande Nube di Magellano

Henize 206



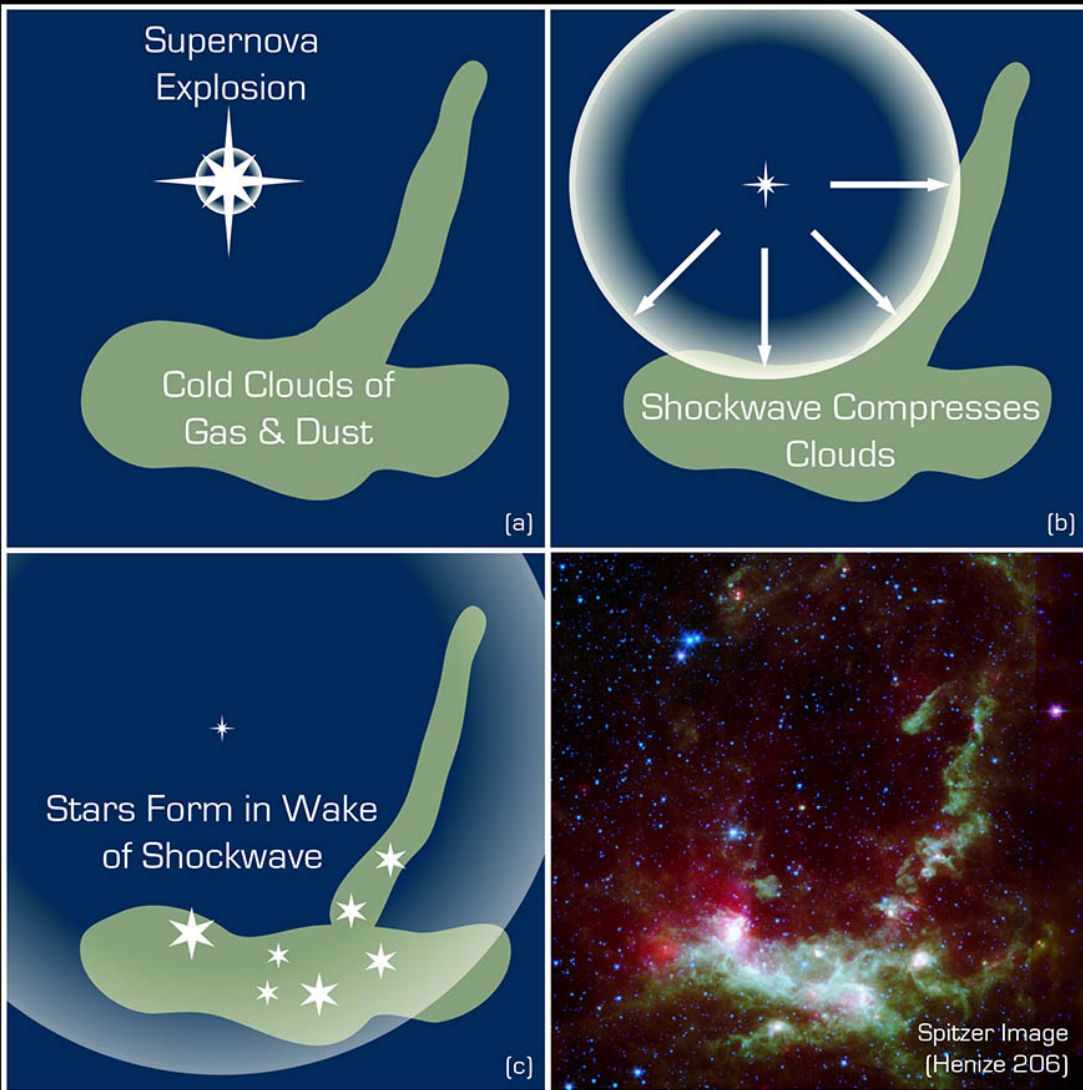
Star Formation in Henize 206

NASA / JPL-Caltech / V. Gorjian (JPL)

Spitzer Space Telescope • IRAC • MIPS

Visible: R.C. Smith (NOAO)

ssc2004-04a



Spitzer Space Telescope • ssc2004-04b



Star Formation in Henize 206

NASA / JPL-Caltech / V. Gorjian (JPL)

Spitzer Space Telescope • IRAC • MIPS

Visible: R.C. Smith (NOAO)

ssc2004-04a

